Milankovitch-Driven Cyclicity and Climate Controlled Dolomitization of a Late Triassic Carbonate Platform, Hungary

by

Anna Balog

Dissertation submitted to the Faculty of the
Virginia Polytechnic Institute and State University
in partial fulfillment of the requirements for the degree of

DOCTOR OF PHILOSOPHY

in

Geological Sciences

APPROVED:

J. Fred Read, Chairman

J. Don Rimstidt

Robert J. Bodnar

Ken A. Eriksson

A. Krishna Sinha

December, 1995
Blacksburg, Virginia

Key words: Geology, Carbonate sedimentology, Milankovitch cyclicity, Dolomitization

MILANKOVITCH-DRIVEN CYCLICITY AND CLIMATE CONTROLLED DOLOMITIZATION OF A LATE TRIASSIC CARBONATE PLATFORM, HUNGARY

by

Anna Balog

J. Fred Read
Department of Geological Sciences

(ABSTRACT)

The Late Triassic platform carbonates of the Transdanubian Range, Hungary were part of a passive margin platform at the southwestern end of the Triassic Tethys now occurs in a single fault-bounded terrain

The Hungarian platform is made up of meter-scale, precessional (~20 k.y.) carbonate cycles. It contains a lower unit, the Main Dolomite Formation (600-1500m thick), which is totally dolomitized. It is overlain by the Transitional Unit (150-400m thick). The overlying Dachstein Limestone is up to 800m thick. The platform is a cyclic succession of subtidal carbonate, laminated tidal flat limestone or dolomitic caps, and reddish or greenish paleosols or reworked paleosols.

The Triassic was a time of global greenhouse conditions and Milankovitch climate forcing has been well documented from lakes and off-shelf facies. The Triassic Hungarian carbonate platform records an imperfect Milankovitch eustatic signal. They lack the bundling of 5 precessional cycles into 100 k.y. eccentricity cycles or 20 cycles/400 k.y. bundle. This is interpreted to be due to many missed beats evidenced by caliches and paleosols, and thick amalgamated subtidal carbonates. These result from precessional sea-level fluctuations either not flooding the platform, or flooding it too deeply to allow shallowing up to sea-level in one precessional beat.

Spectral analysis of the Hungarian carbonates was used to compare the amplitude spectra of different time series including lithology, gamma ray, self potential and neutron density. The spectra based on lithology were compared to synthetic spectra generated by computer from platforms subjected differing Milankovitch signals.

Most dolomitization of the Hungarian carbonates occurred early in tidal flat settings during each high frequency cycle. Intertidal-supratidal dolomites are fine grained , Fe^{2+} and Mn^{2+} rich and slightly enriched in $\delta^{18}O$ compared marine calcite cement, and formed from weakly to moderately reducing marine waters. Subtidal dolomites are slightly coarser grained, low in Fe^{2+} and Mn^{2+} and have heaviest $d^{18}O$ signatures, indicating more evaporative oxidizing brines beneath flats. Repeated emergence stabilized the dolomites to low Sr^{2+} and Na^{+} types similar to Cenozoic dolomites. Later, coarse-grained dolomites with very low Mn^{2+} Fe^{2+} and light $\delta^{18}O$ signatures were formed along the platform margin by thermally driven, warm oxidizing marine water associated with Jurassic rifting of the Pennini Ocean (Neo-Tethys).

The overall vertical distribution of early dolomite on the platform does not reflect long term ecstasy. Instead the regional stratigraphic trends in climatically sensitive sediments, as well as stable isotopes, suggest that intense dolomitization of the lower platform reflects a semi-arid, hot subtropical setting and megamonsoonal climate. Global cooling and increased humidity toward the latest Triassic and Early Jurassic, inhibited pervasive early dolomitization, leaving the upper platform little dolomitized.

TABLE OF CONTENTS

LIST OF FIGURES

LIST OF TABLES

ACKNOWLEDGMENTS

The research presented here could not have been accomplished without encouragement, support and guidance of my scientific advisor, Fred Read. Fred provided generous assistance and advice and was always there when I needed him. I also would like to thank Janos Haas my Hungarian colleague, who introduced me to the carbonates and collaborated on the project. I am indebted to the constructive discussions with Bob Bodnar and Don Rimstidt (Virginia Tech) and their classes on fluid inclusions and geochemistry, as well as their service on my committee. I would like to thank my other committee members (Ken Eriksson and Krisna Sinha) and Cahit Coruh for their help. I would like to thank my fellow students who helped a great deal Aus Al Tawil, Mike Pope, Taury Smith, Sam Peavy, Karl Kirby, Mark Williamson. I would also like to thank Karen Hunt, Mary McMurray, Linda Bland, Sharon Chang and Brenda Kutz making my life much easier here.

My experience as a graduate student at the Department of Geological Sciences at Virginia Tech brought a new dimension to my life. First of all, I realized that I was able to live in another country, to learn about its great people and its different culture and to study and write in English. My daughter Judit, and son David made my hard days a little bit easier and my husband Csaba who shared the good and bad moments with me. Thanks to all.

During my time here I lost both of my parents, which made me more determined to finish my work in their memory.

Chapter 1: INTRODUCTION

The following chapters consist of three related cyclicity, petrologic, and geochemical studies of the Late Triassic platform carbonates of the Transdanubian Range, Hungary.

The Late Triassic platform carbonates of the Transdanubian Range, Hungary were part of a huge passive margin carbonate platform at the southwestern end of a large gulf of the Triassic Tethys, and during the Paleogene it moved eastward to its present position in the central Pannonian Basin as a single fault-bounded tectonic terrane.

The Hungarian segment of the platform is made up of meter-scale, probably precessional (~20 k.y.) carbonate cycles and contains a lower unit, the Main Dolomite Formation which is 600-1500 m thick. The cycles in this lower platform composed of lagoonal subtidal carbonates and algal laminites, and is totally dolomitized. The Main Dolomite is overlain by the Transitional Unit (150-400 m thick) which contains both totally dolomitized cycles and cycles in which caps only are dolomitized; paleosols are developed on some cycles. The overlying Dachstein Limestone is up to 800 m thick. This is a succession of subtidal limestone, laminated tidal flat limestone or dolomitic limestone, and reddish or greenish paleosols or reworked paleosols.

The Triassic was dominated by global greenhouse conditions with little continental ice. Well preserved examples of Milankovitch driven cyclicity in the Triassic sedimentary record include Triassic-Jurassic lake sedimentary cycles, marine cyclic carbonates on small Mid Triassic platforms in the Dolomite Alps, and off-shelf facies equivalent to Late Triassic large passive margin platforms. In contrast, the Late Triassic Hungarian shallow marine carbonate platform that formed on the southern margin of Tethys records a far from perfect Milankovitch eustatic signal.

The Late Triassic Hungarian platform carbonates do not show the clear bundling of 5 precessional cycles into larger eccentricity cycles. The poor record of Milankovitch sea-level changes is interpreted to be due to many missed beats in the platform stratigraphy. Missed beats are evidenced by caliches and paleosols, thick amalgamated subtidal carbonates and may result from precessional sea-level fluctuations either not flooding the platform, or flooding it to deeply to allow shallowing up to sea-level in one precessional beat. Fourth order bundling of the cycles is weak with fewer than the typical 5 cycles/100 k.y. bundle and far less than 20 cycles for inferred 400 k.y. eccentricity bundles. Fischer plots of the Hungarian cycles show third order bundling which match

Aigner's (1992) sea-level curve from the German Muschelkalk basin but is less similar to the Haq et al. (1987) global sea-level curve.

The aim of our work on spectral analysis of the Hungarian carbonates was to study the similarity of amplitude spectrum of different time series using the same datatset and the probable distortion effect of the hiatuses in the Hungarian shallow water carbonates.

The Hungarian platform carbonates have a complex early diagenesis history. The geochemistry of the abundant marine calcite cements on the platform, provide data on Triassic ocean composition as a baseline for the dolomite studies.

Most of the dolomitization occurred early, in tidal flat settings during each high frequency cycle. Intertidal-supratidal dolomites are fine grained , Fe^{2+} and Mn^{2+} rich and slightly enriched in $\delta^{18}O$ compared to the marine calcite cement, and formed from marine water, that were weakly to moderately reducing. Subtidal dolomites are slightly coarser grained, low in Fe^{2+} and Mn^{2+} and they have the heaviest $\delta^{18}O$ signature, indicating more evaporative but oxidizing brines as dolomitizing fluid sinking beneath supratidal flats. Repeated emergence stabilized the dolomites to low Sr^{2+} and Na^{+} types similar to Cenozoic platform dolomites.

Coarse-grained dolomites with very low Mn^{2+} Fe^{2+} and light $\delta^{18}O$ signatures were formed along the platform margin by thermally driven, warm oxidizing marine water associated with Jurassic rifting of the Pennini Ocean (Neo-Tethys).

Early dolomitization of cycles was controlled by high frequency sea-level changes, but the overall vertical distribution of early dolomite on the platform does not reflect long term ecstasy. Rather the intense dolomitization of the lower platform reflects a semi-arid, hot subtropical setting and megamonsoonal climate. Global cooling and increased humidity toward the latest Triassic and Early Jurassic, inhibited pervasive early dolomitization, leaving the upper platform little dolomitized.

Chapter 2: Shallow Marine Record of Orbitally Forced Cyclicity in a Late Triassic Carbonate Platform, Hungary

ABSTRACT

Well preserved examples of Milankovitch-driven cyclicity in the Triassic sedimentary record include Triassic-Jurassic lake sedimentary cycles, marine cyclic carbonates on small Middle Triassic platforms in the Dolomite Alps, and off-shelf facies equivalent to Late Triassic large passive-margin platforms. In contrast, the Late Triassic Hungarian shallow marine carbonate platform that formed on the southern margin of Tethys records a far from perfect Milankovitch eustatic signal.

These carbonate cycles contain subtidal skeletal wackestone/packstone, tidal laminites, and paleosols. The cycles include not only transgressive laminites (the classic Lofer cycles): some cycles contain regressive laminites, whereas other cycles have both transgressive and regressive laminites. The stratigraphic successions do not show the clear bundling of five precessional cycles into larger-eccentricity cycles. The poor record of Milankovitch sea level changes is interpreted to be due to many missed beats in the platform stratigraphy. Missed beats are evidenced by (1) caliches and paleosols and (2) thick amalgamated subtidal carbonates, and may result from precessional sea level fluctuations either not flooding the platform, or flooding it too deeply to allow shallowing up to sea level in one precessional beat. Fourth-order bundling of the cycles is weak, with fewer than the typical 5 cycles/100 k.y. bundle and far less than 20 cycles for inferred 400 k.y. eccentricity bundles. Fischer plots of the Hungarian cycles show third-order bundling that matches Aigner's (1992) sea level curve from the German Muschelkalk basin but is less similar to the Haq et al. (1987) global sea level curve.

INTRODUCTION

There is abundant evidence of orbitally forced changes in climate, lake levels and sea levels in Triassic rocks from many areas of the world (Olsen 1986, Goldhammer et al. 1990, Reijmer and Everaars 1991). Olsen (1986) showed that Upper Triassic-Jurassic lake sediments of the Newark Supergroup, U.S.A. were deposited under the influence of fluctuating lake levels driven by Milankovitch-induced climate changes. Goldhammer et al. (1990) and Hinnov and Goldhammer (1991) showed that Middle Triassic shallow marine carbonates of the small Latemar platform in Italy were formed under the influence of Milankovitch-driven sea level changes, which in some sections showed 5:1 bundling. For the marine Upper Triassic, Fischer (1964, 1975) and Schwarzacher and Haas (1986) suggested a Milankovitch origin for Alpine Upper Triassic marine cycles, but they later pointed out that relating the various scales of carbonate cycles to Milankovitch frequencies is not simple. Goldhammer et al. (1990) thought that the Upper Triassic marine cycles from the Alps showed little evidence of Milankovitch orbital forcing, but subsequent studies by Reijmer (1991) and Reijmer et al. (1993) of off-shelf facies equivalent to the Late Triassic platform, suggested that a Milankovitch signal was recorded in the deeper-water sediments shed from the platform.

Given the evidence of Milankovitch-driven climate and sea level changes during the Late Triassic, we examined the shallow marine carbonate record of the Late Triassic platform in the Transdanubian Range, Hungary (Figs. 2.1, 2.2), a transported tectonic terrain from the Alps and time-equivalent to the classic Alpine Hauptdolomit and Dachstein Limestone (Fischer 1964). We attempt to determine to what extent this huge platform records Milankovitch sea level/climate changes, how the record was affected by sealevel fluctuations that did not flood the platform or caused too deep a submergence to allow rapid shallowing (missed beats of Goldhammer et al. 1990), and whether paleosols can be used to help reconstruct the record. We also test whether Fischer plots could be used to document longer-term changes in sea level, and to what extent missed beats modified the signal. These Alpine carbonates formed the basis for many of the early concepts of cyclic carbonate deposition, especially the dominantly transgressive laminite development of the Lofer cycles (Fischer 1964, Haas 1982, Haas 1991). However, more recent studies have suggested that the Alpine Triassic cycles are upward shallowing and that the laminites are in fact regressive (Bosselini and Hardie 1985, Goldhammer et al.

1990). We present data showing that some of the Hungarian cycles do indeed have significant preservation of transgressive laminites and discuss reasons for this.

STRUCTURAL, STRATIGRAPHIC AND GLOBAL CLIMATIC SETTING, HUNGARIAN TRIASSIC

Structural Setting: The Upper Triassic platform carbonates of the Transdanubian Range, Hungary (Figs. 2.1, 2.2) were part of a huge passive-margin carbonate platform at the southwestern end of a large gulf of the Triassic Tethys (Fig. 2.3) (Kovacs 1982, Kazmer and Kovacs 1985, Tollman 1987). The region probably was situated between the Northern and Southern Alps. From the Mid-Cretaceous onward, the region underwent nappe formation and large-scale strike-slip faulting, and during the Paleogene moved eastward to its present position in the central Pannonian Basin as a single fault-bounded tectonic terrain (Fig. 2.2) (Kazmer and Kovacs 1985, Balla 1988, Haas et al. 1990).

Stratigraphic Setting: Rifting in the Permian was followed by marine flooding in Permian/Triassic boundary time. In the Early Triassic (Scythian), a shallow, mixed siliciclastic-carbonate ramp was formed. The first extensive carbonate platform developed in the Middle Triassic (Anisian), but a brief phase of Middle Triassic tectonism and volcanism in the Late Anisian-Ladinian segmented the platform with a series of grabens. In the east, carbonate platform deposition continued until the Middle Triassic (Early Carnian). However, by the end of the Early Carnian, terrigeneous influx drastically increased, perhaps as the climate became wetter, and the deep basins began to fill with sediment. Large areas of the platforms were incipiently drowned. This resulted in extremely flat topography by the Latest Carnian, which favored development of the huge Late Triassic carbonate platform (Main Dolomite and Dachstein Limestone). Subsidence of the platform in the Late Triassic was relatively rapid, but slowed in the Early Jurassic (Fig. 2.4).

The Late Triassic platform (Fig. 2.5) contains a lower unit, the Main Dolomite Formation, which grades eastward into skeletal limestone (Uppermost Carnian) and is underlain by a thin bituminous lagoonal dolomite and skeletal limestone in the west. The Main Dolomite is Uppermost Carnian in the east but its top becomes younger to the west (Uppermost Carnian to Lower Norian).

The Main Dolomite is 600-1500 m thick, and highly cyclic, with cycles composed of lagoonal subtidal carbonates and algal laminites, and is totally dolomitized. It is overlain

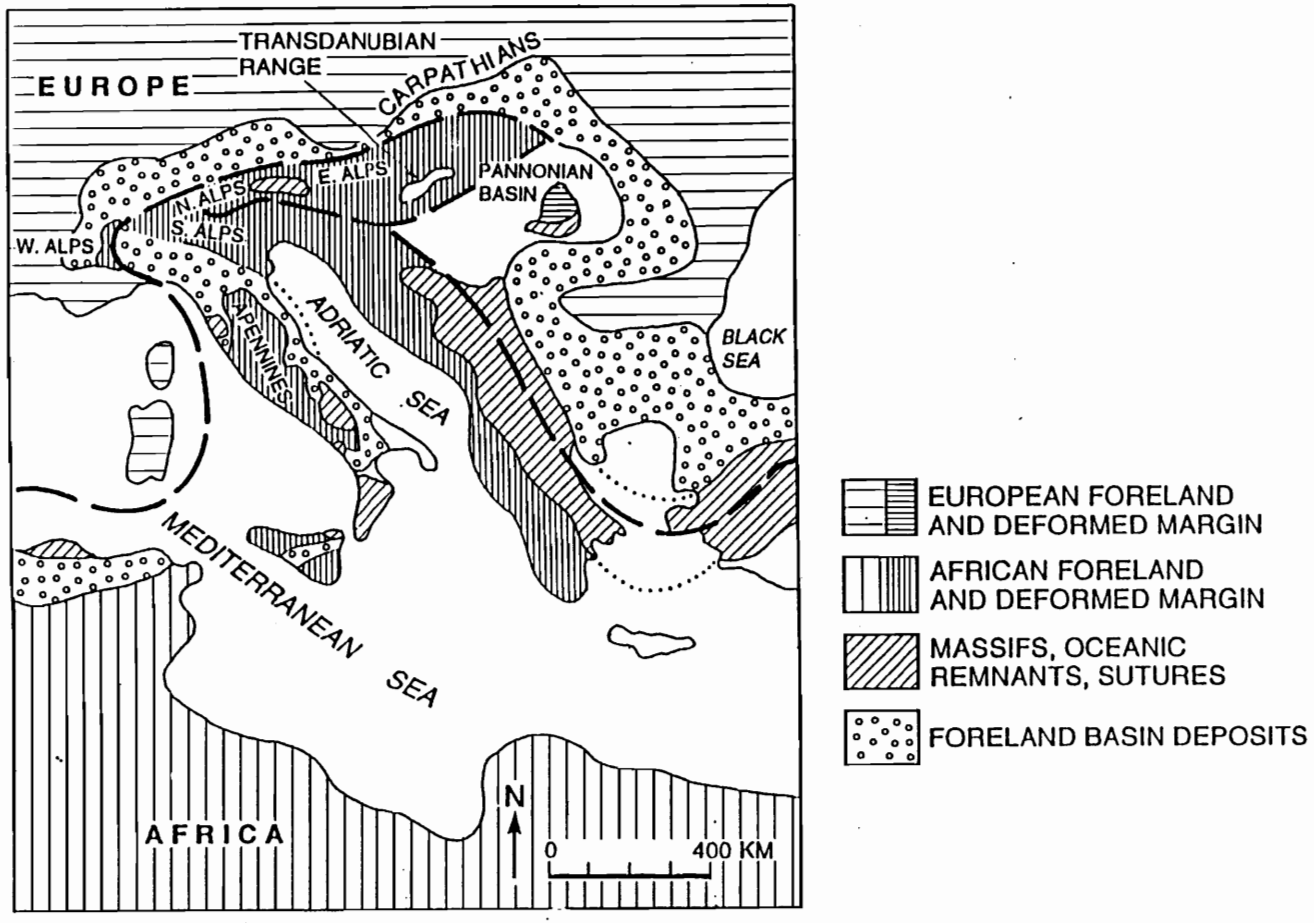

Fig. 2.1. Regional geological location map of the Triassic carbonates of the Transdanubian Range (arrowed), Hungary. Boundaries of major lithotectonic blocks bounded by heavy dashed lines. The Transdanubian carbonates are allochthonous, and were transported by strike-slip faulting from their original position between the Northern and Southern Alps.

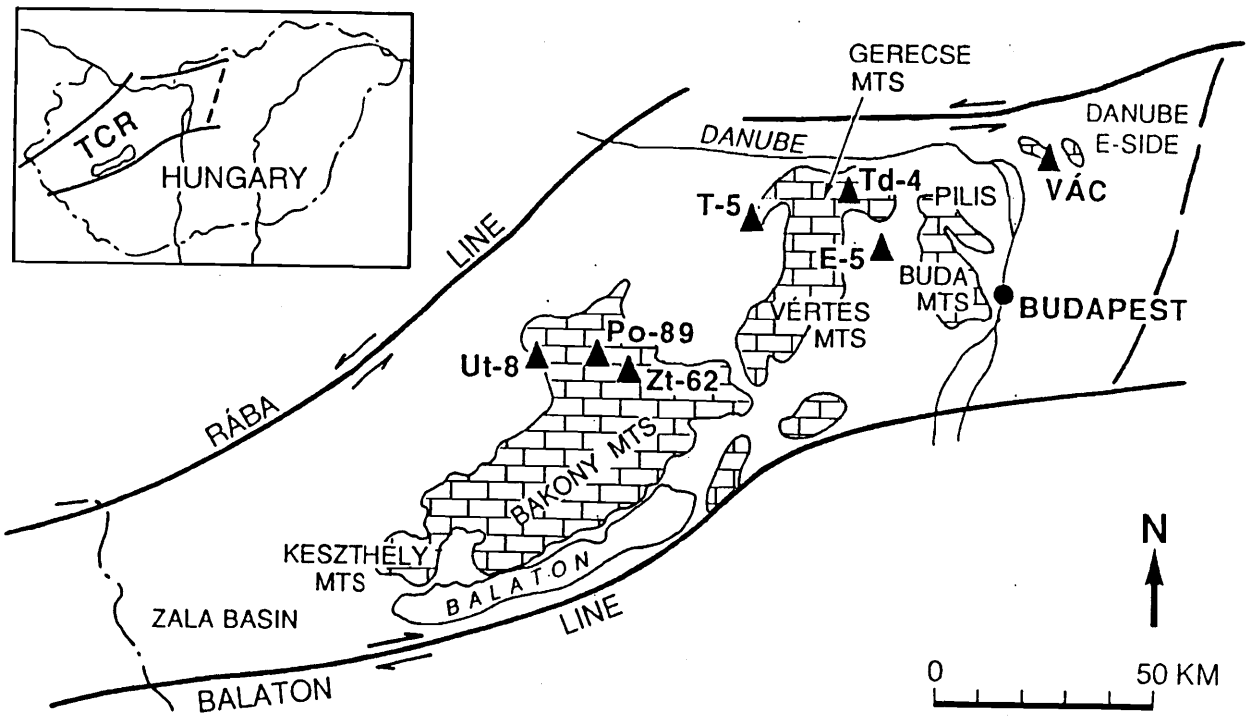

Fig. 2.2. Location map, Transdanubian Range, with inset showing regional location in Hungary. The tectonic terrain containing the Triassic carbonates is bounded by the Raba Line and Balaton Line (shown on inset map as heavy lines bounding the Transdanubian Range labeled TCR). Core locations within the Transdanubian Range (larger map) are shown by solid triangles; VAC is from Vac area; Td-4 is Tardos 4; E-5 is Epol 5; T-5 is Tata 5; Zt-62 is Zirc-62; Po-89 is Porva-89; Ut-8 is Ugod-8.

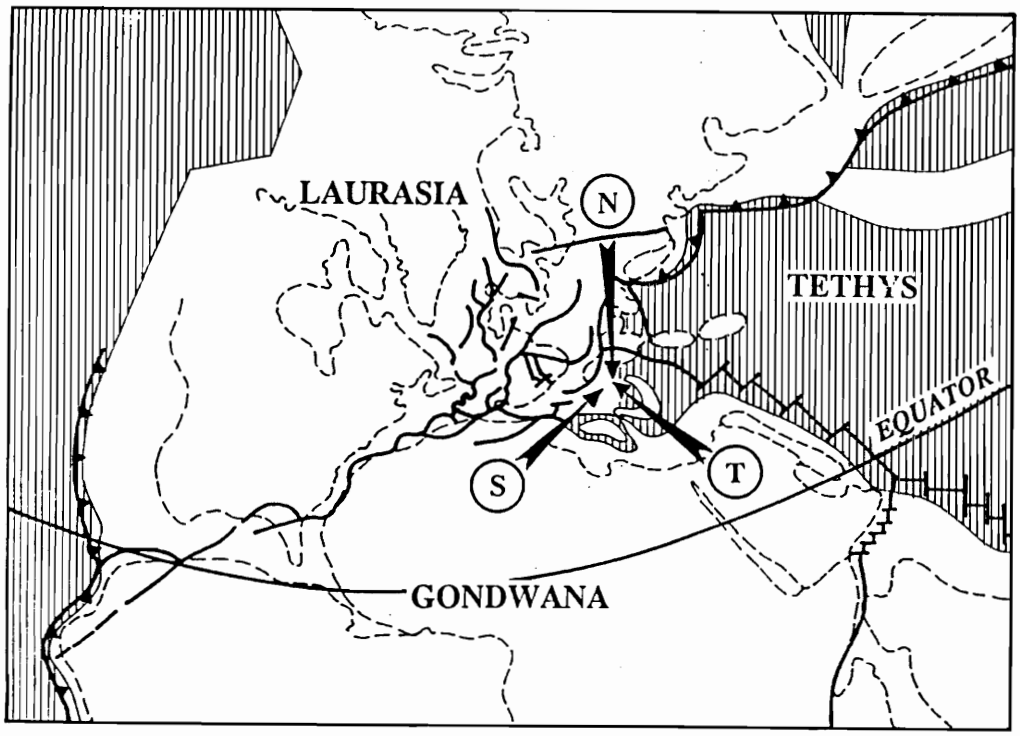

Fig. 2.3. Paleogeographic setting of the Triassic Transdanubian carbonates during Late Triassic time (216 m.y.). Modified from Marcoux et al. (1993). N is Northern Limestone Alps, S is Southern Limestone Alps and T is Transdanubian Range.

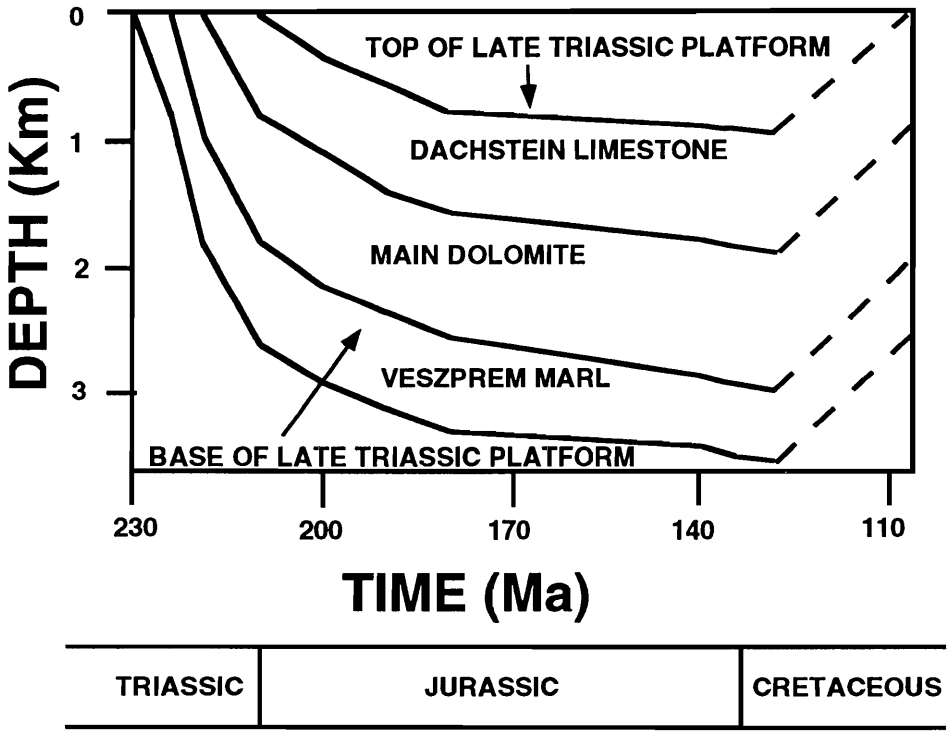

Fig. 2.4. Composite subsidence history plot of the Hungarian Triassic platform for the Late Triassic-Early Jurassic. This study interval includes the Main Dolomite to Dachstein Limestone interval. Individual subsidence history plots for each area, which might demonstrate differential subsidence could not be constructed because of limited well control.

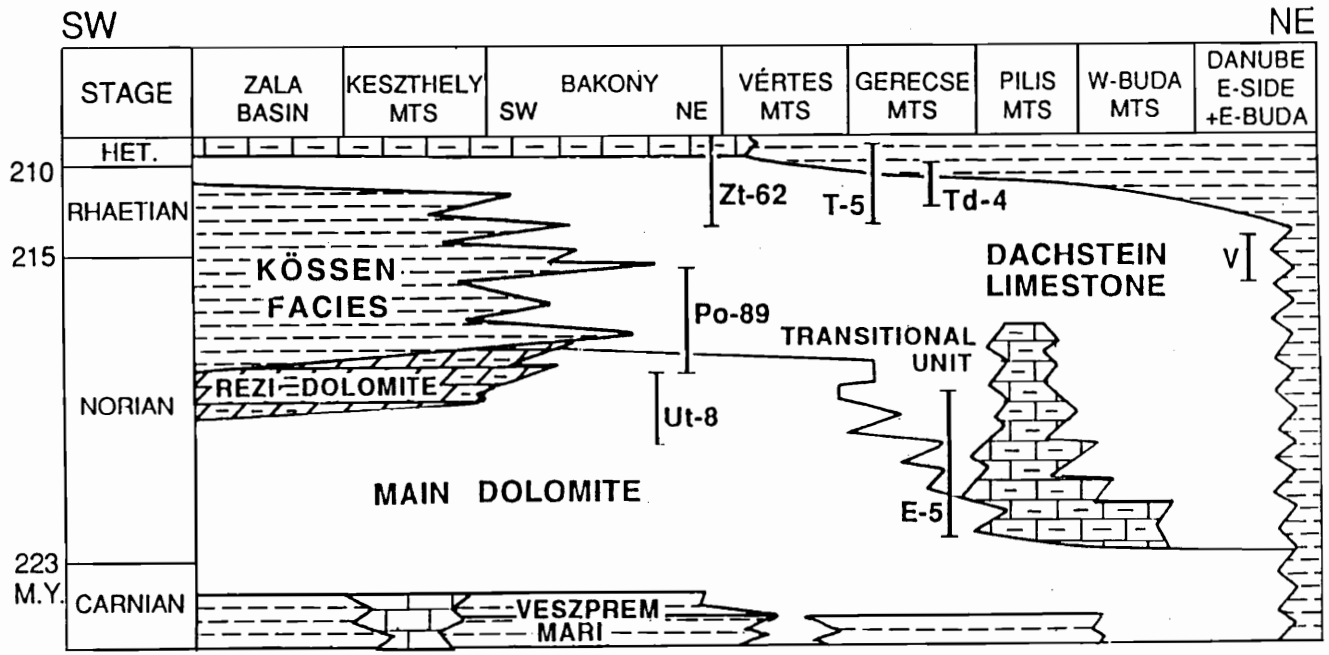

Fig. 2.5. Depth-distance stratigraphic chart showing stratigraphic units of the Triassic carbonate platform, Transdanubian Range. Stratigraphic positions of the cores are shown by heavy vertical bars. Modified from Haas (1988). Time (m.y.) shown alongside depth section for reference. Landward is to left (southwest), and seaward edge of platform is to right (northeast).

by the Transitional Unit (150-400 m thick), which contains both totally dolomitized cycles and cycles in which caps only are dolomitized; paleosols are developed on some cycles.

The overlying Dachstein Limestone is up to 800 m thick. To the west, the base of the Dachstein Limestone becomes younger, and the unit passes into dark gray, argillaceous, intrashelf basin facies (Kossen Formation). The Dachstein Limestone ranges from Lower Norian to Rhaetian in the east, Middle Norian to Rhaetian in the central region and upper Rhaetian in the west. It is a cyclic succession of subtidal limestone, laminated tidal-flat limestone or dolomitic limestone, and reddish or greenish paleosols or reworked paleosols.

The Main Dolomite-Dachstein Limestone succession in the east contains localized bituminous dolomite and limestone deposited in narrow intraplatform basins from the Carnian to Latest Triassic-Early Jurassic. The shallow-water platform drowned in the Early Jurassic, during a phase of rift-related subsidence (Sengor 1985, Haas et al. 1990).

Global Climatic Setting and Orbital Forcing: The Triassic was dominated by global greenhouse conditions with little continental ice (Frakes et al. 1992). There is substantial evidence that Triassic climates were strongly influenced by Milankovitch orbital forcing. Van Houten (1962, 1964), and Olsen (1986) and Olsen et al. (1989, 1993) showed that the Triassic-Lower Jurassic lake deposits of the eastern United States show evidence of Milankovitch-induced, alternating wet-dry climate changes that caused changing lake levels. The resulting sedimentary cycles (Van Houten cycles) typically show a basal, desiccation-cracked mudstone (very shallow lake) overlain by black laminated calcareous claystone (deep perennial lake), up into gray desiccated mudstone (very shallow lake) and capped by red, massive mudstone (playa). These facies changes within cycles are accompanied by changes in sedimentary structures, total organic carbon, percent carbonate, and biota and were used to define relative water-depth rank (Fig. 2.6). Olsen (1986) and Olsen et al.(1989) considered that the lake cycles were bundled into various scales of compound cycles. On the basis of estimated long-term accumulation rates, they showed the various scales of cycles to have Milankovitch periodicities defined by spectral analysis of time series constructed from relative water-depth rank of the cyclic facies; quasi-periodicities were approximately 21, 100, and 400 k.y. Kominz et al. (1991), using gamma analysis, a method in which estimated sedimentation rates for the different facies are taken into account, substantiated the Milankovitch orbital forcing.

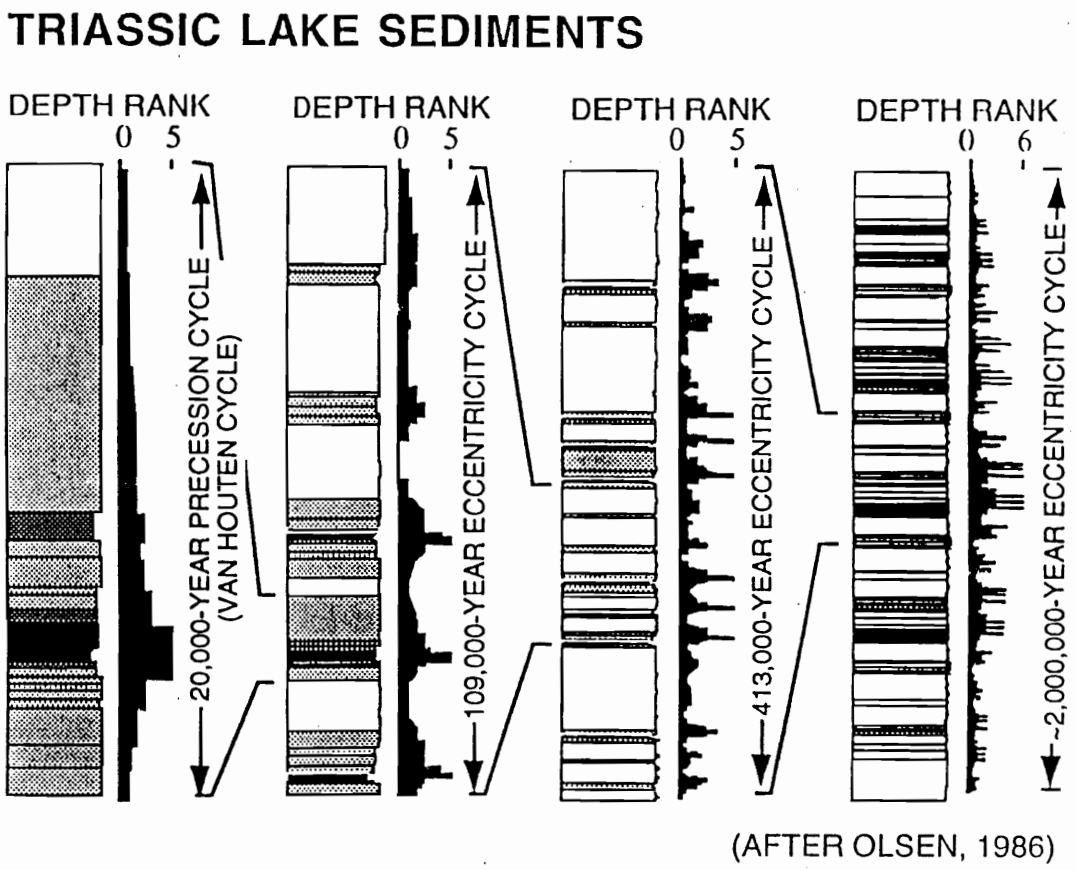

Fig. 2.6. Plot showing cyclicity in the Triassic lake deposits of the Newark Basin, U.S.A based on water depth rank vs stratigraphic position (see Olsen, 1986). The different stipple patterns on the lithologic columns define facies described in text. The cycles show a clear bundling of precessional cycles into short- and long term eccentricity cycles and a third order cycle.

In the Upper Triassic basinal equivalents of the Dachstein Limestone in the Austrian Northern Limestone Alps, Reijmer et al. (1993) showed that there was a rhythmic alternation in the point-counted proportion of platform-derived vs. basin-derived grains in calciturbidites. By spectral analysis of the time series constructed from the calciturbidites, they concluded that the rhythmic variations were due mainly to Milankovitch-driven sea level fluctuations which caused much bank-derived material to be incorporated into the periplatform debris during high-frequency highstands, and a major decrease in bank material during high-frequency lowstands. Their spectra suggested that Milankovitch-driven sea level changes were dominantly due to precession (roughly about 20 k.y.) and short-term eccentricity (100 k.y.); they suggested that an obliquity signal also is present but weak. There is little evidence of a 400 k.y. signal in the data. Reijmer and Everaars (1991) suggested that Milankovitch orbital forcing caused the sea level fluctuations. This Milankovitch orbital forcing also extended back into the Middle Triassic (Goldhammer et al. 1990, Hinnov and Goldhammer 1991).

Data Sources: The study area is a 200 km wide dip-parallel section of the original platform in the Transdanubian Range, Hungary (Figs. 2.1, 2.2). Our data are mainly from cores from two subareas, the Gerecse Mountains, located on the outer part of the inner platform, and the Northern Bakony Mountains, situated 70 km landward from the Gerecse area (Fig. 2.2). Our study is based on detailed bed-by-bed logging of continuous diamond drill cores (Fig. 2.2). Cores from the Bakony Mountains include Po-89 (400 m), Ut-8 (300 m), and Zt-62 (220m); these span the topmost part of the Main Dolomite, the Transitional Unit, and a nearly complete sequence of the Dachstein Limestone (Figs. 2.2, 2.5). From the Gerecse Mountains, cores include E-5 (500 m), T-5 (200 m), and Td-4 (50 m); these span the topmost part of the Main Dolomite, the Transitional Unit and the topmost 50-200 m of the Dachstein Limestone (Figs. 2.2, 2.5). We recorded the field data in tabular form, noting lithologies, sedimentary structures, fossils, color, degree of dolomitization, leaching, internal sedimentation, any obvious marine or sparry cements, presence of paleosol and tectonic fractures.

METER-SCALE CARBONATE CYCLES (LOFER CYCLES)

Description of Late Triassic Meter-Scale Cycles

The Upper Triassic carbonates of the Transdanubian Range contain well-developed carbonate cycles (Haas and Dobosi 1982, Haas 1982, Schwarzacher and Haas 1986). The cycles are from less than 1 m to over 5 m thick and include transgressive types, regressive types, and symmetrical transgressive-regressive types (Fig. 2.7A, B) (Haas and Dobosi 1982). Facies are described in Table 2.1.

Facies of the Idealized Cycle: The idealized facies succession in the Lofer cycles is described below, from the base up, with common European letter designations for each facies given in parentheses (Fig. 2.7B) (Fischer 1964, Haas 1982):

(1) Reworked paleosol (A), composed of red or green carbonate that may be argillaceous, with numerous clasts of the underlying limestone; storm layers of clasts or skeletal debris may be present; in-situ features such as root casts or root mottles are absent (Fig. 2.8A). It commonly rests on in-situ paleosol of underlying cycle.

(2) Transgressive tidal flat laminite (B), containing well developed microbial lamination, fenestrae, and mudcracks (Fig. 2.8D).

(3) Subtidal carbonate (C), typically lime wackestone/packstone or rare ooid grainstone; may have carbonate rip-ups in lower part; biota includes foraminifera, megalodont clams, and calcified green, dasyclad, and amoeboid algae (Fig. 2.8E, F). Subtidal units commonly are preserved as limestone in the Dachstein Limestone, and are dolomitized in the Main Dolomite; aragonitic fossils typically are leached and molds are filled by dolomite spar in the Main Dolomite and marine cement in the Dachstein Limestone.

(4) Regressive tidal flat laminite (B'); similar to transgressive laminites but commonly more dolomitized, mud-cracked and leached, and with internal sediment-floored cavities.

(5) In situ paleosol (A'); in Dachstein cycles, paleosols are composed of red or green, commonly argillaceous carbonate, with numerous angular lithoclasts of the underlying carbonate bed, some of which are blackened; mottles and root casts are common. In Main Dolomite, paleosols are dominated by laminated and pisolitic caliches (Fig. 8B, C). Paleosol rests disconformably on underlying cycle, and may be overlain by transgressive surface.

Table 2.1

Facies	Clayey Paleosol	Caliche	Microbial Laminites	Subtidal Carbonates
Lithology	nodules of underlying carbonates and black pebbles in clayey, dolomitic matrix	laminated or massive cryptocrystalline calcrete	completely to partly dolomitized microbially laminated lime mudstone and pellet intraclast packstone	skeletal peloidal wackestone/packstone or rare ooid grainstone
Color	red or green	light gray to yellow	Light gray, yellow	light gray to cream, dark gray
Sedimentary Structures		very thin laminations of darker organic rich and lighter sediment rich layers; fenestral porosity	Smooth, wavy or crinkled lamination with irregular fenestral porosity	thick- to massively bedded bioturbated, unlayered
Grain Types	in the matrix: skeletal fragments, iron oxides, clay minerals; nodules are fragments of subtidal and peritidal carbonates, some of which are blackened	peloids, lumps, coated grains, intraclasts, vadose pisolite	skeletal fragments, intraclasts, fine to sand sized pellets and peloids	skeletal grains of diverse biota, intraclasts, pellets, peloids, ooids
Biota	Reworked Ostracods, gastropod fragments, some forams	reworked rare fragments of Ostracods, gastropods	some Gastropods, Ostracods, forams; calcified filaments in Dachstein Limestone	forams, gastropods, Ostracods, megalodont bivalves, dasycladacean algae, calcyspheres
Early diagenesis	internal sediment and/or vadose cement in cavities and pores; vadose alteration of underlying carbonates	Calcified, than completely or partly dolomitized aragonite cement; dolomitized host	skeletal grains leached; micrite cements; dolomitization, vadose or phreatic radiaxial or equant calcite in fenestral pores and cavities	leached skeletal grains, micritic, radiaxial or bladed marine calcite in pores, and cavities; some vadose pendant cement and micrite cement
Environment	terrestrial	terrestrial to supratidal	intertidal and supratidal	intertidal and subtidal

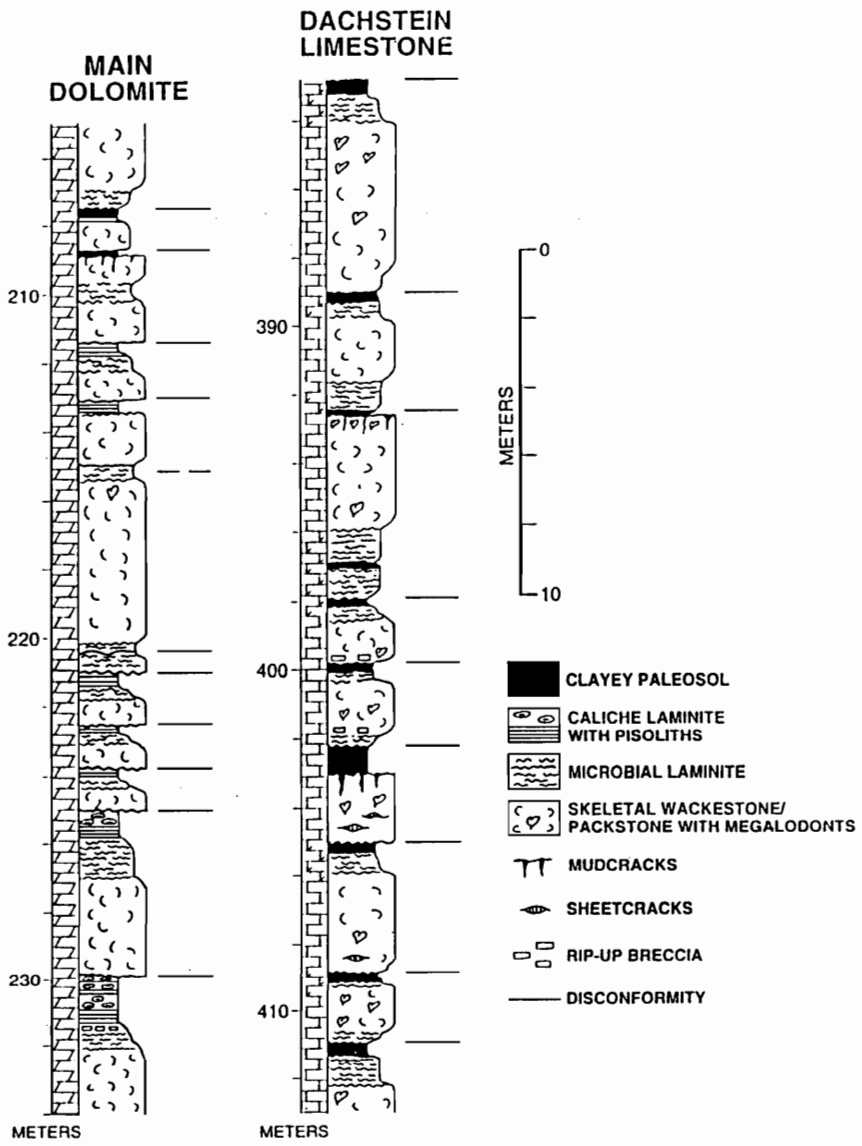

Fig. 2.7.A. Small portions of representative stratigraphic columns showing typical cyclic successions in Main Dolomite and Dachstein Limestone. Cycles in the Main Dolomite are completely dolomitized, whereas those in the Dachstein Limestone are limestone with dolomite caps and paleosols. Cycle boundaries shown by horizontal lines alongside columns.

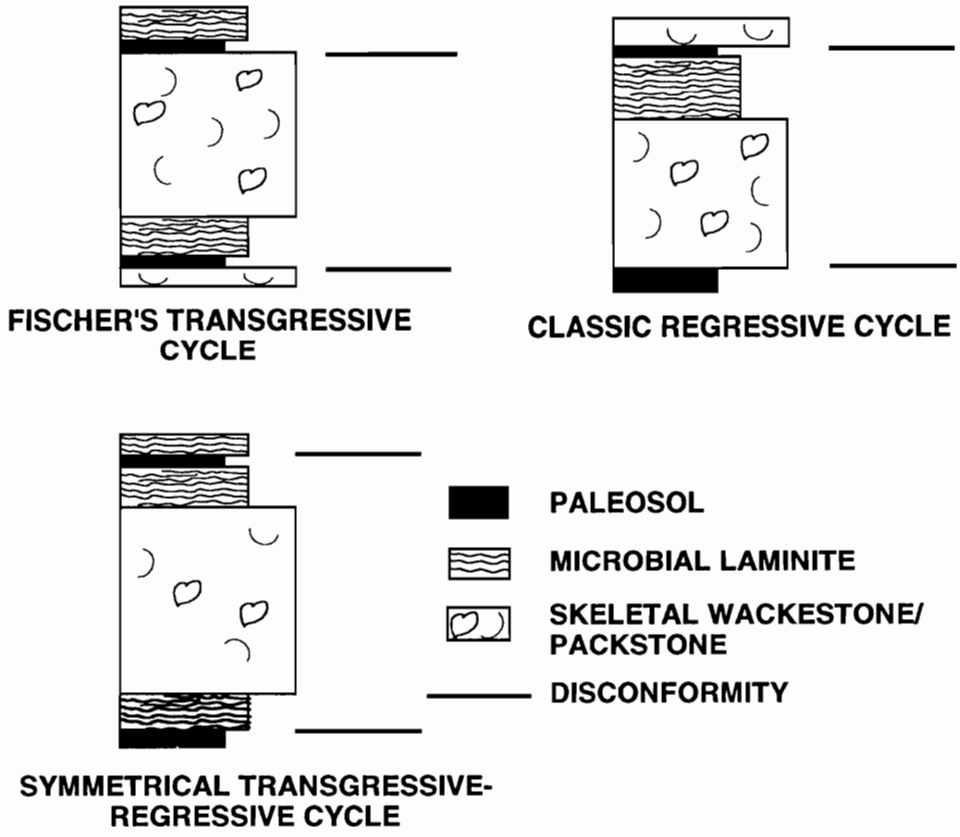

Fig. 2.7.B. Facies of the three cycle types in the Late Triassic carbonates. Note that the cycles differ mainly in presence or absence of transgressive vs regressive tidal flat laminites and paleosols.

Fig. 2.8. Slabs and thin section photomicrographs. A. Slab of paleosol from Po-89 core (Dachstein Limestone), consists of fragments of the underlying limestone and black pebbles in a clayey lime mud matrix.

B. Thin section of dolomitized pisolitic caliche from Ut-8 core (Main Dolomite).

C. Slab of dolomitized laminated caliche from Ut-8 core (Main Dolomite).

D. Thin section of microbial laminite from Po-89 core (Dachstein Limestone).

E. Slab of subtidal limestone with leached Triassinas and megalodont shell fragment from Po-89 core (Dachstein Limestone). The mold is filled by marine calcite.

F. Thin section of subtidal skeletal wackestone from Po-89 core (Dachstein Limestone).

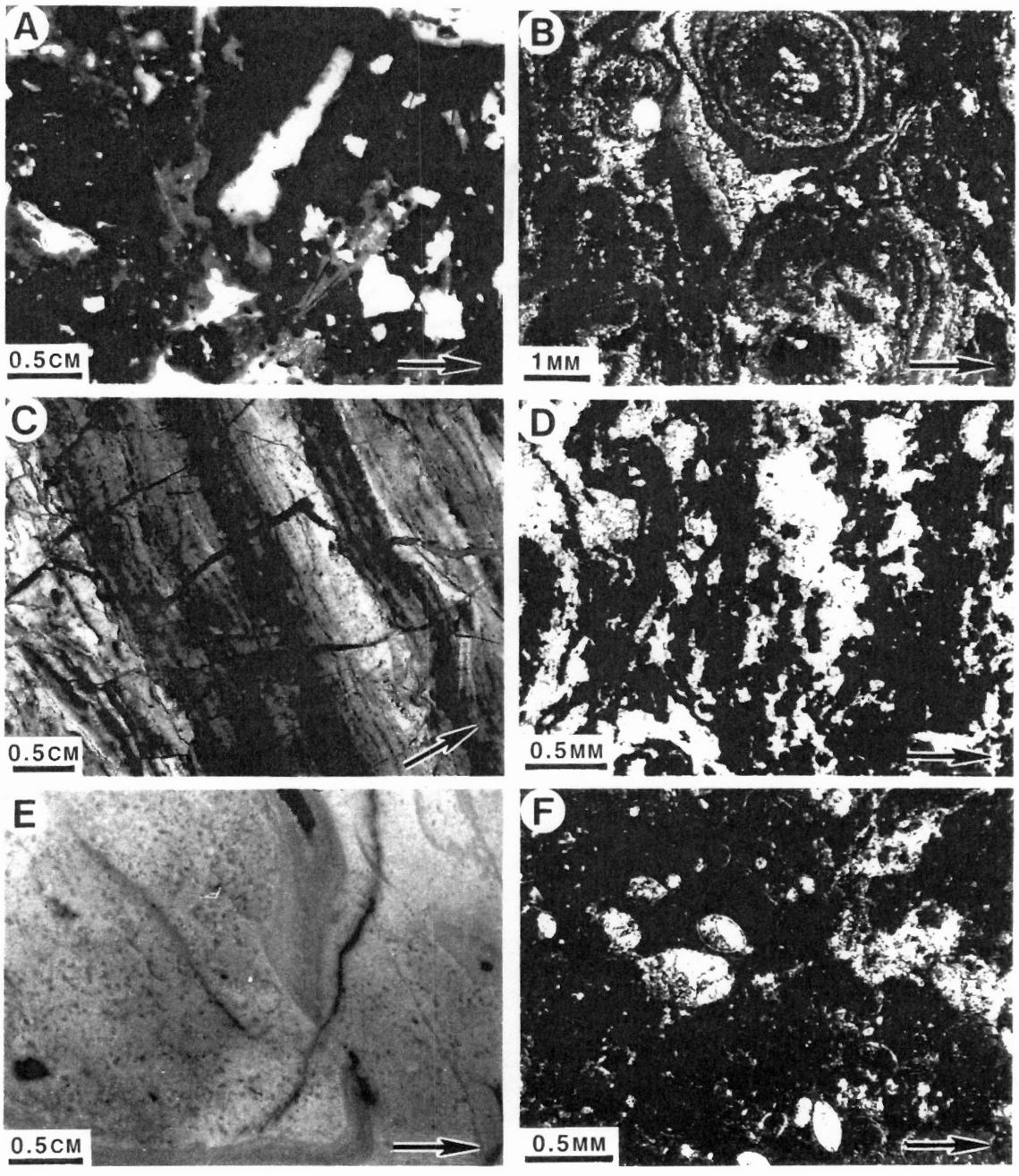
A
0.5CM
B
1MM
C
0.5CM
D
0.5MM
E
0.5CM
F
0.5MM

Cycle Types Defined on Laminite Position: Transgressive laminites (B) are recognizable as such where they overlie a disconformity, paleosol, or reworked paleosol developed on a regressive laminite or subtidal unit (Fig. 2.7B). Transgressive laminites typically pass up via a flooding surface into the overlying subtidal (C) unit. Regressive laminites (B') typically conformably overlie the subtidal carbonate unit (C) and may be capped by disconformities or paleosols (Fig. 2.7B). If paleosols or disconformities are absent from the section, transgressive vs. regressive laminites cannot be recognized: then these laminites were labeled undifferentiated types. Cycles containing the ideal symmetric pattern of both transgressive and regressive laminites (Fig. 2.7A, B) are present in some cases, but most cycles lack one or more of the component facies. Frequency analysis and Markov analysis of the successions show that frequency of the various cycle types differs significantly among the Main Dolomite, Transitional, and Dachstein Units (Fig 2.9) (Haas 1988). Symmetrical transgressive-regressive cycles are abundant in the Dachstein Limestone and Main Dolomite and are least developed in the Transitional Unit. Regressive-laminite-capped cycles are common in all formations. Fischer's (1964) classic transgressive-laminite cycles are dominant only in the Transitional Unit, but are as abundant as regressive-laminite cycles in the Dachstein Limestone and rare in the Main Dolomite.

Paleosols and Paleosol Rank: Clayey paleosols are common in the Dachstein Limestone and in limestone-rich parts of the Transitional Unit, although the thickness and development of paleosol layers is highly variable even within units. Clayey paleosols are thin or absent in other units. The clayey paleosols include both red and greenish gray types, which are equally common, and consist of argillaceous limestone, marl, or clayey marl, containing fragments of the underlying subtidal and intertidal beds and black pebbles (Fig. 2.8A). Bifurcating molds of probable plant rootlets are also present.

Paleosols with caliche fabrics composed of laminated caliche and vadose pisolite are common in upper parts of cycles from the Main Dolomite and the dolomitic Transitional Unit (Fig. 2.8B, C). Intense dolomitization and lack of distinctive color differences from the underlying carbonates makes the caliche paleosols less easy to recognize in core.

Paleosols were qualitatively ranked by thickness, apparent degree of development and presence of single versus multiple soil zones (Figs. 2.10, 2.11). Any such ranking clearly has problems because thickness may not necessarily proportional to time, and can reflect

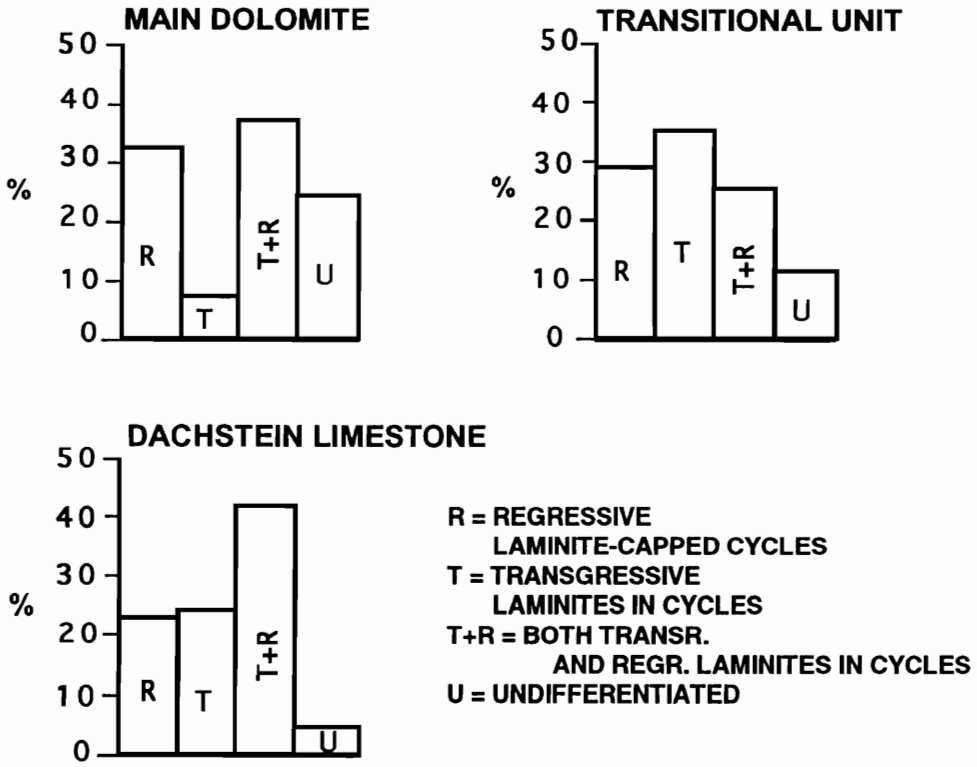

Fig. 2.9. Histograms showing frequency of occurrence of cycles with transgressive laminites and regressive laminites in the Main Dolomite, Transitional Unit and the Dachstein Limestone. Undifferentiated cycles ("U") are those in which laminites could not be classified because they lacked an associated paleosol. Note the common occurrence of transgressive laminites in the Transitional Unit and the Dachstein Limestone.

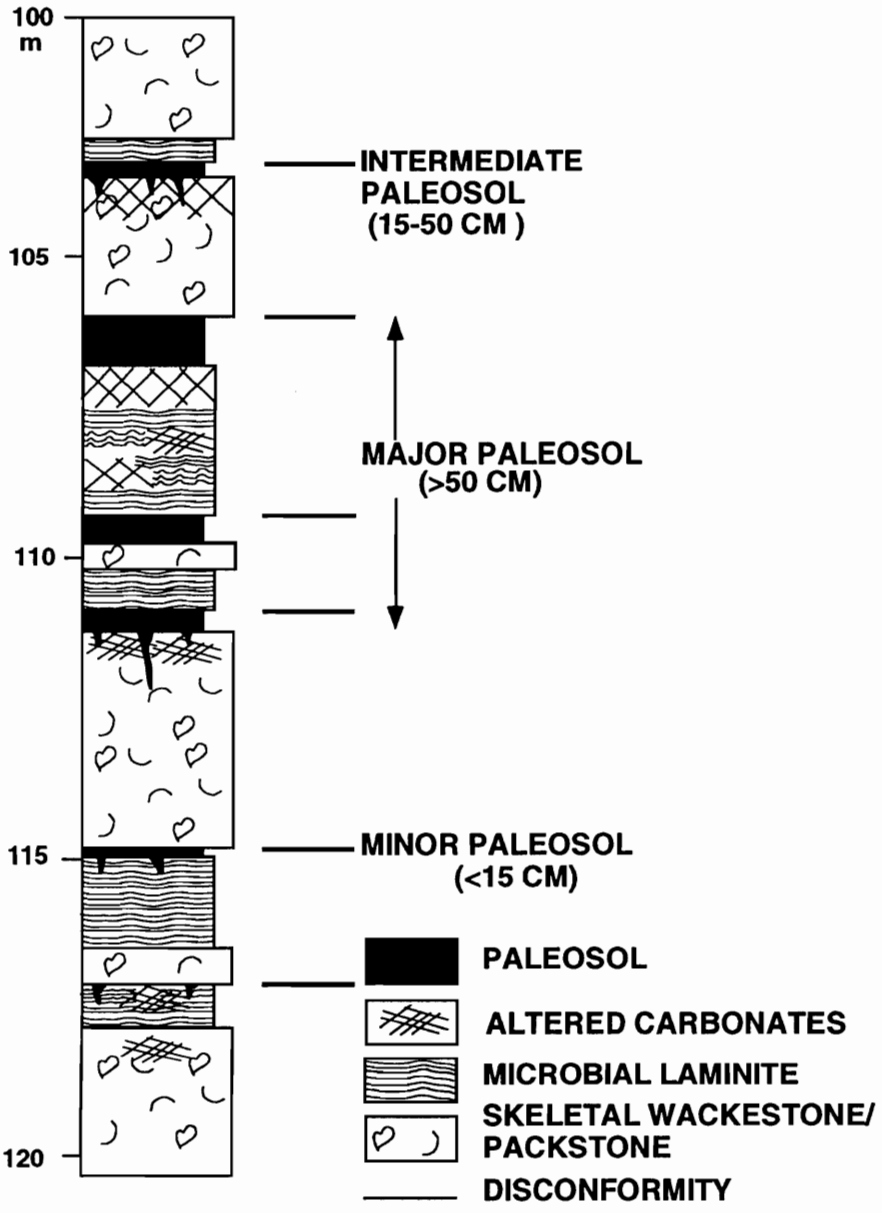

Fig. 2.10. Measured section (core Po-89) illustrating different ranks of paleosols in the Hungarian Triassic sequences. The paleosols ranked 1,2 and 3 in Figure 10 correspond to paleosols labeled minor, intermediate and major types. Such a ranking may be misleading if the soils show great lateral thickness variation, which is likely.

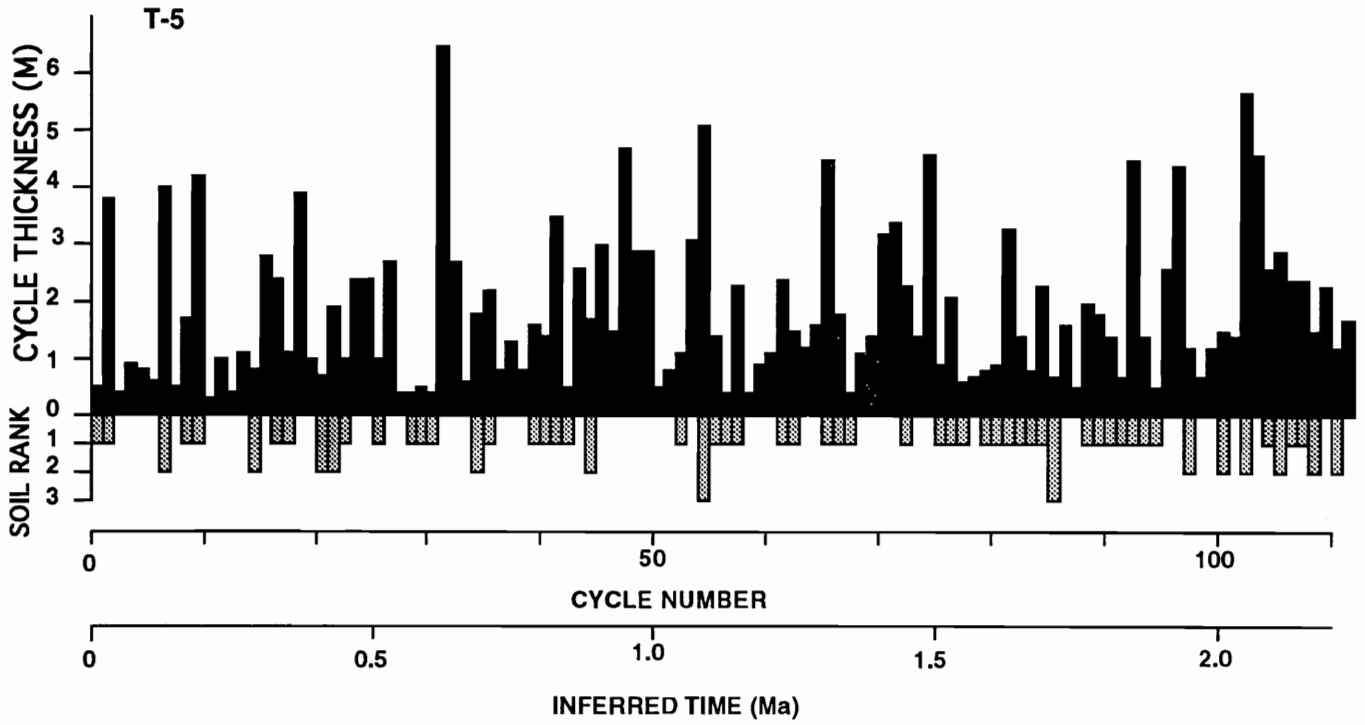

Fig. 2.11. Bar plot of core T-5 showing cycle thickness and rank of associated paleosols capping the cycles (shown below cycle in which they occur) plotted against stratigraphic position (cycle number). Least well developed paleosols are ranked 1, best developed are ranked 3. Gaps mark inferred major stratigraphic breaks.

erosional thinning of the original paleosol or local topography on which the paleosol developed. Also, most of the data are from cores, which give little indication of horizontal variability. The paleosols also were qualitatively ranked in an attempt to determine whether they could be used to better assess the duration of stratigraphic gaps in the section. Incipient paleosols are thin (<10-15 cm) and commonly are reddish or greenish intraclastic carbonate mudstone (Fig. 2.10). Intermediate rank paleosols are 20-50 cm thick units of argillaceous claystone or marl and have common internal erosion surfaces. Major-rank paleosols are thick (>50 cm) and segmented by many internal erosion surfaces. These composite paleosols consist of limestone-marl mini-cycles were completely altered to paleosols during long subaerial exposure (Fig. 2.10). Colors of paleosols appear to change regionally: cores from the seaward part of the platform have reduced, greenish gray paleosols (Core T-5), whereas paleosols in Core Td-4 (mid-platform) are more oxidized, and in the time-equivalent and more landward Zt-62 section only red paleosols are present.

Periodicity of Individual Meter-Scale Cycles

Core T-5 and its topmost exposed outcrop in the Kalvaria Hill Quarry spans the Rhaetian and consists of a 200 m interval of the Dachstein Limestone beneath the Triassic/Jurassic boundary (Fig. 2.5). Foraminiferal studies on Core T-5 by Oravecz-Scheffer (personal communication, 1993) suggests that the Norian-Rhaetian boundary is between 190 and 196.5 m depth, which is evidenced by the last occurrence at 196.5 m of minim Peptic, which is known only from the Norian, and by the appearance of Triasinas and other abundant Rhaetian microfossils at around 190 m. In this section, the upper part (probably a few meters) of the Triassic succession may be missing (Fulop 1975) as well as the Jurassic section (Lowermost Hettangian).

Lack of accurate radiometric ages for the Upper Triassic make estimation of cycle period subject to large errors. Total duration of the Rhaetian is between 2 and 6 m.y. (6 m.y, Albertiana, 1992; 5 m.y, Haq et al., 1987; 4 m.y Menning, 1990; 2 m.y. Harland et al., 1990). If the minimum Rhaetian duration of 2 m.y. is used for the 100 cycles in Core T-5 and the quarry section, this would give about 20 k.y. duration for each cycle. This value is similar to the 23 k.y. average cycle period obtained by Schwarzacher and Haas (1986) using the mean total thickness of the Upper Carnian-Rhaetian Dachstein carbonates, the absolute age data, and the mean thickness of the small-scale cycles.

Schwarzacher (1993) also estimated the cycles in the Po-89 core to be approximately 20 k.y. This was on the basis of the Harland (1990) time scale for the Norian-Rhaetian of 15.4 m.y., which is represented by 2000 m of carbonates. Four hundred meters of Po-89 thus represents about 3 m.y. and contains 25-33 larger bundles (~100 k.y. each) made up of approximately five (20 k.y.) cycles per bundle. The approximately 20 k.y. average period for the meter-scale Hungarian cycles seems reasonable considering the abundant stratigraphic gaps and missing beats manifested by paleosols. On the other hand, if we assume an upper value of 5 m.y. for the Rhaetian, and 50 k.y. period for the basic cycles, the duration of the Late Carnian to Rhaetian is almost twice the accepted value. Similarly the 50 k.y. periods that Fischer (1964) obtained for the 300 cycles in his Dachstein section, Northern Limestone Alps, was due to his over estimation of 15 m.y. for the section.

Formation of the Meter-Scale Cycles

Evidence that Milankovitch Eustasy Formed the Hungarian Cycles: Although some of the Hungarian Triassic cycles may be autocycles, we feel that most show evidence of having formed as a result of high-frequency sea level fluctuations, for the following reasons. A eustatic origin is supported by evidence of subaerial exposure at tops of cycles and intense early leaching of aragonite shells in marine parts of cycles (Haas and Dobosi 1982, Schwarzacher and Haas 1986, Haas 1988). Autocycles would tend to shallow to tide level only, and would not tend to form subaerial paleosols unless carbonate was deposited above sea level in the form of beach ridges or dunes, of which there is little evidence. Similarly, without topographic relief above sea level, a fresh-water wedge or lens could not develop to cause early leaching of aragonitic shells in subtidal facies.

That such eustatic fluctuations apparently were driven by Milankovitch orbital forcing is suggested by the estimated 20 k.y. periodicities of the meter-scale cycles (precessional cycles?), and distinctive ratios between these small cycles and larger bundles of cycles, presumed to be obliquity (minor) and 100 k.y. eccentricity bundles (Haas and Dobosi 1982, Schwarzacher and Haas 1986, Haas 1988). However, because of the lack of a clear 5:1 bundling in some of the Austrian Triassic sections, Goldhammer et al. (1990) ruled out a pure Milankovitch mechanism, but suggested that any Milankovitch

signal was complicated by tectonics and autocyclic shoaling. A Milankovitch origin for the Hungarian cycles is also compatible with the evidence of Milankovitch-forced sea level changes in time-equivalent off-shelf facies in the Alpine Triassic described by Reijmer et al. (1993). The magnitudes of any Late Triassic Milankovitch-driven sea level fluctuations were probably only several meters or so, similar to those proposed for the Middle Triassic by Goldhammer et al (1990). Such relatively small eustatic fluctuations would be compatible with the general lack of Triassic continental ice sheets (Frakes et al. 1992).

Origin of Transgressive, Regressive and Symmetrical Cycles: The idealized Northern Alpine Lofer cycles of the Dachstein Limestone were considered to be transgressive by Fischer (1964) but were reinterpreted by Goldhammer et al. (1990) as classic regressive upward-shallowing cycles (Fig. 2.7B). The histograms of the Hungarian cycle types (Fig. 2.9) show that regressive-laminite-capped cycles are not the dominant cycle type here, but in much of the section are subordinate to transgressive-laminite-capped cycles and transgressive-regressive cycles. The apparent dominance of regressive-laminite-capped cycles in the Main Dolomite may relate to the difficulty in recognizing transgressive vs regressive laminites, in the absence of a paleosol or disconformity within the laminite unit. This is suggested by the abundant "undifferentiated" cycle group in the Main Dolomite (Fig. 2.9).

Cycles that lack a transgressive laminite (Figs. 2.7B, 2.9) may result from the effects of lag time or depth. In the platform interior, sedimentation may not have been triggered until some critical depth after flooding had been reached (given likely rise rates, attainment of such a depth might have taken a few thousand years). Thus, sediment was not supplied to the tidal zone during transgression, and only a reworked regolith, rather than a transgressive laminite, was laid down. Lack of transgressive laminites also could be due to low accommodation (Koerschner and Read 1989). This is because low subsidence rate would create only a small accommodation space during emergence, leaving the platform above the position of the lowstand sea level immediately prior to flooding. Thus by the time the sea flooded the platform, rise rates on the sea level curve would be near maximum. This would favor rapid transgression of the platform, inhibiting deposition of a transgressive tidal-flat laminite. Lack of transgressive laminite also could be due to rapid rise rates associated with highly asymmetric sea level oscillation.

Development of transgressive laminites (Figs. 2.7B, 2.9) probably was favored where or when rate of accommodation creation during emergence was sufficient to drop the platform to near the Milankovitch lowstand of sea level. This allowed the initial lowstand rise rates to be relatively slow, favoring deposition of a transgressive laminite (Koerschner and Read 1989)

Lack of regressive laminites from some cycles (Figs. 2.7B, 2.9) may have resulted from non deposition of tidal-flat facies on subtidal units, perhaps because sea level drop was more rapid than progradation of tidal-flats into the area. This would have resulted in a subtidal unit capped by a soil. Some cycles might also have been capped by regressive laminites that were eroded following sea level fall, causing the paleosol to develop directly on a subtidal unit.

Significance of the Paleosols: Paleosols in the Main Dolomite resemble laminated and pisolitic caliches that were formed in semi arid or seasonally wet-dry settings (James 1972, Read 1974). These commonly developed on microbial laminites, overprinting the original fabrics and undergoing penecontemporaneous dolomitization (Goldhammer et al. 1987). Clayey, red/green paleosols on the Dachstein cycles, in contrast, appear to have formed under more humid conditions, indicated by calcified filament molds in laminites, scarcity of dolomite, and preservation of subtidal units as limestone.

Although we do not know how many beats to assign to the various ranks of paleosols (Fig. 2.10), minor-rank (incipient) paleosols may have formed in less than a few thousand years during the lowstands of 20 k.y. cycles. Similar incipient soils have formed in modern supratidal carbonate settings over the last 3-5 k.y. (Read 1974). Intermediate-rank paleosols, which commonly are thicker, with more internal erosion surfaces and clay, may represent a few missing beats (perhaps 40-100 k.y.). Thick, major-rank paleosols commonly are composite paleosols with many internal erosion surfaces. The multiple, interlayered soil and remnant marine carbonate layers may be due to multiple marine phases that barely flooded the platform. They could also be due to paleosol material extending down into the section along bedding planes and joints, to form an apparently interlayered complex of soils and marine units (James 1972, Rossinsky et al. 1992). These perhaps are comparable to soils developed on Pleistocene carbonates over the last hundred or several hundred thousand years (Semeniuk and Meagher, 1981).

CYCLES AND BUNDLING

Types of Plots Used

In aggraded cycles that formed under low-amplitude (rather than high-amplitude) eustasy, cycle thickness is related to accommodation space created prior to and during deposition of each cycle. This accommodation space is due to subsidence, sea-level rise, and isostatic effects. Although cycle thickness reflects accommodation rate, the relationship is not quantifiable because there are too many complicating effects such as quasi-periodicity of the cycles, variable sedimentation rates, potential for non uniform subsidence rates, and incomplete shallowing to the high-frequency highstand. However, in a general sense, plots of cycle thickness vs. cycle number should record changes in accommodation in both the short term (tens or hundreds of kiloyears) and the long term (Figs. 2.11, 2.12).

Cycle bundling reflecting changes in accommodation rate (rate of change of sea level plus subsidence) should be evident on Fischer plots (Fischer 1964. Read and Goldhammer 1988. Goldhammer et al. 1990). These plots graph cumulative cycle thickness (corrected for linear subsidence) against time by assigning an average cycle duration to each cycle. They can be better envisaged as plots showing the cumulative departure from mean cycle thickness, plotted against cycle number up the stratigraphic section (Figs. 2.13-2.15) (Goldhammer et al. 1993, Sadler et al. 1993). Packages of thick cycles are interpreted on the plots as long-term increases in accommodation space and plot as positive deviations (plot rises to right), whereas packages of thin cycles may reflect decreases in accommodation, and show on the plots as negative departures (plot falls to right). Fischer plots are thus useful in defining bundling of cycles, which may be related to Milankovitch-induced changes in accommodation (Goldhammer et al. 1990) or short periods of increased subsidence. They also record longer-term (0.5-5 m.y.) third-order relative sea level cycles (Read and Goldhammer 1988, Koerschner and Read 1989, Goldhammer et al. 1990, Goldhammer et al. 1993).

Bundling of cycles should also be evident in spectral analysis of time series constructed using some measure of relative water depth plotted against stratigraphic thickness (Schwarzacher and Haas 1986) or cycle thickness vs. cycle number (Fig. 2.16). Consequently, a combination of cycle-thickness vs. cycle number plots, Fischer plots, and spectral analysis of various time series was used to examine the degree of bundling and hence the degree of preservation of any Milankovitch record in the cores.

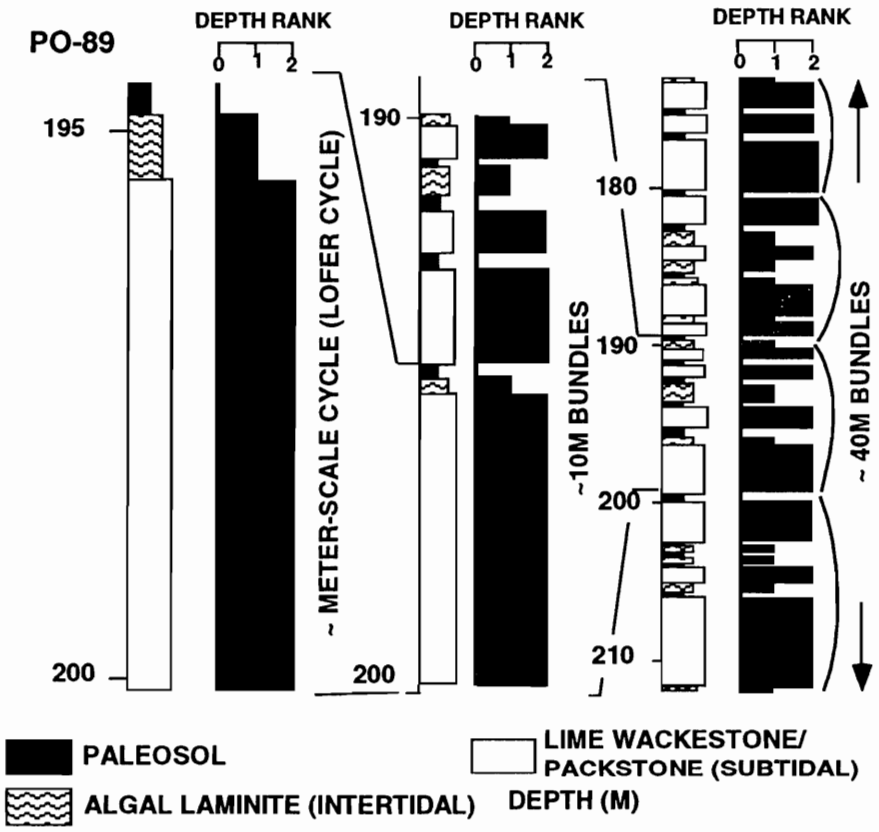

Fig. 2.12. Simplified stratigraphic columns (patterned for lithologies) and water depth rank plots (black bar graphs) from part of core Po-89 in the Late Triassic Dachstein Limestone showing poor cycle bundling. Depth rank is: 0 equals paleosol, 1 equals laminite and 2 equals subtidal limestone. Numbers alongside columns show stratigraphic depth in core. Any cycle hierarchies appear to be far less clear than in the Triassic lake record (Olsen, 1986) shown in Figure 2.12.

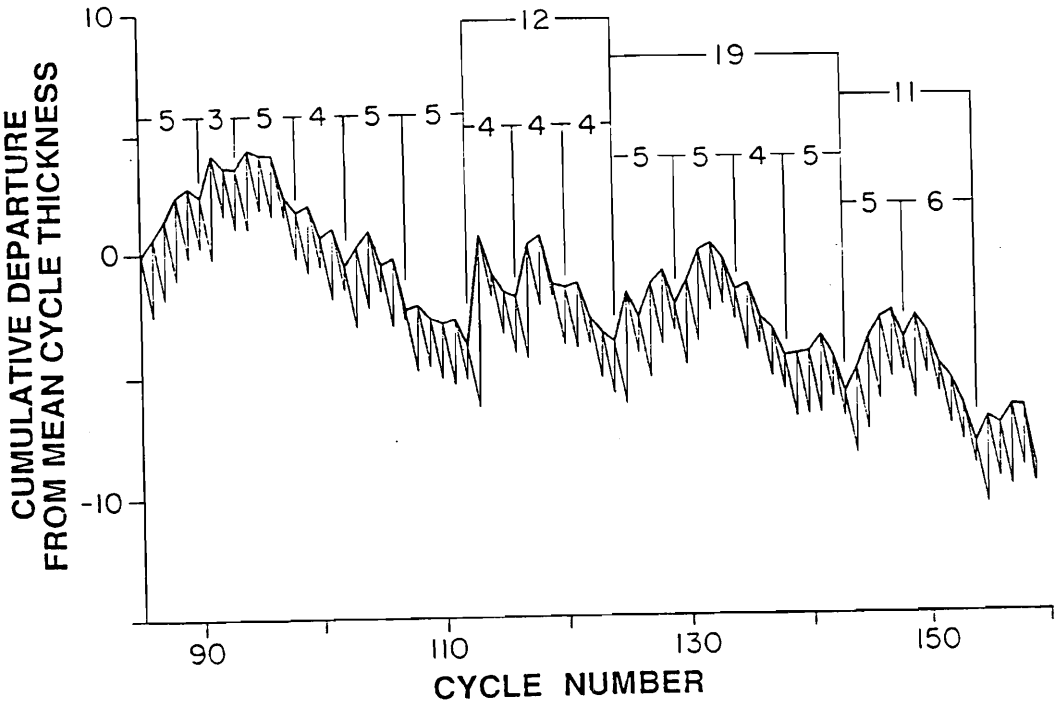

Fig. 2.13. Part of Fischer plot of Dachstein Limestone in upper part of core Po-89 showing possible bundling of carbonate cycles. This plot is the "fall" part of a long term, third order cycle shown on figure 2.14. Higher frequency cycle bundles of 3 to 6 cycles (possibly 100 k.y. bundles) are bundled into larger bundles made up of up to four 100 k.y.(?) bundles; these may be 400 k.y. cycles (11 to 19 cycles/bundle).

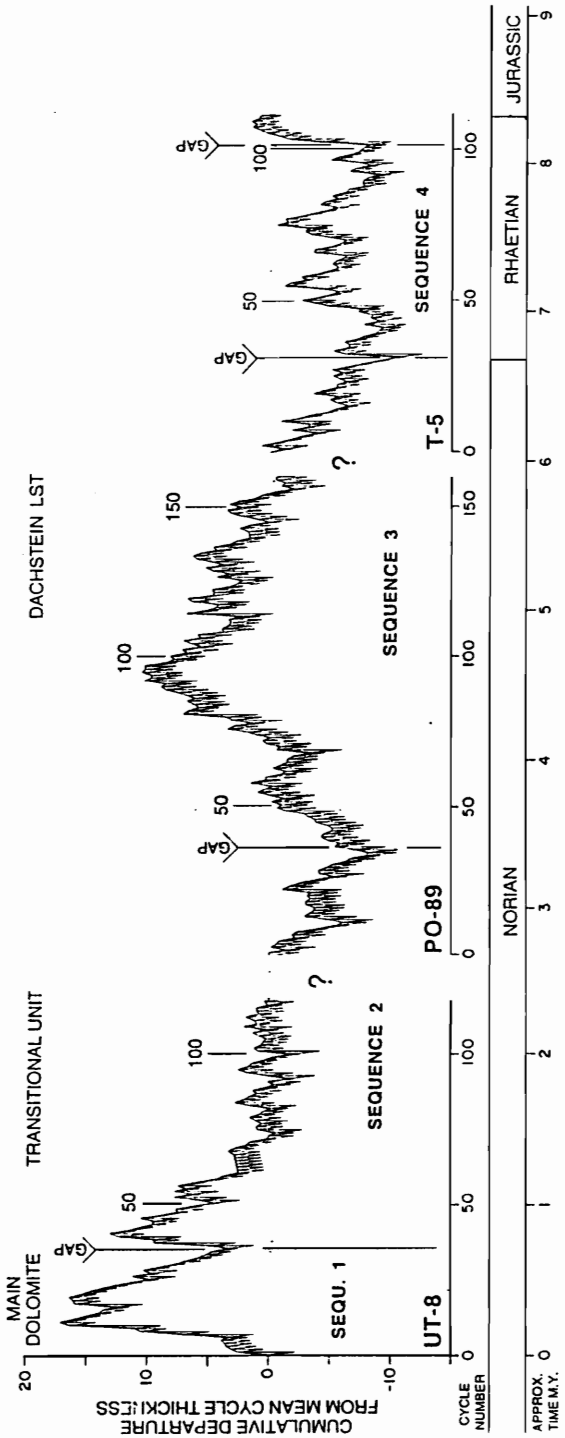

Fig. 2.14. Composite Fischer plot spanning the Main Dolomite to Dachstein interval constructed from cores UT-8, PO-89 and T-5. Non-overlapping portions between the cores are shown by spaces in the plots. The composite plot suggests that possibly four third-order relative sea-level cycles are developed in the section (sequences 1 to 4). The falling limb of the Po-89 plot (sequence 3) is shown in detail in Figure 2.13. Parts of plots marked by "gap" are characterized by several stacked soil zones.

Fig. 2.15. Comparison of Fischer plots of overlapping sections Zt-62, T-5 and Td-4 cores. These cores extend up to the base of the Jurassic. Possible correlative low-stand positions bounding sequence 4 are marked by heavy lines connecting plots. The light line connects a smaller low-stand within sequence 4. Parts of plots marked by "G" for stratigraphic gap, indicate portions of the section with stacked soil zones.

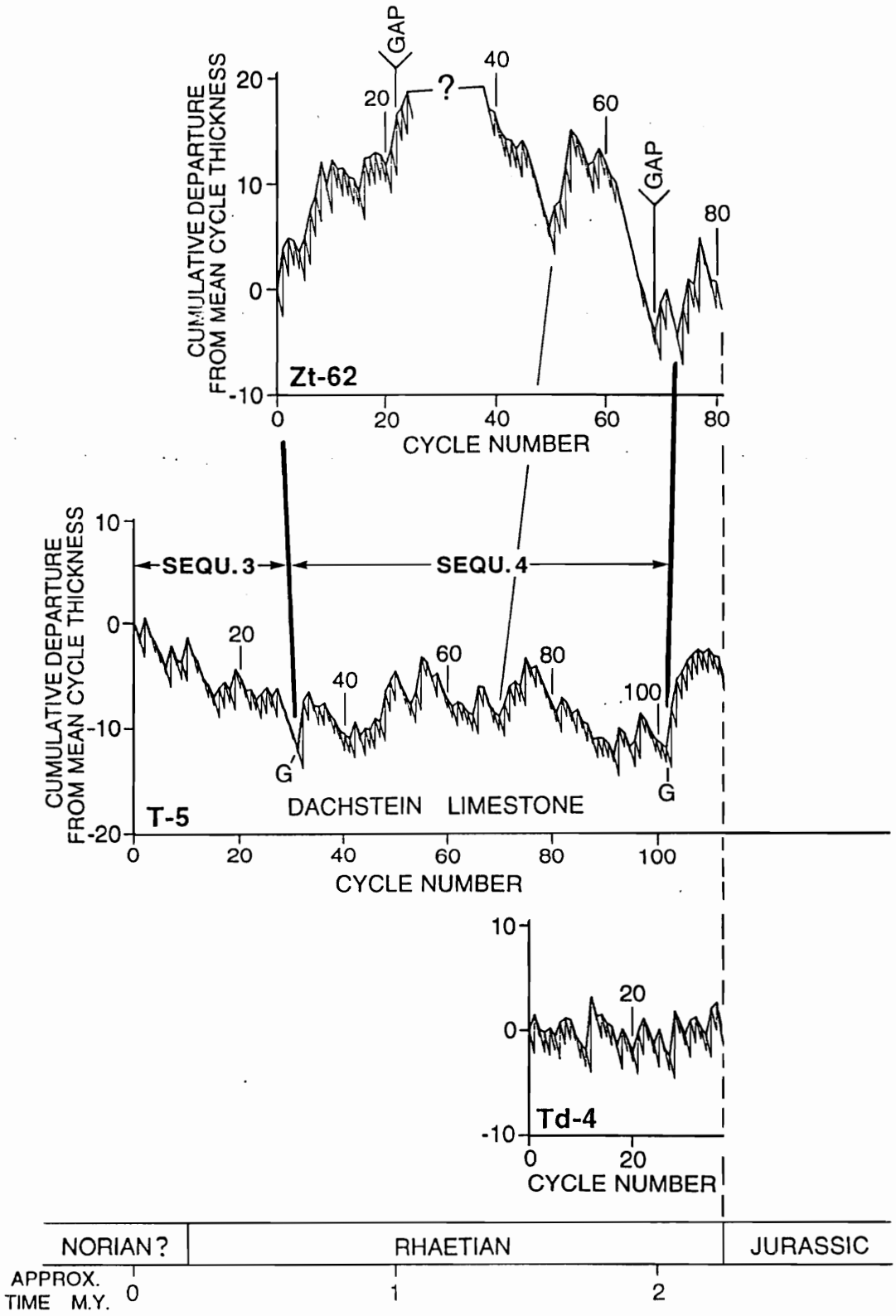
GAP
40
20
?
60
GAP
80
CUMULATIVE DEPARTURE FROM MEAN CYCLE THICKNESS
20
10
0
-10
Zt-62
0
20
40
60
80
CYCLE NUMBER
SEQU. 3
SEQU. 4
10
0
-10
-20
20
40
60
80
100
G
G
T-5
DACHSTEIN LIMESTONE
CUMULATIVE DEPARTURE FROM MEAN CYCLE THICKNESS
0
20
40
60
80
100
CYCLE NUMBER
10
20
0
-10
Td-4
0
20
CYCLE NUMBER
NORIAN?
RHAETIAN
JURASSIC
APPROX. TIME M.Y.
0
1
2

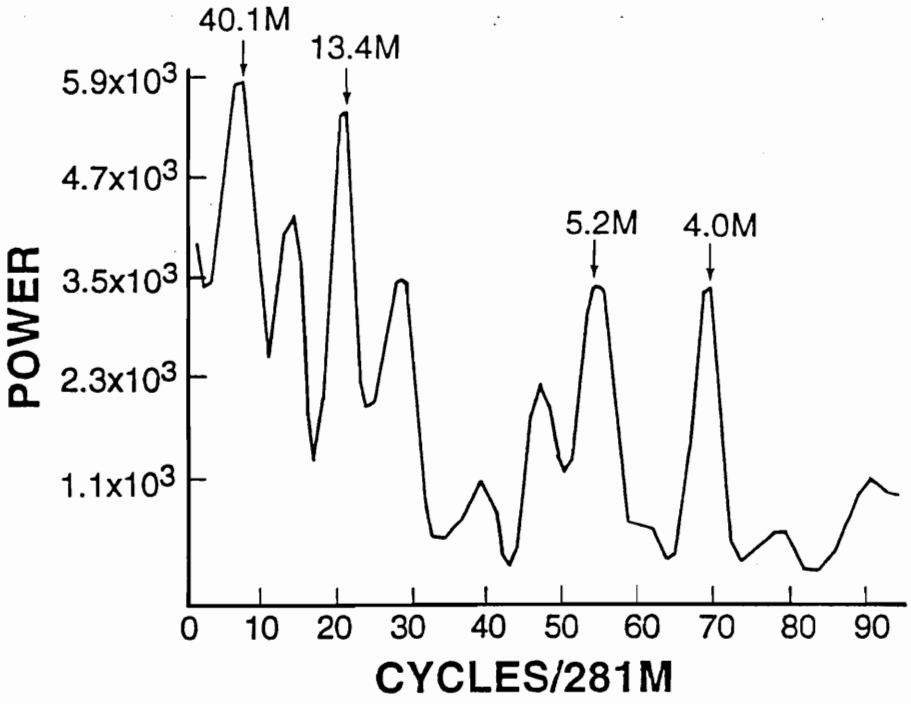

Fig. 2.16A. Walsh power spectrum of composite core sections coded as a two-state sequence of supra-intertidal and subtidal sediments. Modified from Schwarzacher and Haas (1986). Cycle wavelengths shown by numbers in meters above peaks.

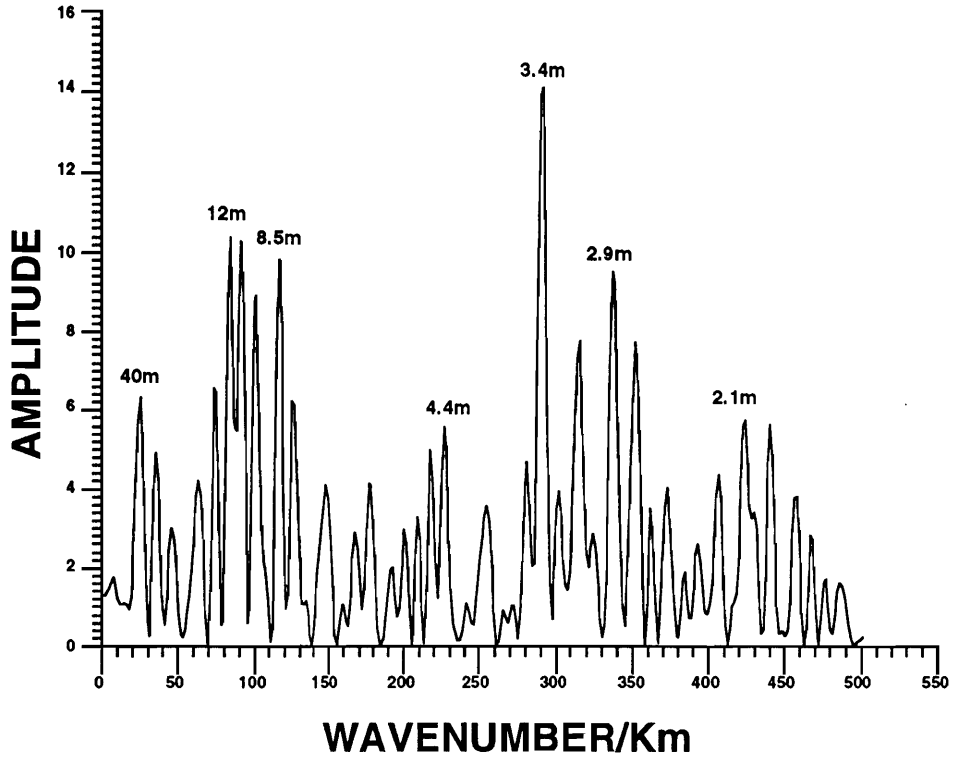

Fig. 2.16.B. Fast-Fourier spectral analysis of PO-89 using debased time-series based on water depth rank (subtidal, intertidal, supratidal/paleosol) vs. stratigraphic position. Sampling interval is 0.2 m. Wavelengths of cycles (in meters) shown by numbers above peaks. The 2 to 3 m peak may be precessional, the 4 m peak may be obliquity, the 12 m cycle may be 100 k.y. eccentricity and the 40 m peak may be 400 k.y. cycle.

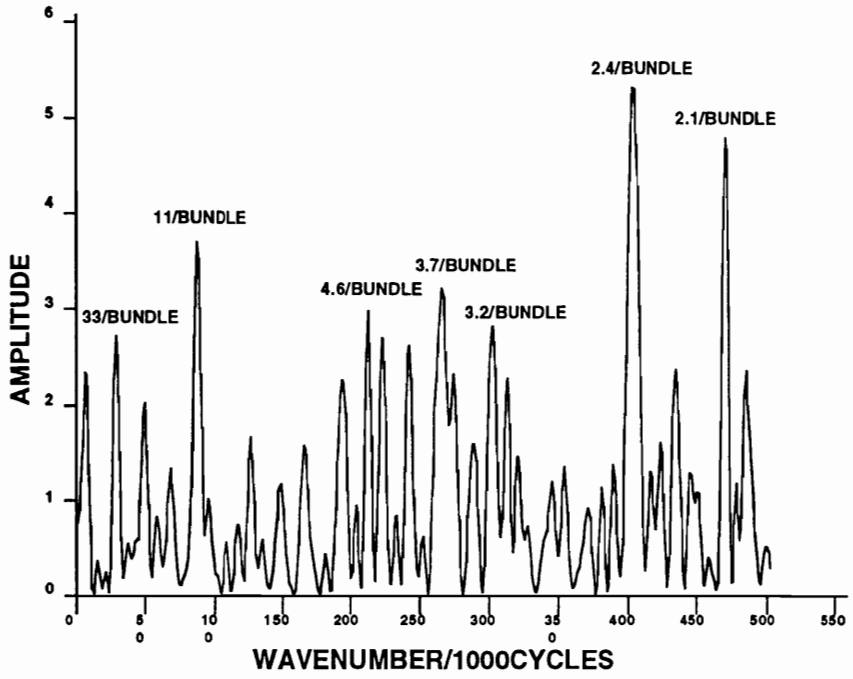

Fig. 2.16.C. Fast-Fourier spectral analysis of debased time-series from PO-89 constructed using cycle thickness vs cycle number (stratigraphic position). Because the meter-scale cycles are the sample interval, the precessional cycles are not evident. Main peaks are labeled according to the approximate number of cycles/bundle. The two cycles/bundle may be due to obliquity, the 3 to 5 cycles/bundle may be eccentricity, and the 11 or more cycles/bundle may be the 400 k.y. cycle.

Fourth- and Fifth-Order Cycle Bundling

Plots of cycle thickness vs. stratigraphic distance for the Triassic lake deposits by Olsen (1986, 1989) Olsen (1986) (Olsen et al. 1989) show a well defined bundling of cycles, strongly suggesting Milankovitch climate forcing, with the precessional cycles grouped into bundles of 5 cycles which in turn are bundled into larger units containing 20 cycles (Fig. 2.6). It is clear that the plot of Triassic marine cycle thicknesses vs. cycle number (Figs. 2.11, 2.12) does not show the clear Milankovitch bundling of the Late Triassic lake record. Although there is a suggestion of bundling of small-scale vs. large-scale cycles in the cycle thickness vs. cycle number plots of the Hungarian Triassic, any bundling of 20, 100, and 400 k.y. cycles is difficult to discern visually (Figs. 2.11, 2.12).

Possible Precessional and Obliquity Cycles: We already have presented evidence that the individual Hungarian Triassic cycles appear to be precessional cycles, given the age constraints for the succession. The individual meter-scale cycles are present on the spectral plots as a peak corresponding to 2-3 m cycle thickness (Fig. 2.16A, B) (Schwarzacher and Haas 1986, Schwarzacher 1993). The spectral data also show a possible obliquity signal (Schwarzacher and Haas 1986) in 5-7 m wavelength cycles, which are roughly twice the common 2-3 m basic cycles (Fig. 2.16A, B). Such a signal results in pairing of thick and thin cycles, which is evident in a few places on the Fischer plots, and on time series based on cycle thickness, along with their spectra (Figs. 11, 12). However, the presence of missing beats in the section would tend to complicate this signal.

Possible Eccentricity Cycles: Eccentricity cycles are evident in spectral data from the cores as a 12-14 m thick cycle bundle which is roughly 4-5 times the basic cycle thickness (Fig. 2.16A, B) (Schwarzacher and Haas 1986). Twenty-five to thirty-three of these bundles were reported in Fischer plots of the Po-89 core, assumed to represent approximately 3 m.y. duration based on the Harland time scale, thus these bundles probably are 100 k.y. cycles (Schwarzacher 1993). Spectra of our time series using water-depth rank vs. stratigraphic distance (Fig. 2.16B) or cycle thickness vs. cycle number strongly suggest incomplete 100 k.y. bundles of 3 and 4 cycles per bundle (Fig. 2.16C). Similar bundling of 3-6 cycles per bundle is evident on parts of our Fischer plots (Fig. 2.13). The best bundling on the Fischer plots (4-5 cycles per bundle), although poor when compared with the Middle Triassic examples of Goldhammer et al. (1990), appears

to be in Core of Po-89 of the Transitional Unit and Dachstein Limestone (Fig. 2.13). If the bundles are approximately 100 k.y. eccentricity cycles, then one or more precessional beats were missed or not recorded by the accumulating platform section. If the Fischer plots are approximately recording accommodation changes, then these bundles may reflect relative sea-level changes of 1-5 m/100 k.y.

The relatively poor development of 5:1 bundling in the Upper Triassic carbonates may in part be due to times when the platform was flooded too deeply for it to shallow to sea-level each precessional beat. This would have formed thick subtidal cycles that do not show meter-scale cyclicity (Goldhammer et al. 1990). However, most of the missing beats were probably associated with times of emergence when caliche-like caps in the Main Dolomite Unit and numerous red and green paleosols in the Transitional Unit and Dachstein Limestone were formed. The well developed, sometimes composite paleosols may even indicate multiple missed beats (Fig. 2.10). However, autocyclic processes or changes in subsidence rate can not be roled out as a cause of the poor bundling observed on the plots.

Possible Long-term Eccentricity Cycles: Spectral analysis shows a 40-50 m wavelength signal in some of the time series of Schwarzacher and Haas (1986) and our data (Fig. 2.16A, B); given that Schwarzacher and Haas (1986) considered the basic precessional cycle to be about 3 m, then these contain only about 75% of the required basic cycles (15 out of 20) if they represent 400 k.y. signals. A strong peak marking bundles of about 11 cycles is present in spectra of cycle thickness vs. cycle number from the lower part of Po-89 (Fig. 2.16 C), suggesting that about 40% of cycles are missing if these are 400 k.y. cycles here.

Some of the Fischer plots also show a very weak suggestion of a longer-wave length bundling that may be a 400 k.y. signal (Fig. 2.13). The number of cycles and the wavelength of these larger bundles is variable, and the signal shows up only in limited parts of the plots. Furthermore, these larger bundles rarely contain the requisite four 100 k.y. bundles. Thus if there is a 400 k.y. signal in the spectral data and Fischer plot data, it tends to be masked by the numerous missing beats evident in most of the section.

Complicating Effect of Differential Subsidence on Bundling: Even accepting that Milankovitch climate forcing was important in forming the cycle bundles, a tectonic influence on the development of poor bundling in the Late Triassic platform can not be roled out. This is because shallow-water carbonate cycles require a limited range of water depth in which to form, so beats may be missed as a result of increased subsidence

rates generating excess accommodation, which can not be filled within a single precessional beat. Differential subsidence on the platform is suggested by the fact that even the fourth-order cycles do not clearly correlate one-for-one between cores (Fig. 2.15). Differential subsidence between various parts of the platform may also have caused some of the non cyclic units (for example, in Zt-62; Fig. 2.15), which might reflect rapid subsidence such that a thick non cyclic interval developed, while on shallower, adjacent blocks of the platform a cyclic section was formed. Periods of decreased subsidence might cause more missing beats because of the decreased accommodation, especially if this was associated with a superimposed fourth-order fall, which would further decrease accommodation.

Third-Order Bundling and Comparison with Other Sea-Level Curves

The Fischer plots can be used to define long-term, 1-5 m.y. third-order changes in accommodation which correspond to depositional sequences (Fig. 2.14) (Read and Goldhammer 1988, Goldhammer et al. 1990). Unless it is known that the Fischer plots record all the systems tracts, we cannot place the timing of the sequence boundary with confidence. If all the beats were recorded on the platform, then the Fischer plots would be a good proxy for sea level, and the sequence boundaries would lie roughly halfway down the descending limb of the plot, marking maximum fall rate and minimum accommodation. Fischer plots, however, may not be a strict proxy for sea level, especially if lowstand systems tracts are not preserved in the platform cores but instead the sequence boundaries are marked by subtle, stacked disconformities. The sequence boundaries thus would be at the lowest points on the Fischer plots, and lowstand deposition would not be represented on the plots; this is how we have arbitrarily located the sequence boundaries or sea level cycles in Figure 2.14.

At least four third-order cycles (labeled sequences 1-4) are evident in the Upper Triassic cores (Figs. 2.14, 2.17). Sequence 1 lies within the Main Dolomite Formation in Core Ut-8. The lowstand between this and the next cycle occurred at a significant gap characterized by well developed subaerial facies (caliches). The stratigraphic position of this break suggests that it is in the Middle Norian. This third-order sea level cycle probably is at least 1 m.y. long judging by the number of cycles evident, and may correspond to the Lower-Middle Norian cycle on the Haq et al. (1987) curve.

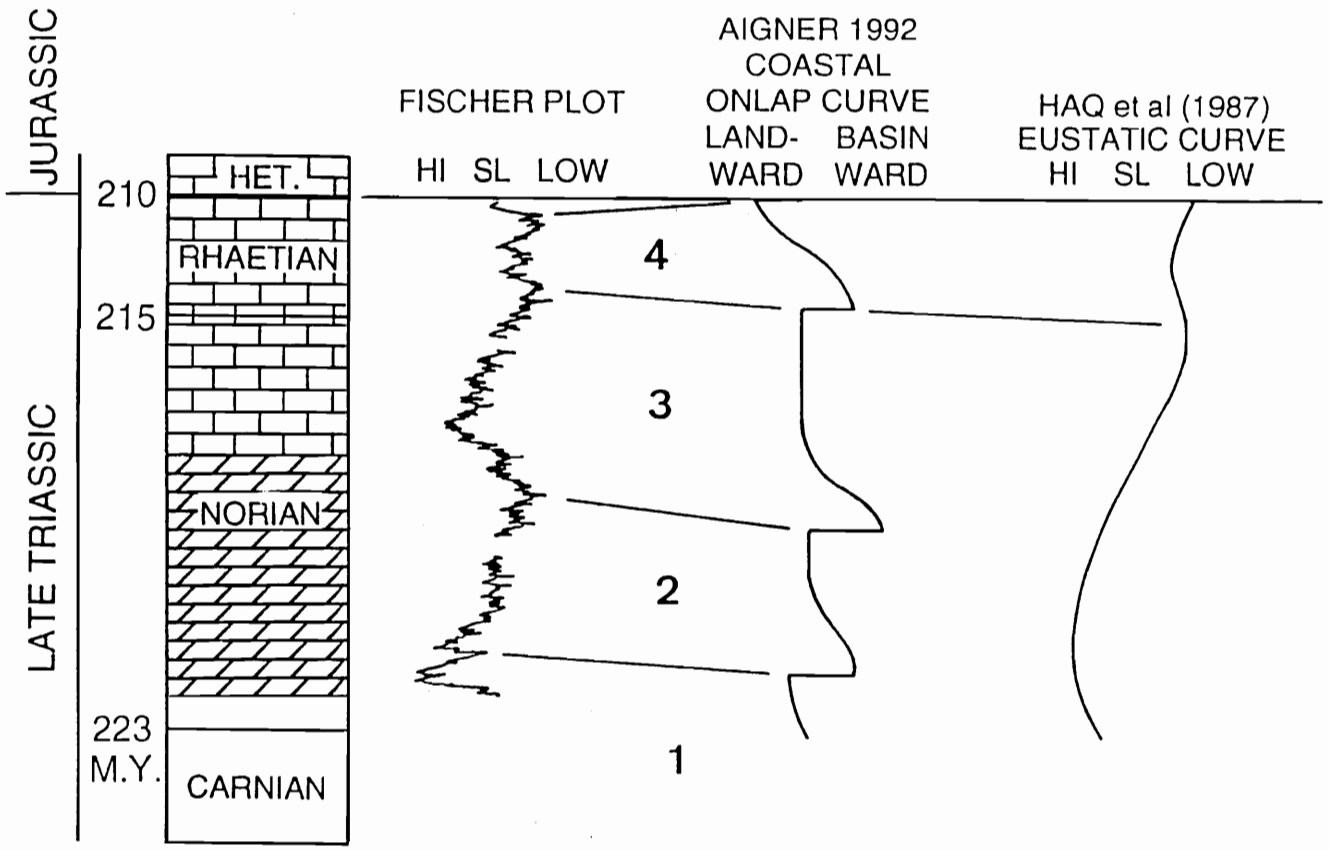

Fig. 2.17. Comparison of Fischer plot (Fig. 2.14) with coastal onlap curve of Aigner (1992) and Haq et al. eustatic curve (1987). Numbers 1 to 4 refer to the sequences on the Fischer plots. There is a reasonable correlation between the Fischer plot and Aigner's curve, but only a weak correlation to the simple Haq et al. curve.

Sequence 2 in core Ut-8 starts above the gap and, on the basis of the Fischer plot, has a rapid relative rise and a gradual fall, with the possible lowstand continuing into the lower part of the Core Po-89 plot. The top of the relative sea level cycle is marked by a subaerially condensed interval with anomalously thick paleosol layers (labeled "gap" in Figure 2.14) at the top of the Transitional Unit. By the number of cycles present, this cycle may be a minimum of 2.2 m.y. long. This boundary probably lies within the Middle to Upper Norian.

Sequence 3 is evident in the rest of Core Po-89 and on the Fischer plot, and it is marked by a long-term symmetrical rise and fall (Figs. 2.14, 2.17). This relative sea-level cycle is a minimum of 3 m.y. long, judging by the number of cycles present. Its upper boundary may correspond to the sequence boundary near the Norian-Rhaetian boundary on the Haq et al. (1987) curve.

Sequence 4 is evident in the plot of Core T-5 (Figs. 2.14, 2.17) representing the Rhaetian upper Dachstein Limestone. Essentially the highstand consists of two smaller peaks, which can be seen in Zt-62 and T-5 (Figs. 2.14, 2.15). In T-5, the upper sequence boundary is drawn at a condensed interval about 20 m beneath the Triassic/Jurassic boundary. This may correspond to the uppermost Rhaetian sequence boundary on the Haq et al. (1987) curve. It is followed on the Fischer plot by a relative rise of an incompletely preserved sequence at the end of the plots.

These four relative sea level cycles defined by the Fischer plots appear to correlate with the coastal onlap plot of Aigner (1992) from the continental Triassic of Germany. However, the more simplistic Triassic sea-level curve of Haq et al. (1987) shows only one cycle for the lower three cycles, but has the uppermost cycle correlating with our topmost cycle. Minimum changes in accommodation for the third-order cycles estimated from the Fischer plots appear to be about 20-30 m per third order-cycle, or approximately 10-15 m/m.y.

Correlation Using Fischer Plots and the Problem of Missing Beats

Fischer plots can provide valuable information on fine-scale correlation between cyclic sections in which biostratigraphic correlation is limited (Read and Goldhammer 1988, Osleger and Read 1991, Goldhammer et al. 1993). Attempts to correlate the Fischer plots of the Hungarian Triassic sections were hampered by non-overlapping

cores, subaerial condensation, and paleosol formation at certain horizons, all of which tend to make direct correlation of the plots on the basis of similar shape difficult. Most of the Fischer plots were constructed assuming that all sea-level fluctuations were recorded in the platform stratigraphy, thus equal duration could be assigned to each cycle (Figs. 2.13-2.15). However, because not all beats may be recorded in the platform stratigraphy, equal time cannot be assigned to all cycles, since the missing beats imply that the data are discontinuous.

To determine what effect inserting missing beats into three Fischer plots from roughly correlative sections would have on their shape, we constructed another set of plots in which missing beats were inserted on the basis of the rank of paleosol formation on each cycle, on the assumption that the plots should be bundled into packages of five, and that large stratigraphic gaps are marked by highly developed paleosol zones (Fig. 2.18). The stratigraphic position of the Fischer plots of To facilitate plotting, each missing beat was assigned a value of 0.1 m (the limit of the plotter). Mean cycle thickness was then recalculated before running the new plots. These reinserted (missing) beats result in a line falling to the right in the position of the condensed interval, which expands the Fischer plots along the cycle number (or approximate time) axis (Fig. 2.18). This experiment is valuable but somewhat subjective, because the number and location of missing beats assigned are difficult to justify because (1) there is not a quantitative relationship between soil thickness and degree of maturity and the number of missing beats, (2) the location of stratigraphic gaps may not be manifested by obvious intense soil development or condensed intervals, and (3) the actual high frequency sea-level curve that generated the Late Triassic cycles, even if it is Milankovitch-driven, can not be known for certain. Given that the plot of Core Zt-62 contains a major non cyclic interval which we plot as a horizontal line, the unmodified Fischer plots of this core and Core T-5 show a reasonable correlation with two major lowstands (shown by heavy lines in Figure 2.15) and an intervening highstand; this highstand is disrupted by a small lowstand in its middle part. Modification of the Fischer plots by inserting missing beats gave mixed results (Fig. 2.18). The plots show a greatly worsened correlation in the lower part. However, the correlative upper parts of the three plots show a slightly improved correlation at the third-order scale, and to some extent, at the fourth-order scale.

In summary, the attempted modification of the Fischer plots using inserted missing beats did not increase the similarity between the shapes of the Fischer plots in a

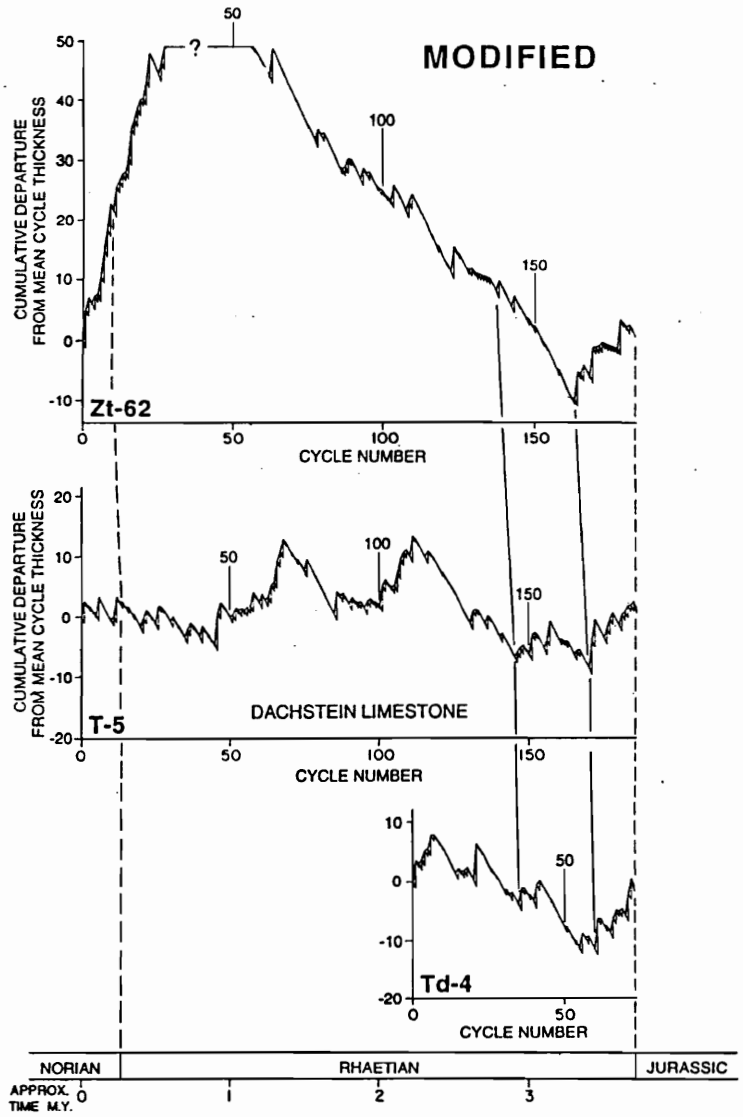

Fig. 2.18. Modification of Fischer plots shown in Figure 2.15, by inserting assumed missing beats into the data sets. Missing beats were inserted on the basis of rank of paleosols plus the inferred 5:1 bundling if section was complete. Note that only the upper part of the plot is improved, while the lower part shows a worsened correlation. Cores T-5, Td-4, and Zt-63 were tied together using the Triassic-Jurassic boundary.

predictable manner. However, it would seem to be worth trying with other data sets that might be more amenable to this approach if a better way is found to assign missing beats to the paleosols.

TRIASSIC LAKE RECORD AND MARINE RECORD COMPARED

The stratigraphy of the continental lakes (Olsen 1986, Olsen et al. 1989, Olsen et al. 1993) has a clear record of Milankovitch climate change with strong precessional (~ 20 k.y.) and short-term and long-term eccentricity (~ 100 and 400 k.y.) cycles as well as third-order cycles of roughly 2 m.y. duration (Fig. 2.6). The Alpine Upper Triassic deep marine, off-platform stratigraphy, in contrast, shows a 20 k.y. and 100 k.y. signal, and possibly a weak obliquity signal, but it does not appear to show a 400 k.y. eccentricity signal (Reijmer and Everaars 1991). Similarly, the shallow platform record from the Hungarian marine Triassic appears to have an incompletely preserved record of precession, obliquity, and short-term eccentricity but also shows a suggestion of a 400 k.y. signal (Schwarzacher and Haas 1986, Schwarzacher 1993). The poor Milankovitch record of the Hungarian Upper Triassic platform appears to relate to the abundance of missing beats, when the precessionally driven sea level fluctuations did not flood the platform. Missing beats are evidenced by the numerous paleosols, caliche-like fabrics, and early leaching of aragonitic shells. Missing beats also may be reflected in scarcity of bundles with 5 precessional cycles to 1 eccentricity cycle and by the spectra that lack simple 5:1 ratios between the fundamental precessional cycles and larger-scale bundles. It also may be evident in the incomplete larger bundles that may represent 400 k.y., which have far less than 20 cycles per bundle and rarely contain the four short-term eccentricity bundles.

The manner in which Milankovitch-driven climate changes that affected the Late Triassic lakes were translated into eustatic sea level changes is not clear given the relatively warm Late Triassic global climate. Perhaps fluctuations in monsoon intensity, coupled with alternate filling and emptying of lake basins and associated ground-water systems, in conjunction with small ephemeral ice caps and Alpine glaciers, were responsible (Jacobs and Sahagian 1993). Perhaps the Milankovitch climate changes are translated very imperfectly into resultant sea-level changes. Whatever the cause, our data

demonstrate that the cyclic stratigraphic record of the large Late Triassic platform in Hungary, although influenced by Milankovitch eustasy, is highly imperfect.

This contrasts with the highly cyclic record observed by Goldhammer et al. (1990) in parts of the Middle Triassic Latemar platform, which may have been too small (5 km wide) and wave-swept to periodically shallow to the level of the precessional highstands and develop extensive tidal-flats. Instead, the cycles resulted in part from unfilled accommodation and incomplete shallowing within the subtidal zone, as well as superimposition of vadose fabrics on subtidal facies when sea level fell below the platform top. The unfilled accommodation allowed flooding of the platform during each precessional highstand so that, given favorable long-term accommodation, the platform stratigraphy preserved a clear Milankovitch signal with 5:1 bundling of cycles. When accommodation was larger or smaller, missed beats appear to have disrupted the Latemar cyclic record (Goldhammer et al. 1990).

For the Norian Dolomia Principale of the Southern Alps, Goldhammer et al. (1990) suggested that lack of simple 5:1 bundling was related to "missed beats" similar to those we propose for the Late Triassic Hungarian platform. They suggested that bundles of cycles capped by teepee zones were the result of an average of two missed beats per fourth-order megacycle but that the thick cycles capped by red soil-like breccias were "super condensed megacycles" in which perhaps only one of the fifth order beats flooded the platform.

The paucity of simple 5:1 bundling and lack of clearly thinning-up megacycles in the Upper Triassic Austrian Dachstein Limestone led Goldhammer et al. (1990) to postulate that cycle development here was largely controlled by short-term variations in subsidence rate rather than Milankovitch eustasy. However, that Milankovitch-driven composite eustasy was indeed an important influence on cycle development on the Austrian Dachstein platform is indicated by the evidence for a Milankovitch signal in time-equivalent off-shelf facies, whose composition was controlled by periodic submergence and emergence of the platform top (Reijmer and Everaars 1991). It is also supported by our interpretation that the time-equivalent and once nearby, Hungarian Late Triassic platform also is a product of imperfectly recorded Milankovitch eustasy. It is difficult to rule out the effects of differential subsidence or uplift on the formation of the cyclic stratigraphy of these platforms without having exactly time-equivalent data from other platforms. In fact, the imperfect correlation between the Fischer plots spanning the same

time interval on the Hungarian platform might suggest that differential subsidence has played a role in forming these Alpine platforms and those in Hungary.

Large, low-energy carbonate platforms that developed under global greenhouse conditions typified by low-amplitude, precessionally dominated sea level fluctuations probably have cyclic stratigraphies reflecting numerous missed beats. This is because sedimentation tends to fill available accommodation during each precessional highstand, resulting in cycles that are capped by tidal-flat facies. Because deposition of the next cycle depends on new accommodation being made for each cycle, superimposed fourth-order falls tend to cause missing beats in the stratigraphy. Small atoll-like platforms are composed of cycles that rarely built to tide level during precessional highstands leaving unfilled accommodation. Consequently, even on fourth order falls on such small platforms, this unfilled accommodation helps capture many of the precessional sea level beats.

Given the poor preservation of Milankovitch sea level changes on large carbonate platforms that develop under global greenhouse conditions, the search for simple, 1, 2, 5, and 20:1 ratios of carbonate cycles as the defining test of Milankovitch orbital forcing may be misleading. Indeed, such criteria may be more applicable to stratigraphies of small platforms and lakes. Furthermore, simple ratio tests of the record of Milankovitch cycles also could be misleading given the added complexity of Milankovitch-driven climate and sea-level changes and the effects of subtle changes in subsidence rates. As pointed out by Sander (1936), Schwarzacher (1954), and Goldhammer et al.(1990), a rhythmic process may leave a poorly "rhythmic" record. This may be true for large carbonate platforms that are aggraded to sea level throughout much of their history.

CONCLUSIONS

(1) Carbonate cycles in the Hungarian Upper Triassic formed in response to precessional sea-level fluctuations of roughly 20 k.y. duration. They contain transgressive laminites (as postulated by Fischer (1964) for the classic Lofer cycles), regressive laminites (suggested to be the major type by Goldhammer et al. (1993), and also symmetrical cycles with both transgressive and regressive laminites. Regressive laminites are easily separated from overlying transgressive laminites where paleosols are

present, but distinction is more difficult if paleosols are absent. Caliche-like fabrics (common in the Main Dolomite) and red and green paleosols (Dachstein Limestone) mark periods when the platform was exposed.

(2) Milankovitch climate changes were important in the Late Triassic, as shown by the lake record of North American rift basins, which show orbital forcing with quasi-periods of 20, 40(?), 100, and 400 k.y. (Olsen 1986). This orbital forcing was also important in the marine realm, as suggested by the record of off-shelf periplatform facies from the Alps. On the large Hungarian platform, however, such a Milankovitch signal, although present, is highly imperfect. The platform does not show the clear 5:1 Milankovitch bundling typical of the small Middle Triassic Latemar platform. The poor Milankovitch record on the large, highly aggraded Hungarian platform is largely due to numerous "missed beats" (evidenced by well developed caliche and vadose fabrics, red and green, simple and composite paleosols), resulting from precessionally driven sea level fluctuations not have flooded the platform. The cycle bundles on Fischer plots and spectra of time series commonly have fewer than the typical 5:1 and 20:1 ratios expected for 100 and 400 k.y. megacycles .

(3) Third-order relative sea level changes defined by the Fischer plots of the Hungarian carbonates are similar to those of Aigner and Bachmann (1992) and to a lesser extent to those of Haq et al. (1987). Condensed, multiple paleosol horizons and non cyclic subtidal intervals are a major problem for the Fischer plot technique. Qualitative ranking of the inferred duration of paleosol horizons was used to attempt to overcome the problem of missing beats and to "stretch" the plots in time. These modifications to the plots gave mixed results; they increased the similarity between some parts of correlative plots, but for other parts they made them more dissimilar. To be successful, such a technique requires a better way of quantifying duration of the missed beats, which is a difficult problem.

REFERENCES CITED

Aigner, T., and Bachmann, G.H., 1992, Sequence-stratigraphic framework of the German Triassic: Sedimentary Geology, v. 80, p. 115-135.

Albertiana, 1992, Albertiana, Cover Table, v. 10.

Balla, Z., 1988, Clockwise paleomagnetic rotations in the Alps in the light of the structural pattern of the Transdanubian Range (Hungary): Tectonophysics, v. 145, p. 277-292.

Bosselini, A., and Hardie, L.A., 1985, Facies e cicli Dolomia Principale delle Alpi Venete: Mem. Soc. Geol. It., v. 30, p. 245-266.

Fischer, A.G., 1964, The Lofer cyclothems of the Alpine Triassic, *in* Merriam, D.F., ed., Symposium on Cyclic Sedimentation: Lawrence, KS, Kansas Geological Survey Bulletin 169, p. 107-149.

Fischer, A.G., 1975, Tidal deposits, Dachstein Limestone of the North-Alpine Triassic, *in* Ginsburg, R.N., ed., Tidal Deposits: A Casebook of Recent Examples and Fossil Counterparts: New York, Springer-Verlag, p. 235-242.

Frakes, L.A., Francis, J.E., and Syktus, J.I., 1992, Climate modes of the Phanerozoic. The history of the Earth's climate over the past 600 million years, Cambridge University Press, 274 p.

Fulop, J., 1975, The Mesozoic basement horst blocks of Tata: Geologica Hungarica, v. 16, p. 1-228.

Goldhammer, R.K., Dunn, P.A., and Hardie, L.A., 1987, High frequency glacio-eustatic sealevel oscillations with Milankovitch characteristics recorded in Middle Triassic platform carbonates in northern Italy: American Journal of Science, v. 287, p. 853-892.

Goldhammer, R.K., Dunn, P.A., and Hardie, L.A., 1990, Depositional cycles, composite sea-level changes, cycle stacking patterns, and the hierarchy of stratigraphic forcing: examples from Alpine Triassic platform carbonates: Geological Society of America Bulletin, v. 102, p. 535-562.

Goldhammer, R.K., Lehmann, P.J., and Dunn, P.A., 1993, Origin of high-frequency platform carbonate cycles and third-order sequences (Lower Ordovician El Paso Gp, west Texas): constraints from outcrop data and stratigraphic modeling: Journal of Sedimentary Petrology, v. 63, p. 318-359.

Haas, J., 1982, Facies analysis of the cyclic Dachstein Limestone Formation (Upper Triassic) in the Bakony Mountains, Hungary: Facies, v. 6, p. 75-84.

Haas, J., 1988, Upper Triassic carbonate platform evolution in the Transdanubian Mid-mountains: Acta Geologica Hungarica, v. 31, p. 299-312.

Haas, J., 1991, Basic model for Lofer cycles, *in* Einsele, Ricken, and Seilacher, eds., Cycles and Events in Stratigraphy: Berlin, Springer-Verlag, p. 722-732.

Haas, J., Csaszar, G., Kovacs, S., and Voros, A., 1990, Evolution of the western part of the Tethys as reflected by the geological formations Hungary: Acta Geod. Geoph. Mont. Hung., v. 25, p. 325-344.

Haas, J., and Dobosi, K., 1982, Felso-Triasz ciklusos karbonatos kozetek vizsgalata bakonyi alapszelvenyeken: Magyar Allami Foldtani Intezet Evi Jelentese 1980-rol, p. 135-168.

Haq, B.U., Hardenbol, J., and Vail, P.R., 1987, Chronology of fluctuating sea levels since the Triassic: Science, v. 235, p. 1156-1167.

Harland, W.B., Armstrong, R.L., Cox, A.V., Craig, L.E., Smith, A.G., and Smith, D.G., 1990, A Geologic Time Scale, 1989: Cambridge, U.K., Cambridge University Press, 263 p.

Hinnov, L.A., and Goldhammer, R.K., 1991, Spectral analysis of the Middle Triassic Latemar Limestone: Journal of Sedimentary Petrology, v. 61, p. 1173-1193.

Jacobs, D.K., and Sahagian, D.L., 1993, Climate-induced fluctuations in sea level during non-glacial times: Nature, v. 361, p. 710-712.

James, N.P., 1972, Holocene and Pleistocene calcareous crust (caliche) profiles: criteria for subaerial exposure: Journal of Sedimentary Petrology, v. 42, p. 817-836.

Kazmer, M., and Kovacs, S., 1985, Triassic and Jurassic oceanic/paraoceanic belts in the Carpathian-Pannonian region and its surroundings, *in* Sengor, A.M.C., ed., Tectonic evolution of the Tethyan region: Dordrecht, London,, Kluwer Academic Publishers, p. 698.

Koerschner, W.F., III, and Read, J.F., 1989, Field and modelling studies of Cambrian carbonate cycles, Virginia Appalachians: Journal of Sedimentary Petrology, v. 59, p. 654-687.

Kominz, M.A., Beavan, J., and McManus, J., 1991, Are cyclic sediments periodic? Gamma analysis and spectral analysis of Newark Supergroup lacustrine strata, *in* Franseen, E.K., Watney, W.L., Kendall, C.G., and Ross, W., eds., Sedimentary

modeling: Computer Simulations and Methods for Improved Parameter Definitio, Vol. 233: Kansas Geological Survay Bulletin, p. 329-334.

Kovacs, S., 1982, Problems of the "Pannonian Median Massif" and the distribution of Late-Paleozoic - Early Mesozoic isopic zones: Geologische Rundschau, v. 71, p. 617-648.

Menning, M., 1990, A new scheme for the Permian and Triassic succession of Central Europe: Permophiles, v. 16, p. 1-11.

Olsen, P., 1986, A 40-million-year lake record of Early Mesozoic orbital forcing: Science, v. 234, p. 842-848.

Olsen, P.E., Kent, D.V., and Cornet, B., 1993, Early Mesozoic lacustrine record of cyclical climate change from core and outcrops of the Newark Basin: SEPM, p. 35.

Olsen, P.E., Schlische, R.W., and Gore, P.J.W., 1989, Tectonic, depositional and paleoecological history of Early Mesozoic rift bains, Eastern North America: International Geological Congress, p. 174.

Osleger, D.A., and Read, J.F., 1991, Relation of eustasy to stacking patterns of meter-scale carbonate cycles, Late Cambrian, U. S. A.: Journal of Sedimentary Petrology, v. 61, p. 1225-1252.

Read, J.F., 1974, Calcrete deposits and Quaternary sediments, Edel Province, Western Australia, *in* Logan, B.W., Read, J.F., Hagan, G.M., Hoffman, P., Brown, R.G., Woods, P.J., and Gebelein, C.D., eds., Evolution and Diagenesis of Quaternary Carbonate Sequences, Shark Bay, Western Australia: Tulsa, OK, American Association of Petroleum Geologists Memoir 22, p. 250-282.

Read, J.F., and Goldhammer, R.K., 1988, Use of Fischer plots to define third-order sea-level curves in Ordovician peritidal cyclic carbonates, Appalachians: Geology, v. 16, p. 895-899.

Reijmer, J.J., Sprenger, A., Ten Kate, W.G.H.Z., Schlager, W., and Krystyn, L., 1993, Periodicites in the composition of the Late Triassic calciturbidites (Eastern Alps, Austria), *in* Boer, P.L., and Smith, D.G., eds., Orbital Forcing and Cyclic Sequences, Vol. Special Publication of IAS 19.: Oxford, Blackwell Scientific Publications, p. 323-345.

Reijmer, J.J.G., and Everaars, J.S.L., 1991, Carbonate platform facies reflected in carbonate basin facies (Triassic, Northern Calcareous Alps, Austria): Facies, v. 25, p. 253-278.

Rossinsky, V., Jr., Wanless, H.R., and Swart, P.K., 1992, Penetrative calcretes and their stratigraphic implications: GEOLOGY, v. 20, p. 331-334.

Sadler, P.M., Osleger, D.A., and Montañez, I.P., 1993, On the labeling, length and objective basis of Fischer plots: Journal of Sedimentary Petrology, v. 63, p. 360-368.

Sander, B., 1936, Beiträge zur Kenntnis der Ablagerungsgefüge (rhythmische Kalke und Dolomite aus der Trias): Tschermaks Mineralogische und Petrographische Mitteilungen, v. 48, p. 27-139.

Schwarzacher, W., 1954, Die Grossrhythmik des Dachstein Kalkes von Lofer: Tschermaks Mineralogische und Petrographische Mitteilungen, v. 4, p. 44-54.

Schwarzacher, W., 1993, Cyclostratigraphy and the Milankovitch Theory, v. 52: London, Elsevier, 225 p.

Schwarzacher, W., and Haas, J., 1986, Comparative statistical analysis of some Hungarian and Austrian Upper Triassic peritidal carbonate sequences: Acta Geologica Hungarica, v. 29, p. 175-196.

Sengor, A.M.C., 1985, The story of Tethys: How many wives did Okeanus have?: Episodes, v. 8, p. 3-12.

Tollman, A., 1987, Neue Wege in der Ostalpengeologie und die Beziehungen zum Ostmediterran: Mitteilungen der Österreichischen Geologischen Gesellschaft, v. 80, p. 47-113.

Van Houten, F.B., 1962, Cyclic sedimentation and the origin of analcime-rich Upper Triassic Lockatong, west-central New Jersey and adjacent Pennsylvania: American Journal of Science, v. 260, p. 561-576.

Van Houten, F.B., 1964, Cyclic lacustrine sedimentation, Upper Triassic Lockatong Formation, central New Jersey and adjacent Pennsylvania, *in* Merriam, D.F., ed., Symposium on Cyclic Sedimentation: Lawrence, KS, Kansas Geological Survey Bulletin 169, p. 495-531.

Chapter 3: Climate controlled early dolomite, late Triassic cyclic platform carbonates, Hungary

ABSTRACT

The 3 km thick Late Triassic Hungarian carbonate platform has a completely dolomitized lower part and a limestone-dominated upper part. The platform is made up of meter-scale, probably precessional (~20 k.y.) carbonate cycles. Cycles are completely dolomitized and capped by caliche laminites and pisolites in the lower platform, whereas in the upper platform, dolomite is confined to laminite caps, and cycles are bounded by clayey paleosols. The geochemistry of the abundant marine calcite cements on the platform provide data on Triassic ocean composition as a baseline for the dolomite studies.

Most of the dolomitization occurred early, in tidal flat settings during each high frequency cycle. Subtidal dolomites are slightly coarser grained, low in Fe^{2+} and Mn^{2+} and they have the heaviest $\delta^{18}O$ signature, indicating more evaporative but oxidizing brines sourced from supratidal flats. Intertidal-supratidal dolomites are fine grained, may be Fe^{2+} and/or Mn^{2+} rich and slightly enriched in $\delta^{18}O$ compared to the marine calcite cement, and formed from marine water, that was weakly to moderately reducing. Dachstein paleosols have light $\delta^{18}O$ and $\delta^{13}C$ reflecting meteoric soil waters. Repeated emergence stabilized the dolomites to low Sr^{2+} and Na^{+} types similar to Cenozoic platform dolomites. In contrast to these early cyclic dolomites, coarse-grained platform margin dolomites with very low Mn^{2+}, Fe^{2+} and light $\delta^{18}O$ signatures were formed by thermally driven, warm oxidizing marine water associated with Jurassic rifting of the Pennini Ocean (Neo-Tethys).

Early dolomitization of cycles was controlled by high frequency sea-level changes, but the overall vertical distribution of early dolomite on the platform does not reflect long term eustasy. Rather the intense dolomitization of the lower platform reflects a semi-arid, hot subtropical setting and megamonsoonal climate. Global cooling and increased humidity toward the latest Triassic and Early Jurassic inhibited pervasive early dolomitization, leaving the upper platform little dolomitized.

INTRODUCTION

The large, Late Triassic carbonate platform (2 to 3 km thick), of the Transdanubian Range, Hungary is highly cyclic and intensely dolomitized in its lower part but little dolomitized in its upper part, a pattern reminiscent of many Cenozoic carbonate platforms. Dolomitization of Cenozoic platforms has been attributed to a reflux of hypersaline or slightly evaporative marine fluids (De Groot 1973; McKenzie et al. 1980; Simms 1984; Mazzullo et al. 1987; Whitaker and Smart 1990; McKenzie 1991) mixing zone dolomitization (Ward and Halley 1985; Humphrey 1988) and dolomitization by normal marine water, where fluid circulation is driven by tidal pumping (Carballo et al. 1987; Mazzullo et al. 1987), by topography driven flow (Vahrenkamp and Swart 1991) and by thermal convection (Kohout et al. 1977; Simms 1984; Saller 1984; Hein et al. 1992). The understanding of dolomitization of Cenozoic platforms has been hampered by the complex sea level and climate history involving high amplitude, high frequency sea level fluctuations driven by glacio-eustasy and continental glaciation in the late Cenozoic (Vahrenkamp and Swart 1991).

In contrast to Cenozoic platforms, the Hungarian Triassic platform developed under global greenhouse conditions and high frequency but low amplitude sea level fluctuations likely driven by precessional orbital forcing (Balog et al. 1995). The Triassic platform was studied to determine to what extent the dolomitization was early and related to high frequency precessionally-driven sea level changes, or to longer term 2nd- and 3rd-order eustasy, or was influenced by climate change associated with plate motion, the Pangean mega-monsoon, global temperature and humidity. We also assess the importance of early burial dolomitization associated with warm marine pore fluids. The geochemistry suggests that the platform has undergone only limited deep burial diagenesis, and because it preserves much of the early diagenetic signatures of the marine calcite cements and dolomites, should provide an important data set to better understand regional platform dolomitization.

Our study suggests that platform dolomitization was strongly controlled by widespread aridity during the Late Triassic under a mega-monsoonal climate, and that early dolomitization decreased rapidly as the climate cooled and became wetter through time. Also, the study shows that the dolomites were stabilized rapidly, even under low

amplitude greenhouse sea level fluctuations, so that they now resemble many Cenozoic platform dolomites.

STRUCTURAL AND STRATIGRAPHIC SETTING

The Late Triassic platform carbonates of the Transdanubian Range were part of the southwestern passive margin of the Tethys seaway (Kovacs 1982; Kazmer and Kovacs 1985; Tollman 1987). The carbonates were situated between the Northern and Southern Alps, and moved eastward to their present position during the Paleogene (Kazmer and Kovacs 1985; Balla 1988; Haas et al. 1990) (Fig. 3.1). They occur in a single, fault-bounded megatectonic unit in the central Pannonian Basin (Fig. 3.2). Inside this megatectonic unit, the approximately 200 km long platform segment consists of a series of fault blocks. The platform margin is exposed in the Vac area on the eastern side of the Danube River (Fig. 3.2).

The Late Triassic carbonate platform was an aggraded, flat-topped platform. The "lower platform unit" is the Main Dolomite Formation (600-1500 m thick, Norian-Rhaetian age), which is Upper Carnian in the east but its top becomes younger to the west (Lower-Middle Norian). It consists of completely dolomitized meter-scale carbonate cycles. The Main Dolomite is overlain by the "upper platform" Dachstein Limestone (up to 1200 m thick), which youngs westward before passing laterally into dark gray argillaceous intrashelf basin facies (Kossen Formation). The Dachstein Limestone is a cyclic succession of subtidal limestone, laminated tidal flat limestone or dolomitic limestone, and reddish or greenish paleosols that cap cycles. The Dachstein Limestone contains both totally dolomitized cycles and limestone cycles in its lower part (Transitional Unit), and in its upper part limestone cycles in which only cycle caps are dolomitized. The shallow water platform was faulted and drowned in the Early Jurassic, during initial rifting of the Pennini Ocean (Neo-Tethys) (Tollman 1987; Kazmer and Kovacs 1985). From the Mid-Cretaceous onward, the region underwent nappe formation and large scale strike-slip transport of the platform, which moved it to its present position.

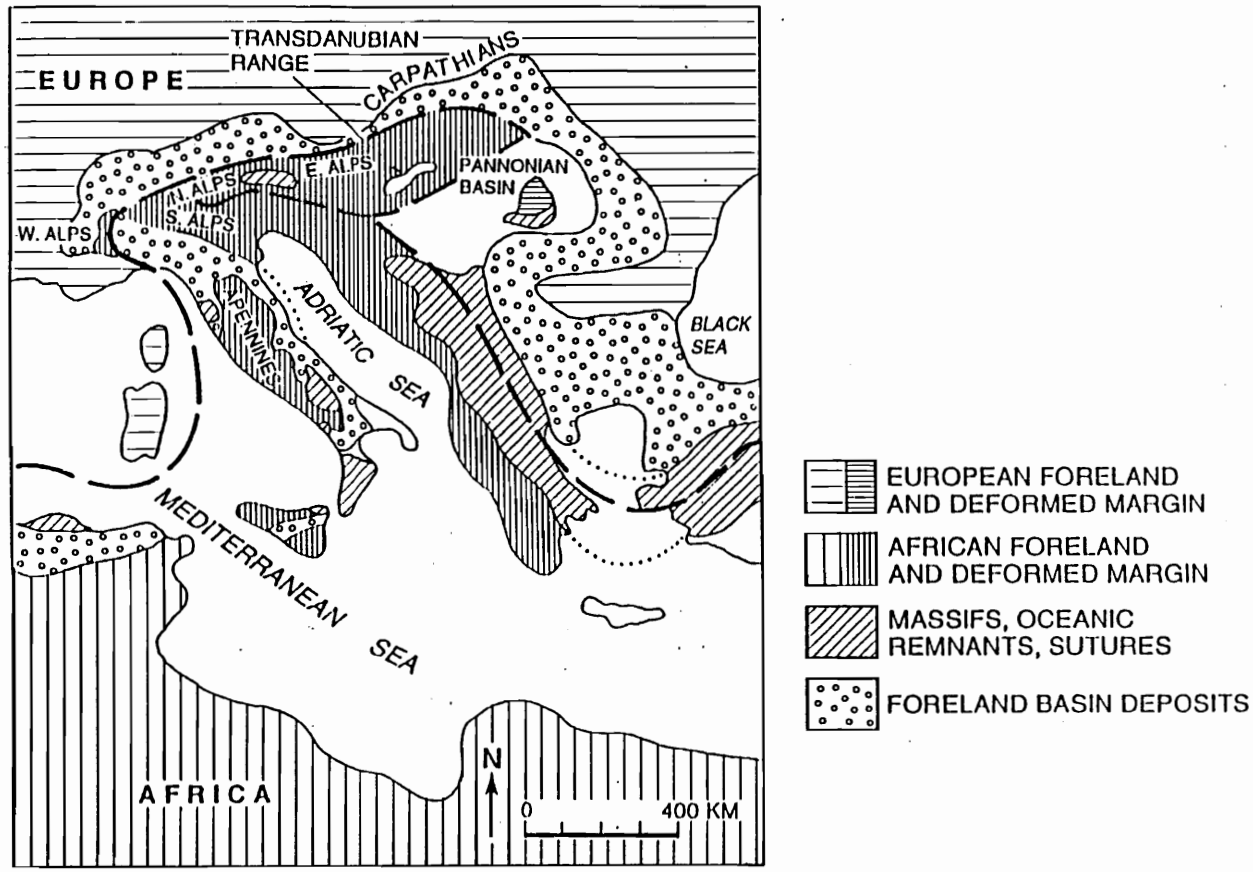

Fig. 3.1. Regional location map of the Triassic carbonates of the Transdanubian Range (arrowed), Hungary. Major lithotectonic blocks are bounded by heavy dashed lines. The Transdanubian carbonates were transported by strike-slip faulting from their original position between the Northern and Southern Alps.

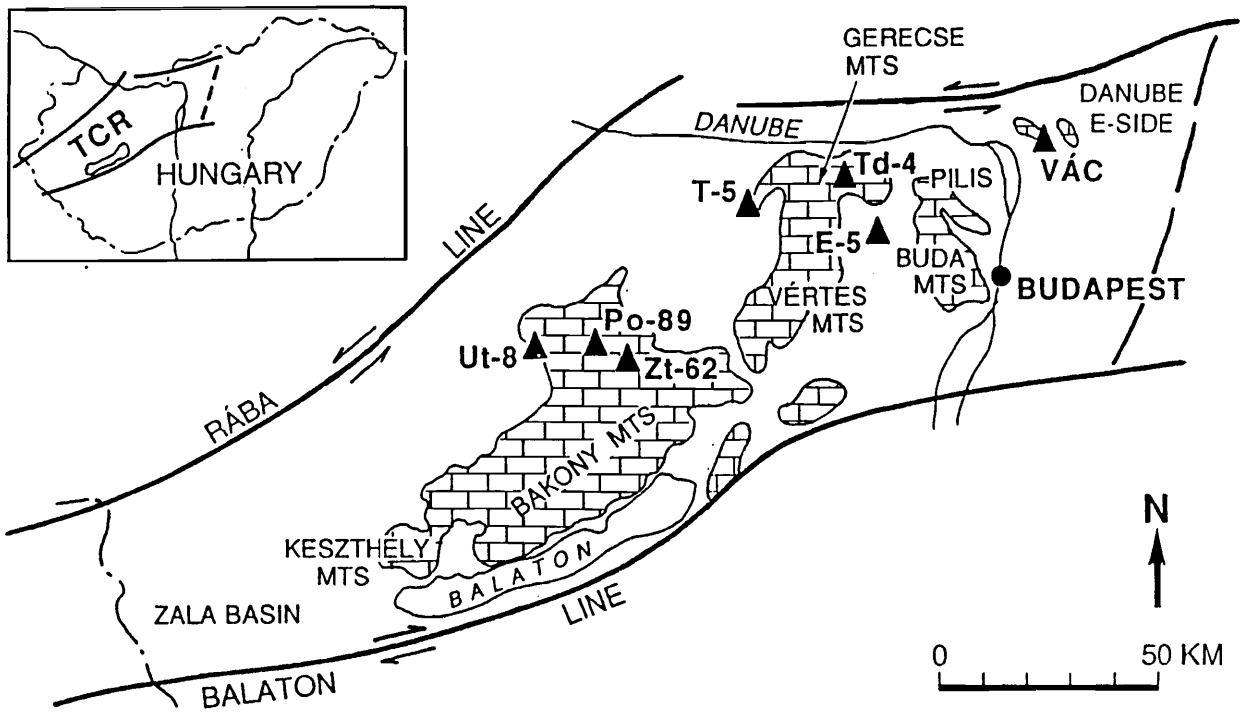

Fig. 3.2. Location map , Transdanubian Range, with inset showing regional location within Hungary. Triassic carbonates are located in a single megatectonic unit bounded by the Raba Line and Balaton Line; on inset map these are shown as heavy lines bounding the Transdanubian Range (TR). Core locations are shown by solid triangles; VAC is from Vac area; Td-4 is Tardos 4; E-5 is Epol 5; T-5 is Tata 5; Zt-62 is Zirc-62; Po-89 is Porva-89; Ut-8 is Ugod-8.

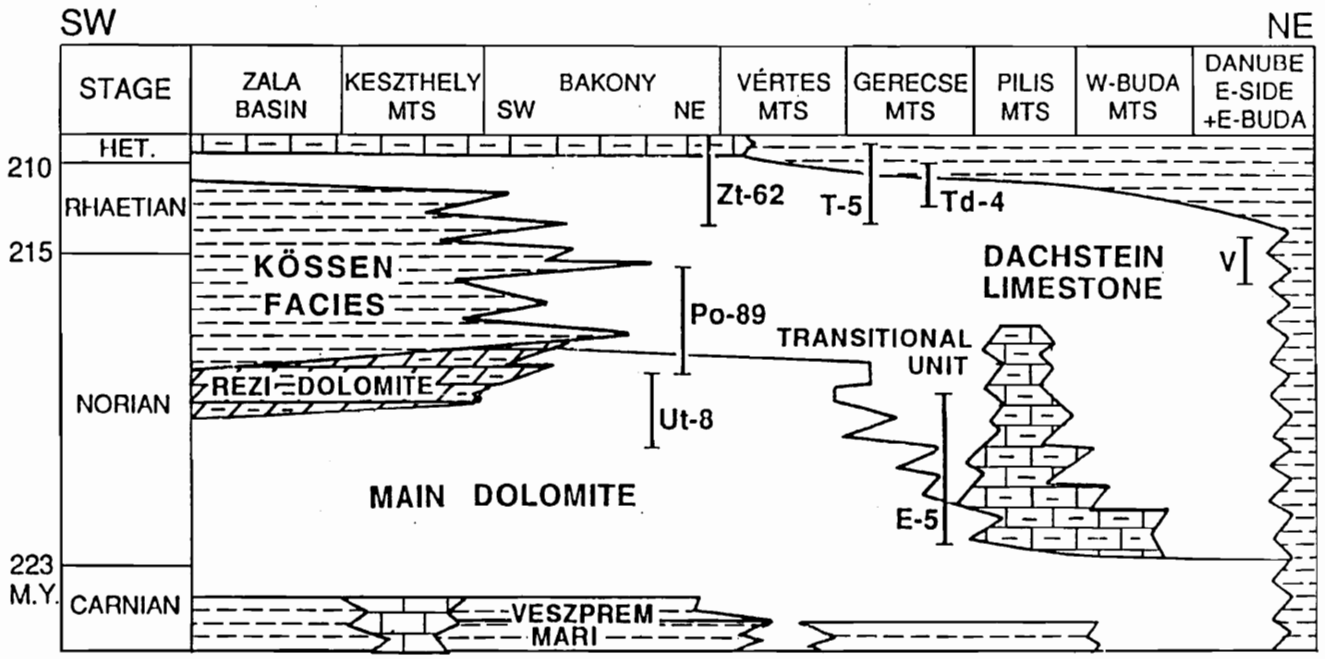

Fig. 3.3. Stratigraphic chart showing units of the Triassic carbonate platform, Transdanubian Range. Stratigraphic positions of the cores are shown by heavy vertical lines. Modified from Haas (1988). Relative time shown alongside depth section for reference. Landward is to left (southwest) and seaward edge of platform is to right (northeast).

METHODS

Data on the dolomites are from several cores from the Gerecse Mountains, originally located in the outer part of the inner platform zone, and the Northern Bakony Mountains about 70 km landward from the Gerecse area (Figs. 3.2 and 3.3). Detailed bed-by-bed logs were made of the continuous diamond drill cores Po-89 (400 m), Ut-8 (300 m) and Zt-62 (220m) E-5 (500 m), T-5 (200 m) and T-4 (50 m) (Figs. 3.2 and 3.3). Between 70 to 150 samples were taken from each measured core for study.

One half of each thin section was stained with alizarin red S and potassium ferricyanide (Dickson 1965) and analyzed using conventional and cathodoluminescent petrography with a Technosyn Cold Cathodoluminescence Model 8200 Mk II (15-20 kV gun potential, 0.4-0.5-milliamps beam current, 1 cm diameter focused beam current and 0.3 torr vacuum).

Samples for fluid inclusion study were cut and polished on low speed polishing wheels. Microthermometric data were collected using USGS-type gas-flow heating/cooling stage, calibrated at -56.6 °C, 0.0 °C, 374 °C using synthetic fluid inclusions (Bodnar and Sterner 1987). The measured freezing and homogenization temperatures are accurate to at least 0.1 °C and 0.5 °C respectively.

Samples for trace element and isotope analysis were ultrasonically cleaned. Dolomite and calcite types were microsampled (2-20 mg) using a bench-mounted milling machine equipped with dental drills (250-500 mm Tungsten carbide tips) and a binocular microscope. Major (Ca, Mg) and trace (Mn, Fe, Sr) element compositions were determined by Inductively Coupled Plasma Spectroscopy (ICP). Between 0.005-0.020 g of powdered sample were dissolved in 10 ml of 0.2N HCl for four hours under constant agitation. After dissolution, samples were acidified to 0.5N by adding 1 ml of 3.5N HCl. Samples then were centrifuged and placed in polyethylene bottles. Insoluble residues were weighed and subtracted from the total weight of the sample. Analytical accuracy was determined by using blind multi-element solution standards (prepared by SPEX Industries) and was less than 5% error. Routinely analyzed blind blanks were always below detection limit. Analytical precision was based on replicate analyses of Brithis Chemical Standard (BCS) No. 368 (dolomite) and 393 (limestone), and are (±1d): Ca=±3.8%; Mg=±3.2%; Mn=±4.1%; Fe=±10.1%; Sr=±2.3% for dolomite and Ca=±3.5%; Mg=±3.7%; Mn=±3.9%; Fe=±9.3%; Sr=±2.4% for limestone.

Stable isotope analysis of the powdered samples (2 to 20 mg) were done by the Stable Isotope Laboratory, University of Miami with analytical precision of $\delta^{18}O=\pm0.03‰$; $\delta^{13}C=\pm0.02‰$ (Dawans and Swart 1988). No correction was made for dolomite-phosphoric acid fractionation.

METER-SCALE CARBONATE CYCLES OF THE HUNGARIAN CARBONATE PLATFORM

The Hungarian Late Triassic carbonates show well developed cyclicity (Haas and Dobosi 1982; Haas 1982; Schwarzacher and Haas 1986; Balog et al. 1995). Meter-scale cycles are from less than 1 m to over 5 m thick, and consist of, from base to top (Fig. 3.4):

1. Supratidal Sediments: These are generally dolomitized caliche laminite and vadose pisolite in the dolomitized lower platform. Laminites are commonly 5 to 35 cm thick, well laminated, fine grained units. Pisolites have numerous concentric to irregular lumpy or scalloped laminations and their size range is between 0.5-3.0 mm. Pore space between pisolites is filled by replacive dolomite cement with orthorhombic terminations suggesting precursor aragonite mineralogy. Supratidal facies of the upper platform are red or green, and composed of partly dolomitized clayey lime mudstone with commonly blackened intraclasts from the underlying limestone. Mottles and root casts are also present.

2. Transgressive Tidal Flat Laminite: These dolomites have well developed microbial lamination, fenestrae, and mudcracks. The laminoid fenestral fabric consists of sub-parallel organic-rich laminas alternating with chains of flattened fenestrae up to 1 mm high. The microbial lamination may be flat or crinkled. The fenestrae are filled by internal sediment, crystal-silt, pellet-silt and/or pendant, radiaxial or blocky calcite or rarely dolomite cement overlain by marine calcite.

3. Subtidal Facies: These are dolomite in the lower platform, and mainly limestone in the upper platform. They are typically peloidal skeletal wackestone/packstone with rare oolitic grainstone. Rip-up breccias with dolomitized flat pebbles are common in the lowermost part of cycles. Biota includes calcified green and dasyclad algae, foraminiferas, megalodont clams, and gastropods.

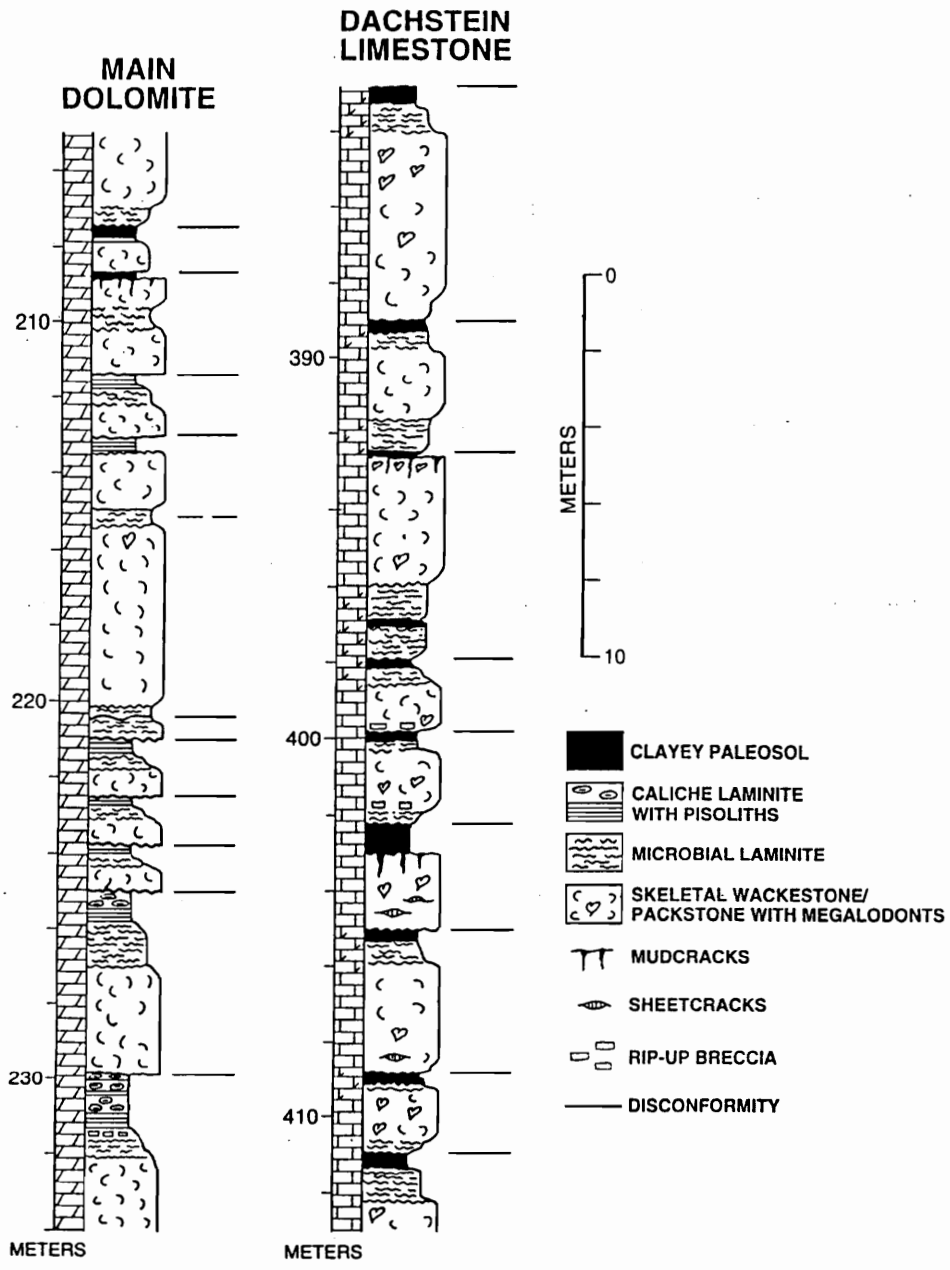

Fig. 3.4. Idealized cycles typical of the lower dolomitized platform (Main Dolomite) and the upper limestone-dominated platform (Dachstein Limestone). Main Dolomite cycles are completely dolomitized and capped by caliche laminites and pisolites, whereas Dachstein Limestone cycles have dolomitization restricted to laminites beneath clayey paleosol.

4. Regressive Tidal Flat Laminites: These dolomites are similar to transgressive laminites, but commonly are more leached, especially in the Dachstein Limestone cycles, with abundant internal sediment and mudcracks filled by internal sediment. Regressive tidal flat laminites are overlained by a disconformity, paleosol, transgressive laminites or subtidal facies of the next cycle.

Origin of the Meter-Scale Cycles

Given the age constraints Schwarzacher and Haas (1986) calculated that the meter scale cycles are approximately 20 k.y. in duration, which suggests a precessional origin. That these cycles formed due to the high frequency sea level fluctuations is evidenced by repeated emergence of the platform, which is indicated by caliche and soil formation on the platform. Balog et al. (1995) showed that there is a poorly developed bundling of 3 to 6 cycles per bundle, rather than the classic 5:1 bundling shown by for the Middle Triassic Latemar buildup (Goldhammer 1990); these bundles appear to be 100 k.y. bundles. Parts of the Hungarian section also show a weak suggestion of larger scale bundles made up of four 100 k.y. bundles; These may be larger 400 k.y. bundles. However, the number of cycles and the wavelength of these larger bundles is highly variable, the bundling only shows up on limited parts of the plots (Balog et al. 1995).

PETROGRAPHY OF DIAGENETIC PHASES IN HUNGARIAN TRIASSIC

Marine Cement

Former Marine High-Mg Calcite: This cement forms banded isopachous crusts up to several centimeters thick lining primary intergranular and fenestral pores, dissolution cavities, skeletal molds, and desiccation cracks. The calcite cement consists of fibrous to bladed crystals oriented normal to the substrate. They have undulatory, radial-fibrous or radiaxial extinction, and are turbid with abundant micro-dolomite inclusions. Fibrous calcite may have elongate subcrystals that locally show small recrystallization patches. Bladed crystals have planar intercrystalline boundaries and rhombohedral terminations. These calcite cements are nonluminescent except for some dully luminescent patches. The marine cements predate, are inter-layered with, and even postdate infiltrated internal

sediment . They commonly postdate early replacement dolomite and dolomite cement. In completely dolomitized cycles of the Main Dolomite, marine calcite is replaced by fabric-retentive dolomite.

Former Aragonite Cement: This is recognized by orthorhombic crystal terminations, neomorphic replacement by low Mg-calcite, and botryoidal form. Former aragonite cement is relatively rare in the Hungarian carbonates, and is associated with supratidal facies. In the lower platform, aragonite is completely dolomitized whereas in the upper platform it is only partly dolomitized, the undolomitized aragonite having been neomorphosed to calcite.

Dolomite

Dolomite generations recognized in the Hungarian carbonates on the basis of textural characteristics and cathodoluminescence are: (1) early replacement dolomite and cement, (2) later vein- and pore-filling dolomite cement, and (3) coarse-grained, fabric-destructive dolomite observed near the platform margin in the Vac area (Balog et al. 1990; Juhasz et al. 1995). In general the dolomitization of the Hungarian Triassic platform decreases upward from the Norian to the Rhaetian lower to upper platform.

Early Replacive Dolomite and Early Dolomite Cement: This comprises an estimated 90% of the total dolomite by volume. It replaces both subtidal and intertidal facies in the Main Dolomite, and partially to completely replaces intertidal facies in the less dolomitized Dachstein Limestone. It forms fabric-preservative, very fine to finely (3 to 35 μm) crystalline mosaics of euhedral dolomite rhombs with planar crystal boundaries (Fig. 3.5A-C). The average crystal size is coarsest in subtidal facies (9 to 35 μm), whereas dolomitized intertidal laminites are the finest grained (3 to 6 μm). Early dolomite generally is non-luminescent, but can be dully luminescent where it replaces organic-rich algae laminites.

Early dolomite cement is distinguished petrographically from later dolomite where it is postdated by marine calcite. Early dolomite cement forms a very thin, isopachous rim cement of non-luminescent euhedral rhombs (6 to 9 μm) lining on the pore walls. They are common in transgressive laminites. It could not be sampled because it only makes an estimated 1 to 2% of the total dolomite volume throughout the section, forming thin linings around cavities.

Fig. 3.5. SEM and thin section photomicrographs of dolomites.

A. SEM photograph of intertidal-supratidal fine-grained dolomite and slightly coarser dolomite cement filled fenestra from Ut-8 core (Main Dolomite).

B. SEM photograph of subtidal dolomite from UT-8 core (Main Dolomite).

C. Higher powered SEM photograph of subtidal dolomite from UT-8 core (Main Dolomite). D. Thin section photograph of pore and fracture filling dolomite cement followed by Fe-calcite cement from Ut-8 core (Main Dolomite).

E. Thin section photograph of platform margin early burial coarse grained dolomite from Vac core (Dachstein Limestone).

F. SEM photograph of platform margin early burial coarse grained dolomite from Vac core (Dachstein Limestone).

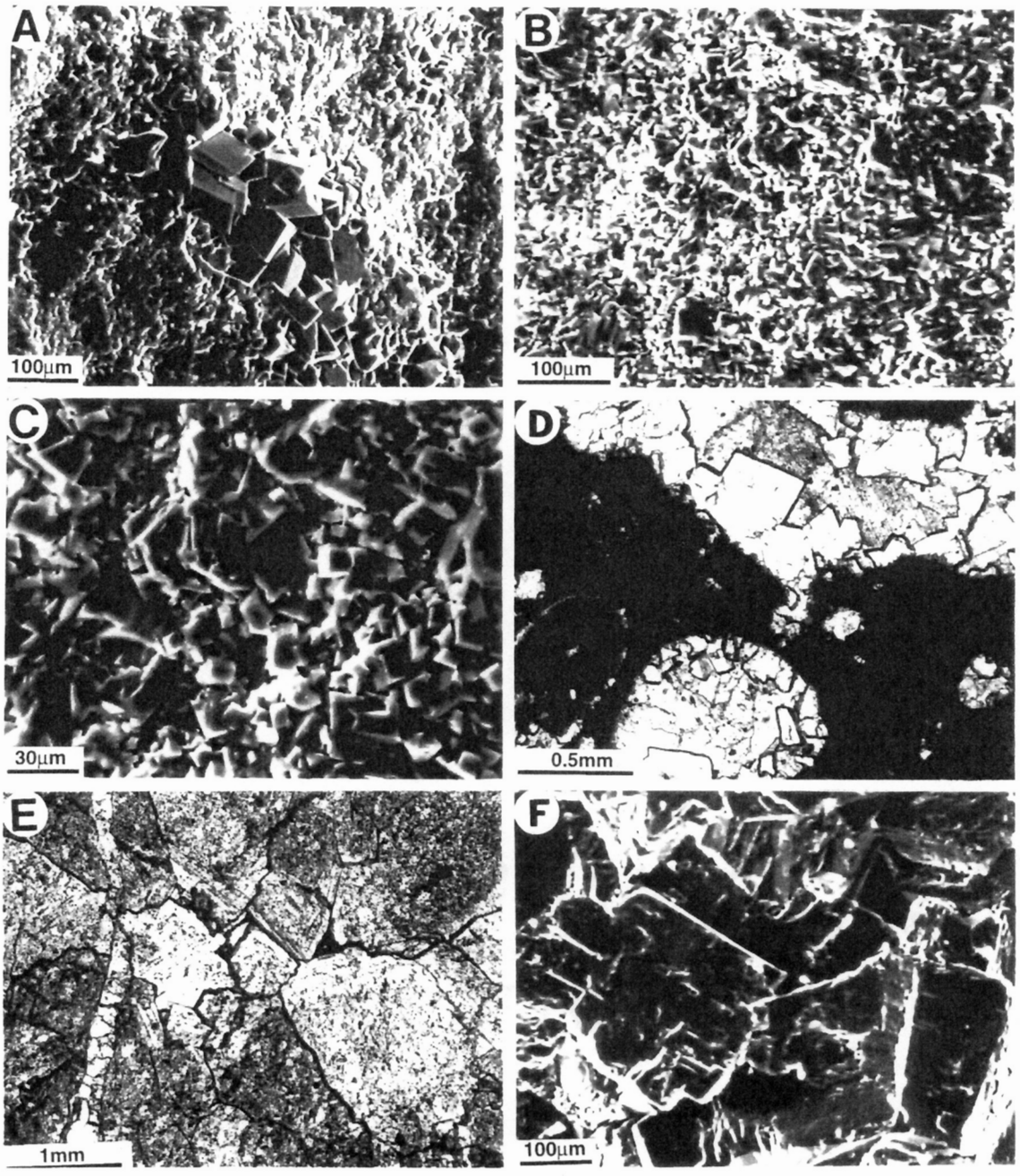
A
100μm
B
100μm
C
30μm
D
0.5mm
E
1mm
F
100μm

Coarse Grained Fabric-Destructive Dolomite: This dolomite occurs locally in the platform margin carbonates of the upper platform in the Vac area (Fig. 3.2). The dolomite has well defined, irregular boundaries with the host limestone and crosscuts original sedimentary fabrics (Balog et al. 1990) The dolomite is fabric destructive and consist of xenotopic, fine- to coarse-crystalline (80 μm - 120μm) mosaic. Remaining large primary interparticle pores are partly filled with large, zoned dolomite crystals that have inclusion-rich cores and clear rims and saddle dolomite cement (0.2 to 1.3mm)(Fig. 3.5E-F). The pore centers usually are filled with late poikilotopic calcite spar with complex CL zonation. This dolomite typically is nonluminescent. Clear rims on the host dolomite and later saddle dolomite crystals contain two-phase, primary fluid inclusions in the form of very small (1-5 μm) negative crystal-shaped aqueous inclusions. At room temperature the vapor bubble occupies less than 10% of the inclusion. The uncorrected homogenization temperatures in the dolomite range from 74-134 °C. The last melting temperatures range from -2.6 to -2.4 °C equivalent to normal or slightly hyper saline sea-water (Bodnar 1994).

Later Vein and Pore-Filling Dolomite Cement: This was too thin to sample and makes up only a few percent of the total dolomite volume, and it is more common in the lower platform dolomite. It occurs as isopachous rim cement of clear euhedral rhombs (15-25 μm) with planar crystal boundaries filling primary and secondary cavities or fractures. It is nonluminescent with a later dull zone (Fig. 3.5D). It commonly is overlain by pink to blue staining late calcite cement.

GEOCHEMISTRY

The geochemistry of the dolomites and marine cements is summarized in figures 3.6 to 3.15 and Table 3.1.

Calcium/Magnesium: Former marine, hi Mg-calcites contain 0.4 to 2.6 mol% of $MgCO_3$ and are now low Mg-calcites (Fig. 3.6, Table 3.1). Early dolomites are calcium-rich, with 44 to 48 mol% $MgCO_3$ and a poorly developed ordering peak (Table 3.1, Fig. 3.7). Early burial coarse-grained dolomites are more stoichiometric with 47.5 to 49.2 mol% $MgCO_3$ (Table 3.1, Fig. 3.7).

Strontium: Marine calcites and Dachstein bulk limestone have 66 to 211 ppm Sr^{2+} (Table 3.1). On a Mg^{2+}/Sr^{2+} plot, the Dachstein marine calcite cement appears to fall on

a line collinear with Holocene Mg-calcite cements, but are not collinear with Devonian cements (Carpenter et al. 1991) (Fig. 3.6).

The Hungarian dolomites show two populations in terms of their Sr^{2+} content, the early dolomites with 44 to 246 ppm Sr^{2+}, and early burial coarse-grained dolomite with less than 50 ppm Sr^{2+} (Figs. 3.7, 3.8). Sr^{2+} content of early dolomite overlaps marine calcite and bulk limestone (Table 3.1). There is little difference in Sr^{2+} content between intertidal/supratidal dolomites, and dolomitized subtidal facies (Figs. 3.7, 3.8). Except for a few outliers, the dolomites tend to plot along a trend of decreasing Sr^{2+} with increasing $MgCO_3$ content (Bahamian line of Figure 3.7) (Vahrenkamp and Swart, 1990). The Sr^{2+} composition of the Hungarian dolomites resembles many Cenozoic dolomites (Figs. 3.8, 3.9).

Sodium: Na^+ content of the marine calcites range from 6 to 185 ppm. Dachstein bulk limestone has 102 to 324 ppm Na^+ (Table 3.1). Na^+ content of early dolomite (14 to 1142 ppm) is elevated relative to marine calcite (Table 3.1). Na^+ content of the early burial coarse-grained dolomite is low (less than 150 ppm). Na^+ vs. Sr^{2+} of the various early dolomites tend to have overlapping fields (Fig. 3.8A). Generally Na^+ increases with increasing Sr^{2+} content with the early burial coarse-grained dolomites having the lowest values (Fig. 3.8A).

Manganese and Iron: Marine calcites have 4 to 18 ppm of Mn^{2+}, their Fe^{2+} content ranges between 12 to 749 ppm (Table 3.1, Fig. 3.10).

Bulk subtidal limestones have Mn^{2+} contents between 32 to 257 ppm and low Fe^{2+} (6 to 138 ppm) (Table 3.1). Mn^{2+} is low in subtidal dolomite (average 83 ppm), but a few intertidal-supratidal dolomite samples from the Main Dolomite show Mn^{2+} enrichment (up to 741 ppm) (Fig. 3.10). Mn^{2+} is high in Dachstein paleosol horizons (204 to 1120 ppm) (Table 3.1, Fig. 3.10). Fe^{2+} contents of different early dolomite facies generally are low but may be up to 1165 ppm in some inter-supratidal facies (Fig. 3.10). In general, Fe^{2+} and Mn^{2+} are inversely related (Fig. 3.10).

Stable Isotopes: Stable isotope compositions of each diagenetic phase are relatively tightly clustered, except for paleosols (Figure 3.11). The marine calcites have $\delta^{18}O$ values of -1.4 to -0.2 ‰PDB, and $\delta^{13}C$ values of 1.5 to 2.3 ‰ PDB, which are similar to other Triassic marine calcites (Wilkinson 1982; Veizer 1983; Lohmann and Walker 1989; Railsback 1990; Hoffman et al. 1991)(Table 3.2, Fig. 3.11).

Table 3.1

TRACE ELEMENTS	Na		Sr		Mn		Fe	
	Avg (n)	Range	Avg (n)	Range	Avg (n)	Range	Avg (n)	Range
Marine calcite	53 (24)	6 to 185	142 (24)	66 to 200	9 (24)	4 to 18	111 (24)	12 to 749
Main Dolomite								
Inter-supratidal	410 (15)	146 to 1142	162 (15)	44 to 217	211 (15)	18 to 741	354 (15)	13 to 1165
Subtidal	465 (13)	190 to 758	172 (13)	99 to 233	83 (13)	9 to 213	168 (13)	2 to 1148
Dachstein Limestone								
Paleosol	437 (6)	198 to 590	237 (6)	70 to 304	669 (6)	204 to 1120	126 (6)	21 to 510
Intertidal dolomite (Dachstein dolomite)	204 (6)	14 to 751	156 (6)	114 to 246	36 (6)	11 to 137	386 (6)	232 to 956
Subtidal limestone	233 (4)	102 to 324	157 (4)	121 to 211	154 (4)	32 to 257	58 (4)	6 to 138
Late Coarse Dolomite	71 (8)	42 to 124	37 (8)	28 to 46	40 (8)	17 to 68	67 (8)	31 to 136

Table 3.2

ISOTOPES	$\partial^{18}O‰PDB$			$\partial^{13}C‰PDB$		
	Avg	(n)	Range	Avg	(n)	Range
Marine calcite	-0.8	(8)	-1.4 to -0.2	1.9	(8)	1.5 to 2.3
Main Dolomite						
Inter-supratidal dolomite	2.0	(15)	1.1 to 2.5	2.2	(15)	1.7 to 2.9
Subtidal dolomite	3.1	(13)	2.6 to 3.5	2.3	(13)	1.9 to 2.7
Dachstein Limestone						
Paleosol	-1.6	(12)	-7.2 to 1.1	1.0	(12)	-1.5 to 2.7
Intertidal dolomite	1.3	(6)	1.2 to 1.8	2.7	(6)	1.9 to 3.2
Subtidal limestone	-1.4	(4)	-2.5 to -0.5	1.1	(4)	0.4 to 1.7
Early burial coarse grained dolomite	-6.3	(8)	-7.8 to -2.7	2.6	(8)	1.8 to 3.5

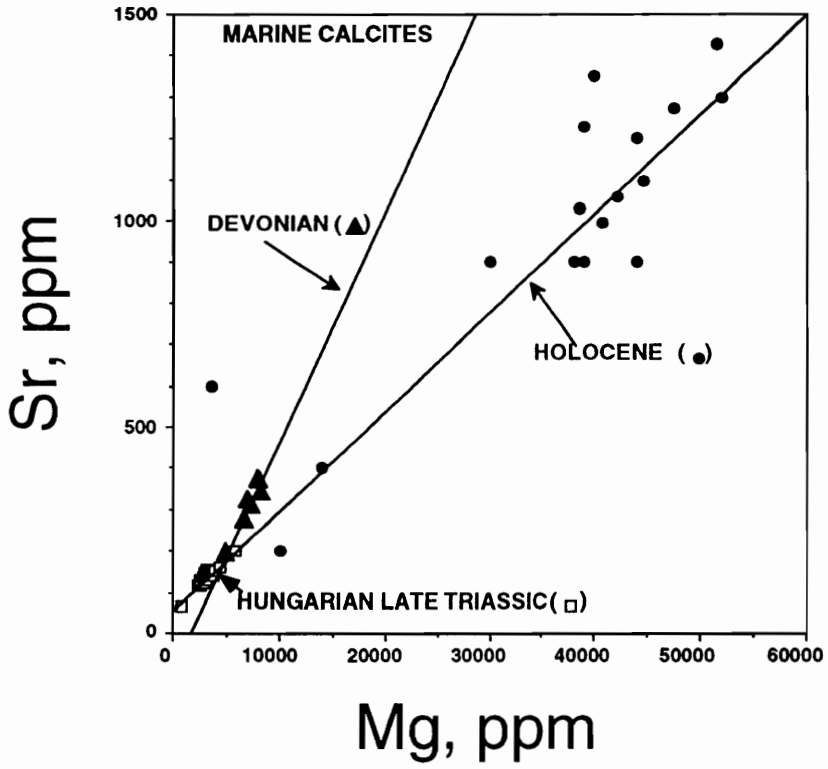

Fig. 3.6. Plot of Mg^{2+} vs. Sr^{2+} content of Hungarian Late Triassic (open squares) and Holocene marine calcites (black circles) and Devonian marine calcites (solid triangles) (Carpenter et al. 1991). Holocene and Devonian trends are shown by lines (Carpenter et al. 1991). The Hungarian marine calcites have low Mg content, and they tend to lie on the Holocene line.

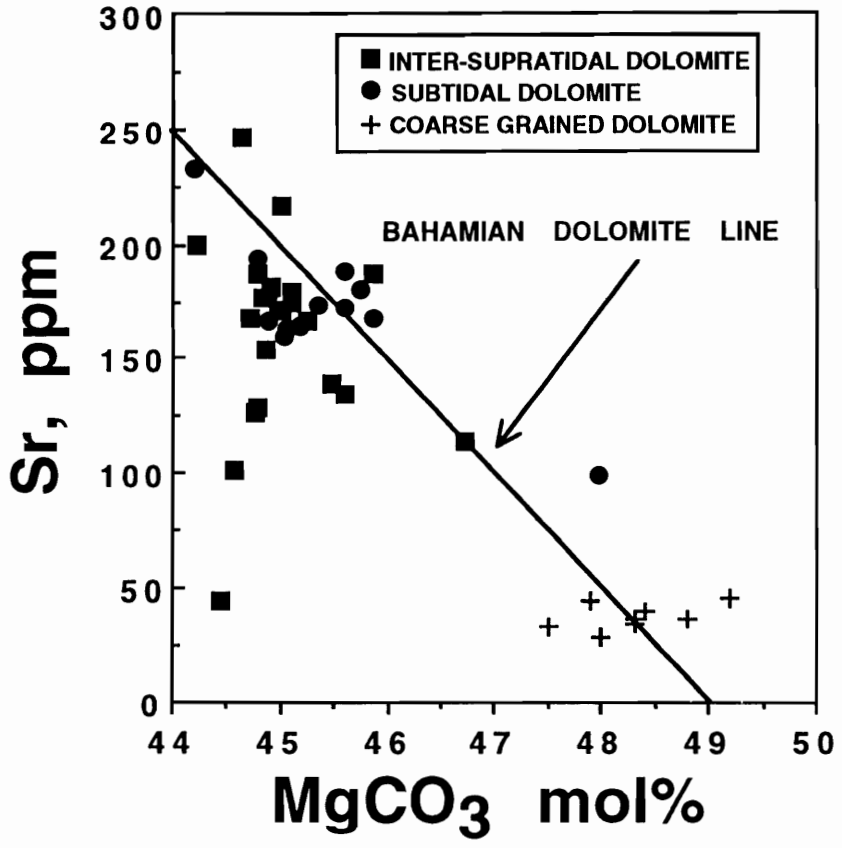

Fig. 3.7. Sr^{2+} vs. mole% $MgCO_3$ of the Hungarian dolomites. The diagonal line shows the Tertiary Bahamian dolomite line of Vahrenkamp and Swart (1990). The early dolomites are less stoichiometric than the platform margin coarse-grained dolomite (pluses).

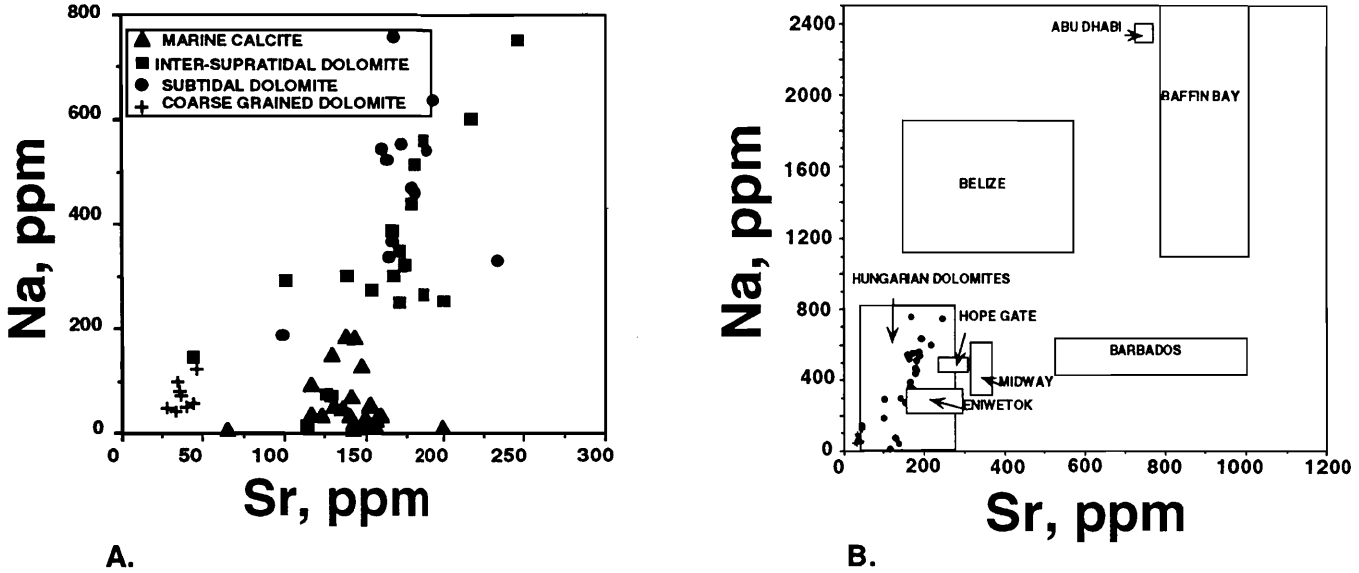

Fig. 3.8A. Sr^{2+} vs Na^{+} plot of the Hungarian dolomite and marine calcites. The coarse-grained platform margin dolomite has very low Sr^{2+} and Na^{+} content compared to the early dolomites.

8B. Comparison of Sr^{2+} vs. Na^{+} content of the Hungarian Triassic dolomites with Cenozoic platform dolomites from Baffin Bay (Behrens and Land 1972); Abu Dhabi (Land and Hoops 1973) Hope Gate (Land 1973); Midway (Major, 1984); Eniwetok (Saller 1984); Belize (Mazullo 1987); Barbados (Humprey 1988).

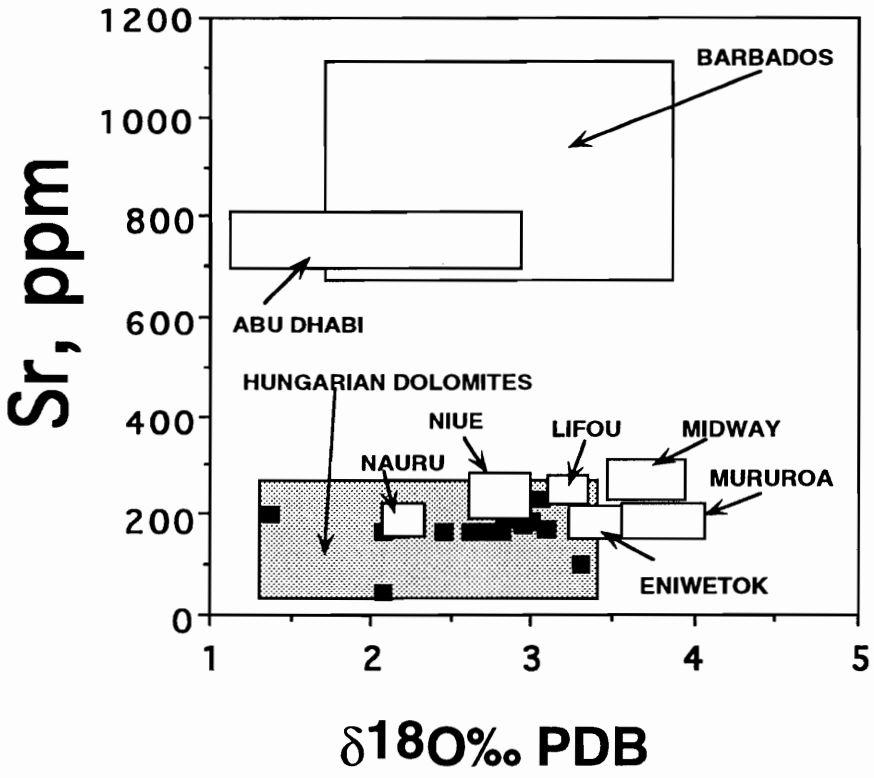

Fig. 3.9. Plot showing Sr^{2+} vs. $\delta^{18}O‰$ PDB composition of the Hungarian Triassic dolomites compared with Cenozoic dolomites from Baffin Bay (Behrens and Land 1972); Abu Dhabi (Patterson and Kinsman 1982); Eniwotak (Saller, 1984); Barbados (Humprey 1988); Niue and Nauru (Aharon et al. 1987); Belize (Mazullo 1987); Midway and Lifou (reported in Aharon et al. 1987). The Hungarian dolomities have similar Sr^{2+} and Oxygen isotopic composition to Cenozoic dolomites.

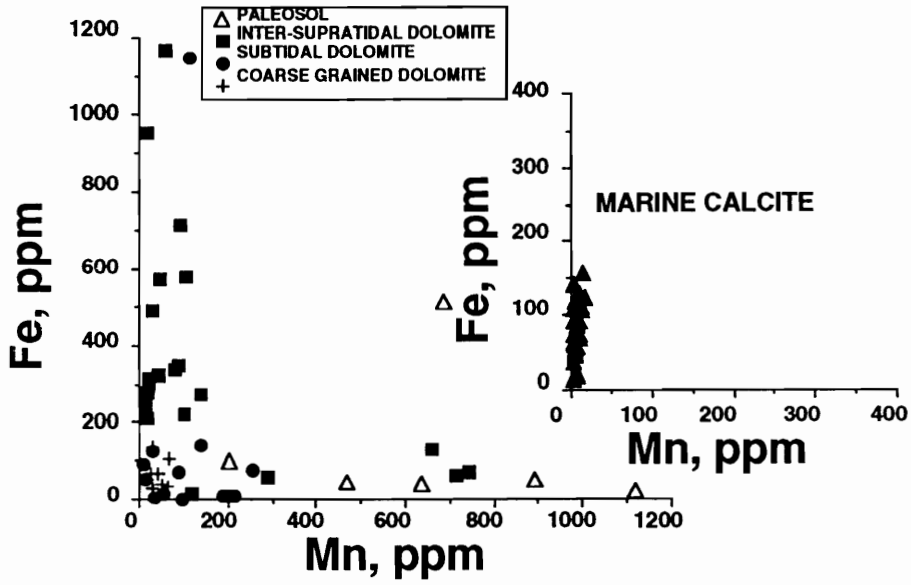

Fig. 3.10. Mn^{2+} vs Fe^{2+} plot of various dolomite facies of the Hungarian Late Triassic carbonates. Marine calcite is shown in inset . There is an inverse relationship between Fe^{2+} vs. Mn^{2+} in some of the intertidal-supratidal dolomites and paleosols. Many of the Mn-rich dolomites are paleosols.

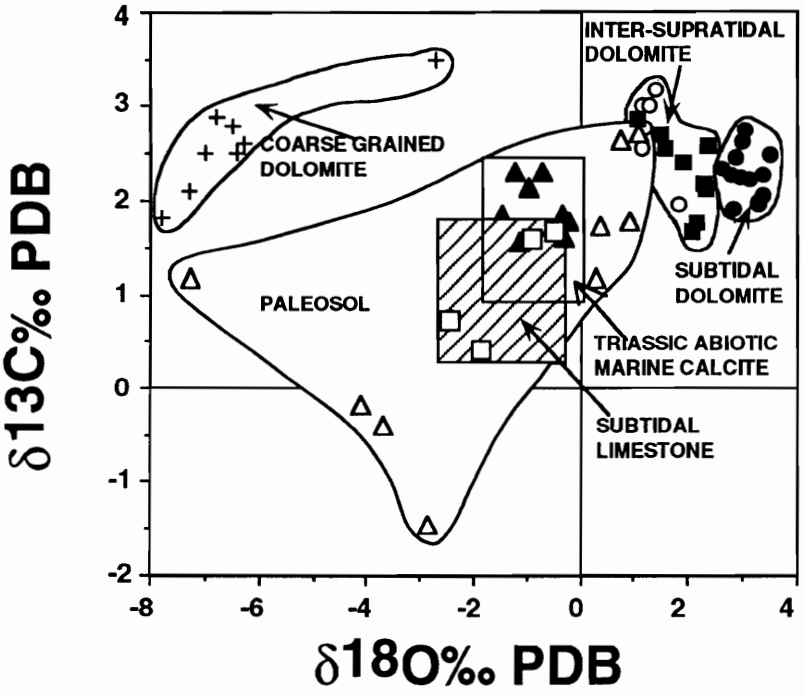

Fig. 3.11. Isotopic composition of the Late Triassic Hungarian dolomites, limestones and marine calcite. Rectangle shows the field of Triassic abiotic marine calcite based on the Hungarian Triassic samples and published values (Wilkinson 1982; Veizer 1983; Lohmann and Walker 1989; Railsback 1990; Hoffman et al. 1991). Cross-hatched square shows the field of subtidal Dachstein Limestone.

The isotopically heaviest dolomites are those replacing subtidal beds ($\delta^{18}O$ 2.6 to 3.5 ‰ PDB; $\delta^{13}C$ of 1.9 to 2.7 ‰ PDB). These are about 4 ‰ heavier in $\delta^{18}O$ than marine calcites (Table 3.2, Fig 3.11). Intertidal-supratidal dolomites have slightly lighter $\delta^{18}O$ values (1.1 to 2.5‰ PDB) than the subtidal dolomites. Of the intertidal-supratidal dolomites, in general the Main Dolomite samples are slightly heavier than the Dachstein dolomite samples (Table 3.2, Fig. 3.11). Dachstein paleosols have $\delta^{18}O$ values that range from slightly heavier than, to several per mil lighter than the Triassic marine calcites (Table 3.2, Fig. 3.11). Del ^{13}C values of the paleosols range from slightly heavier than, to 3 ‰ lighter than marine calcite (Table 3.2, Fig. 3.11).

In an attempt to define isotopic trends within cycles, all the dolomite isotope data for the Main Dolomite and the Dachstein Limestone were plotted relative to their position above or below the intertidal/subtidal boundary within the cycles to form composite isotope profile (Figs. 3.12, 3.13). In the Main Dolomite overall, the $\delta^{18}O$ values of the intertidal-supratidal dolomites increase toward the base of the tidal flat cap (zero datum); $\delta^{18}O$ of the subtidal dolomite remains uniformly heavy with depth in the cycles (Fig 3.12A). Del ^{13}C for the Main Dolomite is relatively invariant with depth in the cycle (Fig. 3.12.B). In the Dachstein composite profiles, the $\delta^{18}O$ and $\delta^{13}C$ trends are " V " shaped with lightest values in some paleosols, and heaviest values in the intertidal dolomites, the subtidal limestones have values between the intertidal dolomites and the paleosols (Fig. 3.13AB). From the base to the top of the platform, the $\delta^{18}O$ values of the platform carbonates show a trend that becomes slightly lighter from the Main Dolomite up into the lower Dachstein Limestone, and becomes highly depleted in the upper Dachstein Limestone which contains many paleosols (Fig. 3.14).

INTERPRETATION

Triassic Sea-water Composition Based on Marine Calcite Geochemistry: The bladed habit and micro-dolomite inclusions in the marine calcites suggest that they were originally high Mg-calcite. The Sr^{2+} and low $MgCO_3$ content suggest that marine calcite has been stabilized to low Mg-calcite (Fig. 3.6). Stabilization occurred in the near-surface because there is no evidence of major burial alteration; this is supported by the nonluminescent character of the cement, indicating stabilization under relatively oxidizing conditions. Its low Mn (<20 ppm), and Fe (average 111 ppm) content and $\delta^{18}O$ and $\delta^{13}C$ values are similar to other Triassic abiotic marine calcites

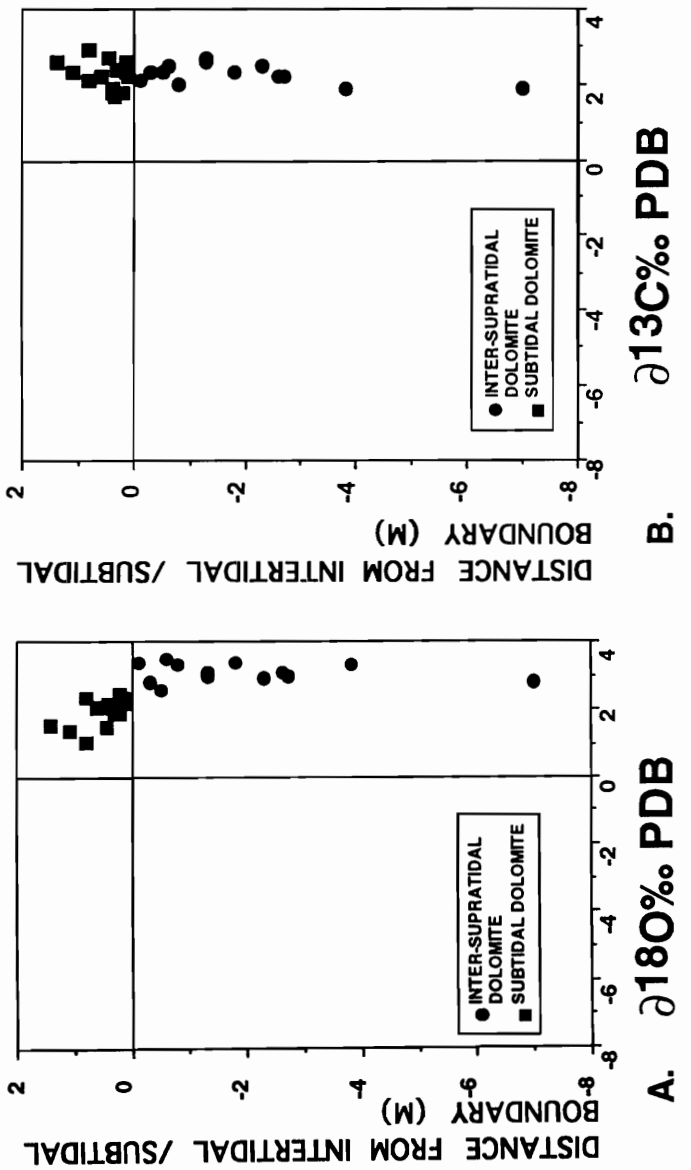

Fig. 3.12A. Composite plot showing $\delta^{18}O‰$ PDB of dolomites vs. sample depth relative to intertidal/subtidal boundary within Main Dolomite cycles (lower platform).

B. Composite plot showing $\delta^{13}C‰$ PDB vs. sample depth relative to intertidal/subtidal boundary within Main Dolomite cycles in the (lower platform).

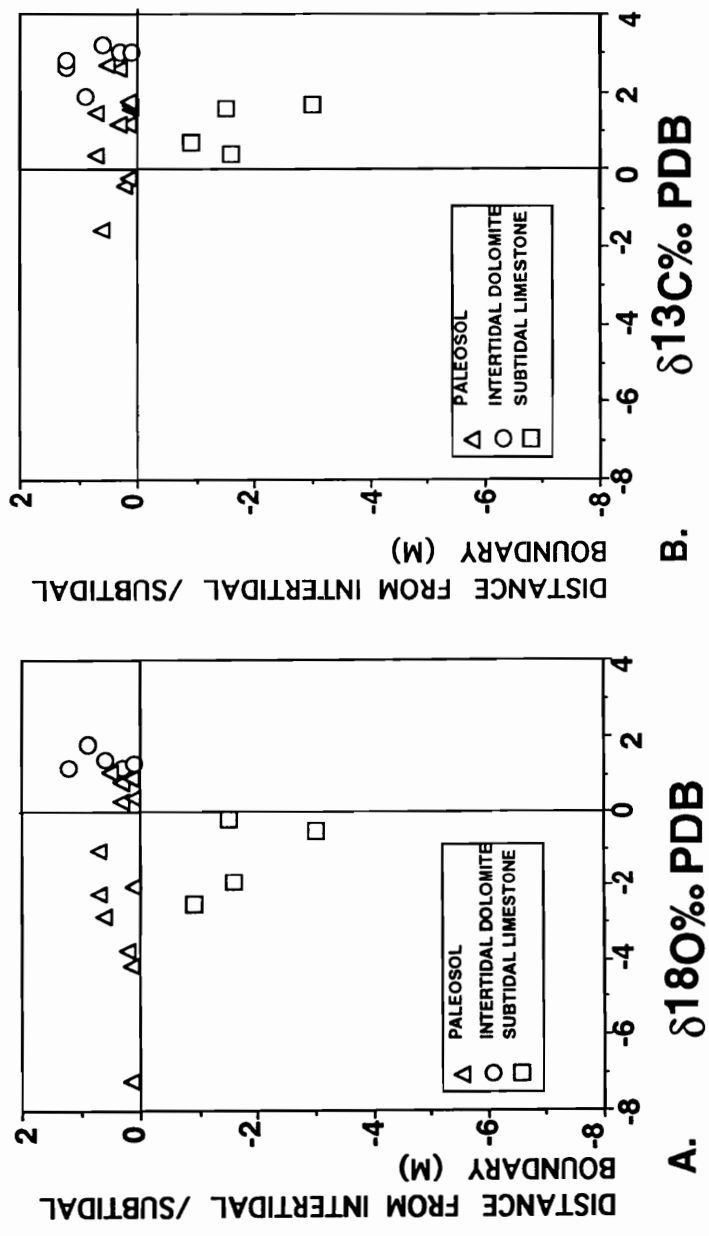

Fig. 3.13A. Composite plot showing $\delta^{18}O‰$ PDB dolomite/limestone vs. sample depth relative to intertidal/subtidal boundary within Dachstein Limestone cycles (upper platform). B. Composite plot showing $\delta^{13}C‰$ PDB of dolomite/limestone vs. sample depth relative to intertidal/subtidal boundary within each Dachstein Limestone cycles (upper platform).

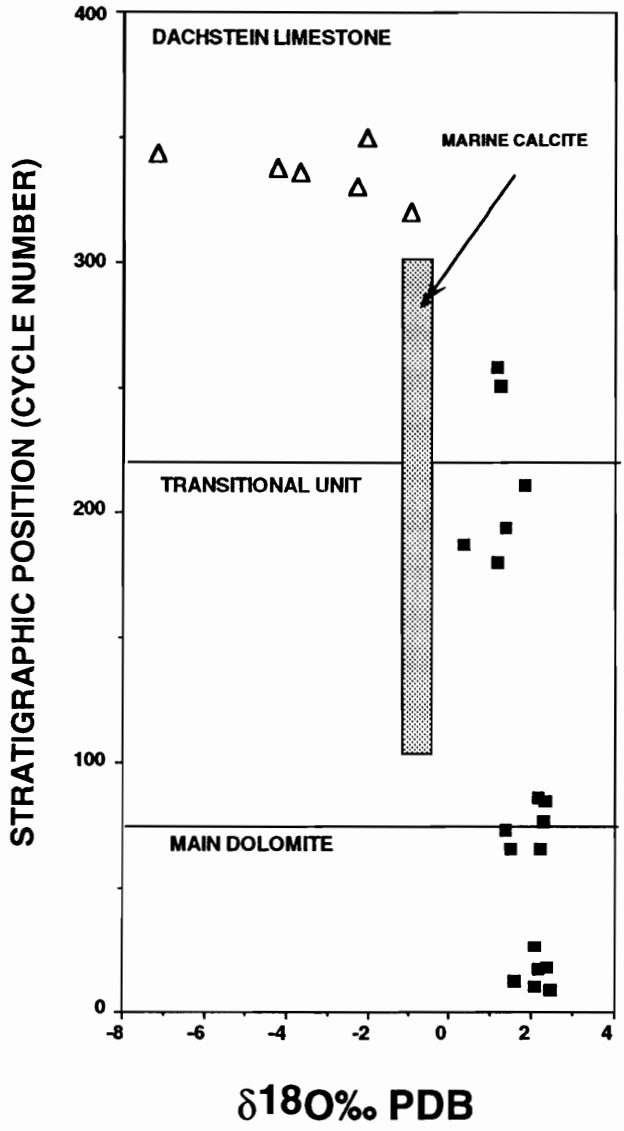

Fig. 3.14. Composite plot showing up-section change in oxygen isotopic composition of intertidal/supratidal facies vs. cycle number (proxy for stratigraphic position) from Main Dolomite to Dachstein Limestone. Solid circles are dolomite samples from intertidal/supratidal facies; open triangles are partly dolomitized clayey carbonates, from Dachstein paleosols. Stippled column shows range of marine calcites. Even taking into account the calcite - dolomite fractionation, some paleosol samples still show a significant depletion in ^{18}O relative to the dolomites.

(Wilkinson 1982; Veizer 1983; Lohmann and Walker 1989; Railsback 1990; Hoffman et al. 1991). Furthermore, the ranges of isotopic and trace element values are relatively narrow, and there is no evidence for a diagenetic trend from the marine calcites toward later diagenetic calcites (Banner and Hanson 1990).

Carpenter et al. (1991) compared Sr^{2+} and Mg^{2+} contents of modern and Devonian marine calcites, in an attempt to characterize Devonian sea-water composition. This was based on the strong dependence of $K_D Mg^{2+}$ in calcite on sea-water Mg/Ca ratio, and the similarity of K_D values of Sr^{2+} (0.03 to 0.07; (Carpenter et al. 1991) and Mg^{2+} (0.01 to 0.03; Morse and Bender 1990). The Hungarian Late Triassic abiotic marine calcite Sr/Mg composition appears to plot along a trend through Holocene cements that is quite distinct from the Devonian trend (Carpenter et al. 1991)(Fig. 3.6). Railsback and Anderson (1987) attempted to calculate the paleo sea-water composition of the Triassic ocean, and suggested that Mg/Ca ratios were ten times higher than today, because of widespread evaporite precipitation during Permian and Early Triassic. However at the end of the Triassic, sea-water composition may have approached the composition of today's ocean, perhaps due to Mg loss along active mid oceanic ridges during rifting and formation of the Pennini ocean (Neo-Tethys), and the break up of Pangea (Wilson et al. 1989).

Precursor Mineralogy of Host Sediment: Modern warm, shallow-water carbonate sediments are dominated by a mixture of high Mg-calcite and aragonite, their local ratio being dependent on the climate, Mg/Ca ratio, and the dominant carbonate producing organisms.

The Hungarian carbonates were formed as a mixture of aragonite and high Mg-calcite because the major biota is aragonitic (green algae, bivalves, gastropods) along with high Mg-calcite forams and ostracodes. Most of the marine cements were originally high Mg-calcite with only minor supratidal aragonite. The Triassic is placed at the transition between aragonitic/calcitic seas by Sandberg (1983), whereas Wilkinson (1982), places the Triassic in a time of aragonite-dominated seas.

Evidence of Early Near Surface Dolomitization vs Early Burial Dolomitization: Much of the dolomitization of the Hungarian carbonates occurred during deposition of each cycle, which is evidenced by fragments of dolomite reworked in paleosols and subtidal carbonates above cycle capping disconformities, the fine replacement dolomite, which is postdated by marine calcite, and the presence of internal lime sediment resting

on early dolomite. Early dolomite is mostly nonluminescent, which also supports oxidizing near-surface conditions for dolomitization.

In contrast, early burial dolomites crosscut the original depositional features. They are fabric obliterate, anhedral, coarse-grained, and may be associated with saddle dolomite cement (Balog et al. 1990). Dolomite crystals are frequently zoned, with two-phase fluid inclusions along growth zones. Their nonluminescent character suggests oxidizing dolomitizing fluids (Juhasz et al. 1995).

Significance of Strontium in the Dolomite: Strontium content of the Hungarian early replacement dolomites is similar to Tertiary low Sr-dolomites and is significantly lower than Holocene dolomites (Figs. 8 and 9). Modern high Sr-dolomites that formed during the last three to five thousand years have 400 to 2000 ppm Sr^{2+} (Behrens and Land 1972; Land 1973; Land and Hoops 1973; Mazzullo et al. 1987; Humphrey 1988). Those formed from high Mg-calcite, have Sr^{2+} contents of only 400 to 600 ppm and higher Sr^{2+} content if they formed from aragonite. The only older high Sr-dolomite is the Golden Grove Formation, Barbados which was dolomitized during the Pleistocene with little evidence of any meteoric stabilization predating dolomitization (Humphrey 1988).

Pleistocene and older peritidal dolomites generally have recrystallized to form low Sr-dolomite (Dawans and Swart 1988; Gregg et al. 1992). The Sr^{2+} loss could have occurred during repeated emergence events as sealevel fluctuations exposed the early formed platform dolomites (Haas 1982; Balog et al. 1995). Aragonite leaching, dissolution enhanced vuggy porosity, internal sediment, vadose and meteoric cement indicate that meteoric diagenesis affected the Hungarian cyclic section, but it is difficult to determine if dolomitization actually predated or postdated meteoric diagenesis. It seems likely that dolomitization may have been interspersed with diagenesis by mixed or meteoric waters, given the sea-level fluctuation affecting the platform. The low Sr^{2+} content of Hungarian dolomites resembles many Cenozoic dolomites, which are low Sr-dolomites with 250 to 380 ppm Sr^{2+}, that formed mainly during Late Miocene-Pleistocene (Figs. 3.8, 3.9) (Randazzo and Hickey 1978; Aharon et al. 1987; Land 1991; Vahrenkamp and Swart 1991; Hein et al. 1992). In some Cenozoic dolomites, there is evidence that meteoric stabilization predated dolomitization (Vahrenkamp and Swart 1990; Hein et al. 1992) and the resulting low Mg-calcite formed dolomites with relatively low Sr^{2+} content. In Aitutaki (Cook Islands), the Sr^{2+} content of the original reef limestone is approximately 6100 ppm, only 455 ppm in the stabilized low Mg-calcite and only 250 ppm in the dolomite (Hein et al. 1992). Similarly, some subtidal facies in the

Hungarian Triassic could have been stabilized prior to dolomitization. This would have required that some subtidal facies escaped dolomitization during cycle progradation, and on exposure, the subtidal facies were stabilized in ground water of mixed meteoric-marine or meteoric origin. With subsequent transgressions and regressions associated with overlying cycles, the remaining undolomitized limestone could have been dolomitized by refluxing brines. Repeated emergence of the platform following the deposition of each cycle would have promoted stabilization and recrystallization of the underlying platform dolomites to form low Sr-dolomites.

The extremely low Sr^{2+} content of the coarse-grained platform margin dolomite, which is also more stoichiometric than the other dolomites, may have resulted from slow dolomitization of previously stabilized carbonates. These were formed by early burial dolomitization by warm marine fluids (indicated by the fluid inclusions), which would have acted on platform margin sediments that had been subjected to repeated emergence events, although duration of emergence here would have been less frequent than in the shallow platform interior. Slow precipitation rate also may have favored the formation of a stoichiometric low Sr, early burial dolomite (Figs. 3.8, 3.9.) (Lorens 1981).

Significance of Sodium in the Dolomite: Na^{+} in dolomites may be in fluid inclusions adsorbed onto clays, or in the carbonate lattice. Overlapping Na^{+} content of the different Hungarian early dolomites is similar to most Cenozoic dolomites (300 to 1000 ppm), which have been repeatedly exposed to meteoric water during high frequency glacio-ecstasy, but is significantly lower than highly evaporative Holocene dolomites which have up to 2500 ppm Na^{+} (Behrens and Land 1972; Land and Hoops 1973) (Fig. 3.8). The restricted facies of the Main Dolomite likely would have formed from hypersaline water, given the interior platform setting, but even these are low Na-dolomites. It is likely that the Hungarian dolomites were relatively high Na-dolomites that stabilized into low Na-dolomite as a result of meteoric exposure due to repeated cyclic sea-level falls.

The very low Na^{+} content of early burial, coarse-grained dolomite (less than 150 ppm) may reflect their early burial origin from warm marine pore waters, their very low Na^{+} content reflecting slow, high temperature precipitation to form more stoichiometric dolomite with low trace element content (Lorens 1981).

Significance of Iron and Manganese in Dolomites: The nonluminescent character of the early dolomite, its generally low Fe^{2+} content and lack of zoning, all suggest that these dolomites were not subjected to deep burial diagenesis. Instead, the Fe^{2+} and Mn^{2+} contents of the dolomites appear to be primary and related to depositional setting.

Mn^{2+} and Fe^{2+} in carbonates are strongly influenced by redox of the pore fluids (Carpenter and Oglesby 1976; Veizer 1983; Montañez and Read 1992).

In the Dachstein Limestone, Mn^{2+} rich paleosols probably formed from moderately reducing pore waters, with wind blown dust perhaps providing an Mn^{2+} source. Similarly high Mn^{2+} and low Fe^{2+} intertidal-supratidal dolomites in the Main Dolomite also may have formed in supratidal paleosol settings with moderately reducing groundwaters, but lack of the clayey soil horizon makes these difficult to recognize as soils. Fe-rich intertidal dolomite would have formed beneath organic-rich microbial mats associated with reducing pore-waters containing much Fe^{2+}, but little reduced sulfate (Fig. 3.10). The low Fe^{2+} and Mn^{2+} concentration of most of the dolomitized subtidal facies suggests that the dolomite formed from relatively oxidizing marine fluids with low Mn^{2+} and Fe^{2+} content (Fig. 3.10). Relatively oxidizing marine pore fluids are compatible with the light color and probably low organic content of these subtidal facies.

Significance of Stable Isotopes in the Hungarian Triassic Dolomites: The limited $\delta^{18}O$ and $\delta^{13}C$ data in bulk subtidal limestones of the Dachstein Limestone, which are lighter than the marine calcites, suggests for this unit at least, that the limestones were stabilized by meteoric fluids, since their field lies within the paleosol field (Fig. 3.11). The $\delta^{18}O$ values of early dolomites, which are 2 to 4 ‰ heavier than the marine calcite ($\delta^{18}O$ of -1.4 to 0.2), suggests dolomitization by normal or slightly modified sea-water, and is compatible with the calcite - dolomite fractionation observed in modern dolomitizing peritidal settings (Friedman and O'Niel 1977; McKenzie 1981) (Figs. 3.11, 3.12).

Main Dolomite laminite caps were formed from slightly more evaporative marine waters than dolomitized laminites of the Dachstein Limestone which have lighter $\delta^{18}O$ values (Figs. 3.11, 3.13). This is compatible with the restricted inner platform setting and more abundant arid climate indicators in the Main Dolomite compared to the Dachstein Limestone.

However, the heaviest $\delta^{18}O$ dolomite values occur in the subtidal facies of the Main Dolomite, which are enriched by 1 to 2 ‰ compared to the tidal flat dolomites. This suggests that these formed by evaporative brine sinking through the tidal flats into the underlying subtidal sediment (De Groot 1973; Whitaker and Smart 1990; Montañez and Read 1992) (Figs. 3.11, 3.12).

Early burial, coarse-grained platform margin dolomite is much lighter (-2.7 to -6.3‰) than early dolomite, although carbon is not depleted (Fig. 3.11), which suggests

high temperature oxygen isotope fractionation in an oxidizing environment (Wilson et al. 1990). Given that calcite - water fractionation is $10^3 \ln a = 2.78(10^6 T^{-2}) - 2.89$ (Bottinga 1968) and using the $\delta^{18}O$ value of the Triassic marine calcite (-1.4 to -0.2 ‰ PDB) then the composition of 20 to 25 °C marine water in the Late Triassic would have been approximately zero ‰ SMOW. If the early burial coarse-grained dolomite formed from this marine water, the calculated temperature of the dolomite formation would be 80 to 90°C using the equation $10^3 \ln \alpha_{dolomite\text{-}water} = 3.2X10^6 T^{-2} - 3.3$ (Land 1983) which is compatible with the fluid inclusion data.

The similar $\delta^{13}C$ values of early dolomite and marine calcite suggests that $\delta^{13}C$ composition was inherited from the original marine sediment in a rock-buffered system (Figs. 3.11 and 3.12). They resemble most modern dolomite $\delta^{13}C$ signatures which were not heavily modified by oxidation of plant material or methane-related reactions (Mazzullo et al. 1987; Humphrey 1988) .

DOLOMITIZATION MODELS FOR THE HUNGARIAN TRIASSIC CARBONATES

The restriction of dolomite to laminite facies within cycles in the partially dolomitized Dachstein Limestone suggests that early dolomitization occurred in association with tidal flat settings (Fig. 3.15). The presence of dolomite in both transgressive and regressive laminites suggests that dolomitization was active during both initial transgression and subsequent tidal flat progradation of each cycle, as in Holocene Persian Gulf coastal sabkhas (McKenzie et al. 1980; Patterson and Kinsman 1982; McKenzie 1991). A similar model was invoked for dolomitization of the Early Ordovician Knox Group. Long periods of emergence of wide prograded intertidal - supratidal flats on the huge, gentle sloping carbonate platform would have promoted dolomitization (cf. Montanez and Read 1992). Repeated dolomitization events during each of the high frequency cycles may have generated a deeply refluxing fluid system within the underlying carbonates, causing dolomitization/recrystallization of subtidal limestone units.

Tidal flat dolomitization was initiated during transgression and more intensively during regression, when large supratidal flats developed. The Mg^{2+} source for the dolomite was most likely marine water moving through the sediment by tidal pumping

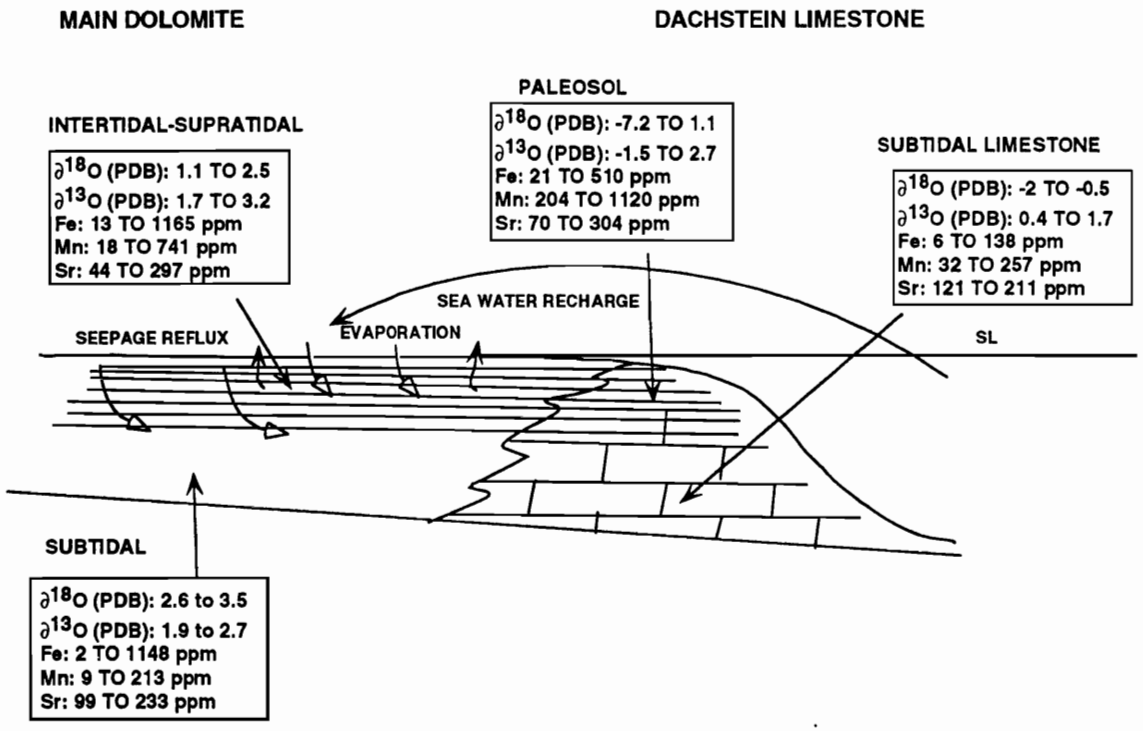

Fig. 15. Schematic model for formation of Hungarian Late Triassic dolomites . Subtidal dolomite is blank; intertidal/supratidal dolomite shown by horizontal lines; subtidal limestone is represented by limestone pattern.Typical trace element and isotope values of the various facies are shown in boxes.

Carballo et al. 1987; Mazzullo et al. 1987), coupled with reflux of marine water following storm-recharge (Illing et al. 1965; McKenzie et al. 1980; Patterson and Kinsman 1982; McKenzie 1991). Dolomitization of the laminite caps formed a very fine grained mimetic dolomite with relatively high Fe^{2+} content (up to 1165 ppm) indicating some reduction, and possible increased HCO_3^- concentration associated with oxidation of organic material in the algal mats, which could have promoted dolomitization (Baker and Kastner 1981; Land 1985; Sibley et al. 1987). Delta ^{18}O values of these dolomites suggest dolomitization by normal marine water (Figs. 3.11, 3.15). Their $\delta^{13}C$ is inherited from the host carbonate. Dolomitized intertidal laminites of the younger Dachstein Limestone have slightly lighter $\delta^{18}O$ values than similar facies of the Main Dolomite, probably indicating dolomitization by slightly diluted marine water (Figs. 3.11, 3.13, 3.15).

As flats became highly prograded, brines beneath them refluxed downward to dolomitize subjacent beds to form completely dolomitized cycles such as those of the Main Dolomite (De Groot 1973; Simms 1984; Kaufman 1994). These brines were enriched in ^{18}O and formed the isotopically heaviest dolomites in the sequence (Figs. 3.11, 3.12, 3.15). The Fe^{2+} and Mn^{2+} contents of these dolomites are low, reflecting the low organic content (light color) which maintained relatively oxidizing pore waters of the subtidal beds (Fig. 3.10).

With each cyclic regression, supratidal caliches, vadose pisolite facies developed on the top of inner platform cycles in the Main Dolomite, whereas clayey paleosol horizons capped the younger Dachstein Limestone cycles. The $\delta^{18}O$ signatures of these paleosols commonly are much lighter than supratidal facies that capped the Main Dolomite cycles, reflecting the influence of meteoric water during Dachstein diagenesis. Similarly, the light $\delta^{13}C$ values of many of the paleosols may reflect soil gas CO_2 in the waters, suggesting that some of the Dachstein supratidal flats were vegetated. However, other supratidal facies and paleosols that have slightly enriched $\delta^{13}C$ signatures may have formed from evaporated ground waters (Fig. 3.11, 3.13). Moderately reducing pore waters favored incorporation of Mn^{2+} in the dolomite/or clayey paleosol, the source of the Mn^{2+} perhaps being wind blown dust. Cyclic sea-level fluctuations repeatedly exposed the sediments to marine, mixed marine - meteoric and perhaps meteoric waters. This may have promoted loss of Na^+ and Sr^{2+} from the high Na- and Sr-dolomites to form low Na- and Sr-dolomites such as those on many Cenozoic platforms that have undergone repeated emergence events (Figs. 8 and 9). Sr^{2+} loss could have been due

gradual recrystallyzation/stabilization in marine pore fluids. Some of these dolomites also could have formed as original low Sr-dolomites where they replaced previously stabilized limestone (Vahrenkamp and Swart 1990; Hein et al. 1992).

Later, perhaps during the latest Triassic or Early Jurassic while the platform was still in communication with marine fluids, warm marine waters circulating through the platform dolomitized the platform margin, to form the relatively coarse-grained replacive dolomite containing fluid inclusions with marine salinities and ≈ 75 to 130°C temperatures of formation. These pore waters were relative oxidizing, which made these dolomites the most Fe^{2+}depleted. The high temperature formed a dolomite with highly depleted $\delta^{18}O$ values and rock buffered $\delta^{13}C$ values (Figs. 3.10, 3.11, 3.15). Circulation of the marine water may have been driven by thermal convection similar to massive late dolomites in the Alps, where intrusions acted as heat sources (Wilson et al. 1990; Miller and Folk 1994). We do not have direct evidence of an igneous heat source, but rocks in the Transdanubian Central Range apparently were never buried to depths where they could have attained these temperatures under normal geothermal gradients (Haas et al. 1990). The dolomitization may have happened during Jurassic rifting of Neo-Tethys with associated high heat flow and igneous activity (Juhasz et al. 1995).

Although most of the diagenetic alteration appears to have been associated with early diagenesis, we can not rule out further meteoric stabilization/or recrystallization of the dolomites with Sr^{2+} and Na^{+} loss during emergence of the platform in the Cretaceous and later, when major unconformities and bauxites were formed. However, the fact that the dolomites far below the top of the platform are stabilized to a similar degree as those in the upper platform argues against major later resetting associated with a single platform capping unconformity. This Sr^{2+} loss could reflect long term stabilization of the platform dolomites.

LONG TERM EUSTATIC AND CLIMATE CONTROL OF LATE TRIASSIC DOLOMITIZATION

Outer platform, limestone-rich Dachstein cycles interfinger with dolomitized cycles of the Main Dolomite to landward, suggesting that intensity of dolomitization increased into the interior of the platform. The inner platform facies became completely dolomitized because they were subjected to dolomitizing brines for longer times than

outer platform cycles whose caps only were dolomitized during the latest stages of progradation of tidal flats. In addition, this landward increase in dolomitization might reflect increasingly arid conditions away from the coast and onto the platform, which is a common feature of most of the Pangean monsoonal climate models (Crowley et al. 1989; Kutzbach and Gallimore 1989). However, the gradual landward onlap of the Dachstein Limestone onto the Main Dolomite through time, and the upward increase in amount of dolomite from the Main Dolomite to the Dachstein Limestone, must reflect some long term control on early dolomitization besides position on the platform.

Long Term Eustatic Control: Although early dolomitization was controlled by high-frequency (5th-order) sea-level changes, 3rd-order eustasy apparently had little influence on the large scale distribution of early dolomitization, in contrast to the model proposed for the Early Ordovician Knox Group, U.S. Appalachians, where 2nd- and 3rd-order eustasy controlled regional, early dolomitization patterns (Montañez and Read 1992). In the Ordovician Knox Group, most early dolomitization occurred during 3rd order relative sea-level fall. During 3rd order relative rise, only the cycle caps of limestone-dominated cycles of the outer platform were dolomitized. In contrast, the large scale distribution of the early dolomite on the Hungarian Triassic platform shows little relationship between intensity of dolomitization and the 2nd- or 3rd-order sea-level curves (Fig. 3.16). The dolomitization pattern shows a gradual trend from a completely dolomitized lower platform to a little dolomitized upper platform. The most intense dolomitization occurs during long term rise and decreases during long term eustatic fall on the haq at al, 1987 curve, which is opposite to that predicted by eustatic control. Furthermore, the decreasing dolomitization trend involved several third order cycles which appeared to have experted little influence (Figs. 3.3 and 3.16).

Climate Control: Evidence of relatively arid climate during deposition of the Main Dolomite, besides the intense early dolomitizaton, is the presence of caliche laminites and pisolites. Evidence of more humid climate during Dachstein time includes calcified filament molds in cycle caps, resembling present day freshwater Scytonema mats, more intense leaching and microkarsting of cycle tops, clayey paleosol horizons capping cycles indicating vegetation of supratidal surfaces, and lighter isotopic signatures up-section (Fig. 3.14).

The Late Triassic was a time of global greenhouse conditions, with little evidence for extensive continental ice sheets (Fischer 1982; Frakes et al. 1992). The Hungarian Triassic carbonates, which were deposited on the southern passive margin of the Tethys,

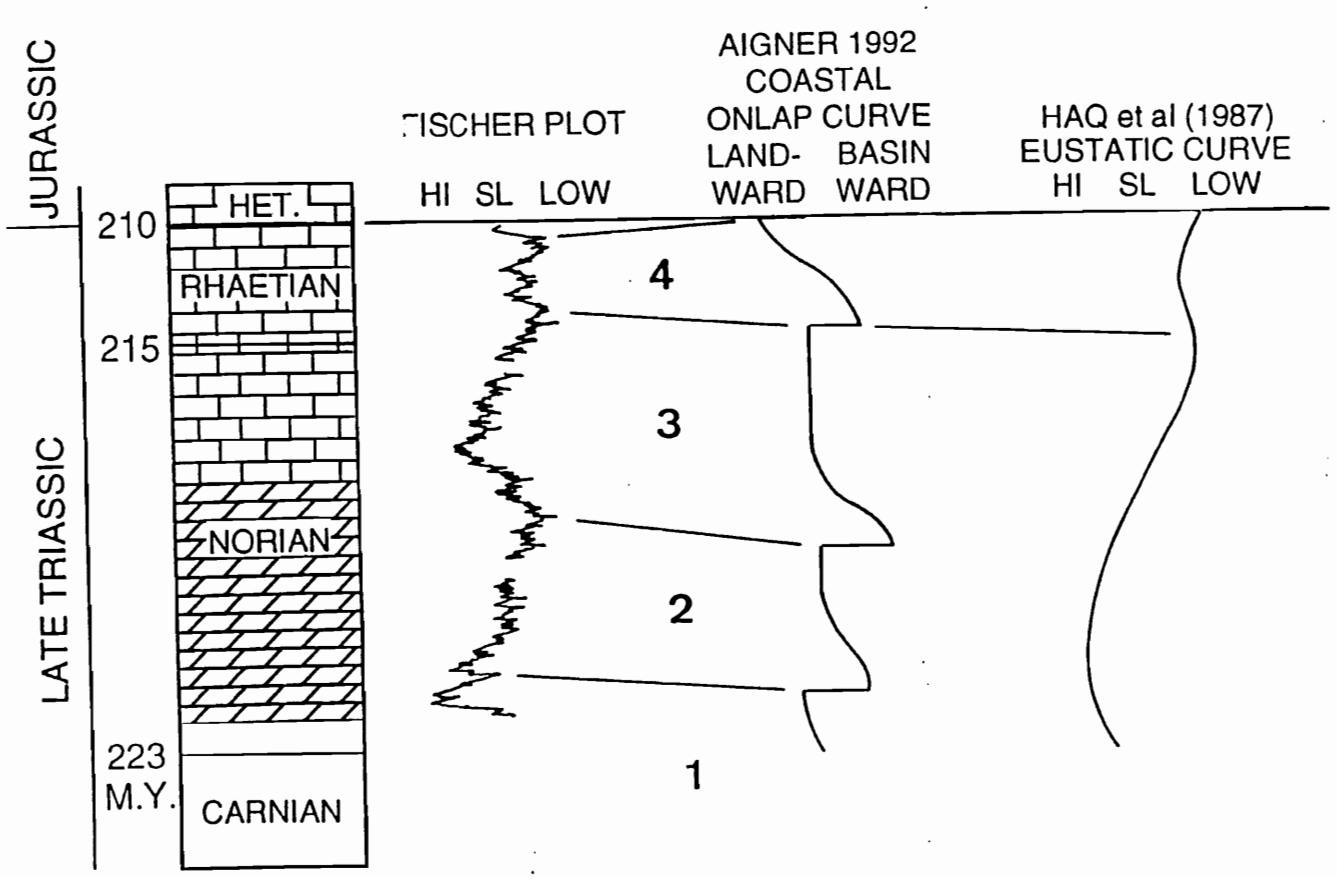

Fig. 16. Comparison of Fischer plot with coastal onlap curve of Aigner (1992) and Haq et al. eustatic curve. Dolomitized lower platform is shown by dolomite pattern; limestone rich upper platform shown by brick pattern. Numbers 1 to 4 refer to the sequences on the Fischer plot from Balog et al. (in press). There is no correlation between dolomitization pattern and the relative sea-level curves.

were part of the northward-moving Triassic Pangea (Klimetz 1983; Ziegler et al. 1983; Parrish et al. 1986; Parrish 1993)(Fig. 3.17). There were high mountain ranges along eastern North America and northwestern Africa from the Late Paleozoic collision (Hay et al. 1982; Parrish 1993) (Fig. 3.17). A mountain range may have occupied the northern part of the Tethys, following subduction of the Paleo-Tethyan plate (Klimetz 1983; Sengor 1985). With breakup of the supercontinent in the Late Triassic, rift-basins and associated highlands developed, peripheral to the Proto-Atlantic Ocean (Hay et al. 1982; Olsen 1986; Manspeizer 1994).

Climate modeling experiments using Pangean paleogeography suggest a strongly monsoonal climate (Robinson 1973; Parrish and Curtis 1982; Parrish and Peterson 1988; Crowley et al. 1989; Kutzbach and Gallimore 1989). Monsoonal climates are humid tropical climates characterized by highly seasonal wind direction and precipitation. They mainly reflect summer heating over large and/or elevated continental areas, which draws in moisture-laden air from the adjacent ocean. The air heats and rises over the land, causing precipitation which generates additional (latent) heat, further intensifying the "low" pressure cell. Highlands or plateaus accentuate this effect because they act as high altitude heat sources to the atmosphere. The strength of the summer monsoon is determined by the size of the continent, which contributes to maximum summer heating, and by the cross-equatorial pressure contrast between the low pressure cell above the continent and the subtropical high-pressure cell above the ocean. The size and surface water temperature of the adjacent ocean also is important as a source of moisture.

Maximum strength of the monsoon effect would occur when the continental areas in each hemisphere were equal in size, favoring alternate development of intense low pressure cells over each continent in northern and southern summers respectively. The Pangean monsoonal circulation probably peaked in the Late Triassic, and formed the "mega-monsoon" (Parrish and Peterson 1988; Dubiel et al. 1991; Parrish 1993). Most reconstructions show an equatorial region that is desert, particularly in the east. In the Tethyan area, the rainfall was concentrated in belts parallel to the northern and southern coasts of Tethys, and on rift highlands (Hay et al. 1982; Parrish 1993). Mountains along eastern North America and northern Tethys may have caused a modified monsoonal circulation, localizing low pressure areas and rainfall, or they may have promoted development of humid lakes at higher altitudes (Manspeizer 1994). A major feature of the Pangean monsoonal, seasonal rainfall model is that much of the tropical equatorial

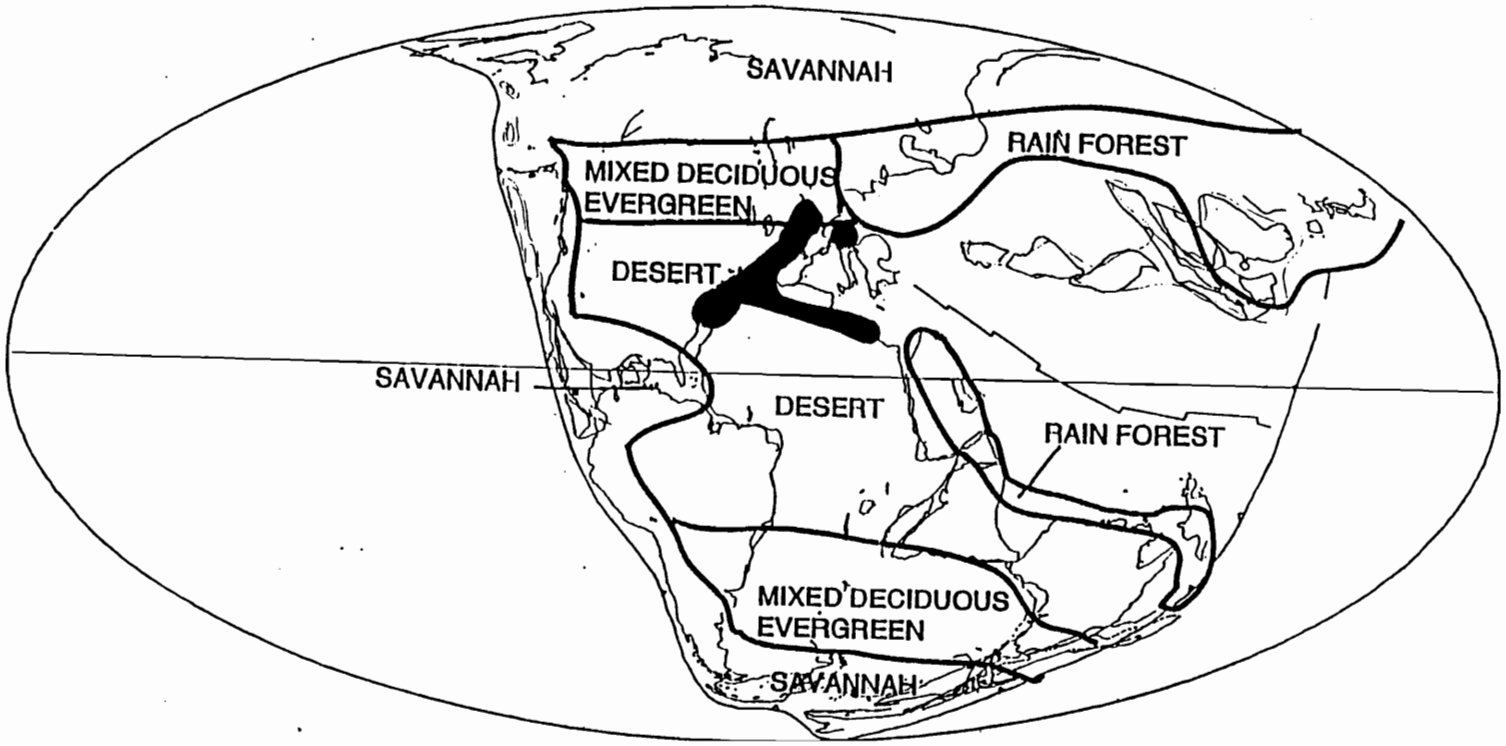

Fig. 17. Generalized paleoclimatic setting of the Hungarian Late Triassic platform (Scotese et al. 1992). The climate regions are a generalized composite from various sources including. During the hot Late Triassic, which was dominated by the megamonsoon, the subtropical and tropical belts were dominantly dry desert. With global cooling the rain forest and mixed forest belts would move equator ward, shrinking the desert belt. This along with northward drift of Pangea brought the Hungarian platform into cooler, wetter climates by Dachstein time.

belt is arid and the rainfall is coastal, and falls off rapidly inland (Robinson 1973; Parrish 1993).

The intensely dolomitized lower platform (Main Dolomite) of the Hungarian Triassic is compatible with such relatively arid equatorial setting, given the paleogeographic setting along the southern margin of the Tethys between 20 to 30° N latitude (Fig. 17) (Scotese and Golonka 1992). Between this huge desert and the Tethyan platform, evaporites were formed in basins in the North American rifts, along northern Africa and western Europe (Aigner and Bachmann 1992; Manspeizer 1994). On the platform, high temperature and high salinities promoted pervasive dolomitization of the Main Dolomite platform cycles. However, some monsoonal seasonal rainfall is indicated by the common early leaching evident in the Main Dolomite cycles.

From the Late Triassic to Early Jurassic, the global climate cooled and become more humid; (Tucker and Benton 1982; Frakes et al. 1992; Weems 1992; Manspeizer 1994). This cooling and increased humidity is indicated by the abrupt decrease in the volume of evaporites from the Late Triassic into the earliest Jurassic (Frakes et al. 1992), increase in the volume of the coal-bearing sediments (Ziegler et al. 1983; Parrish and Curtis 1982; Frakes et al. 1992), and the change from widespread Dicroidium flora of Gondwana to the cooler conifer/Benettitalean flora (Anderson and Anderson 1970; Barnard 1973; Tucker and Benton 1982). There also is a major decline in the ammonite abundance from the Late Triassic to the Early Jurassic (Fischer 1982), from a "polytaxic" to an "oligotaxic" state, reflecting a change from warmer high latitude waters to cooler waters (Fischer and Arthur 1977; Fischer 1982). Such a global cooling would decrease the width of the doldrums or monsoon belt. This would move the areas wetted by seasonal monsoons closer to the formerly drier areas of the equatorial belt, making these wetter.

Besides overall global cooling, some cooling may have been due to the well documented northward motion of the Pangea (Klimetz 1983; Ziegler et al. 1983; Parrish 1993). Paleomagnetic data indicate that the Transdanubian Range (with the Hungarian Late Triassic platform) moved 5 to 10° north during the Triassic (Marton 1986). This in conjunction with global cooling would have placed the platform in a cooler, wetter monsoonal setting by the Rhaetian, when the Dachstein Limestone was deposited. This decreased the intensity of dolomitization of the upper platform cycles, by inhibiting the development of dolomitizing brines on the flats, lowering surface temperature on the flats, and favoring vegetation of the emergent flats and formation of clayey paleosols

capping the Dachstein cycles, analogous to flats in parts of western Shark Bay, Australia (Read 1974).

High frequency precessional climate changes probably occurred during cycle deposition (Perlmutter and Matthews 1989). There is much evidence that Milankovitch orbital forcing strongly influences the intensity of the monsoonal circulation (Rossignol-Strick 1983; Olsen 1986; Jacobs and Sahagian 1993; Kutzbach 1994). Although this is not easily seen in the rock record, because of the restriction of the climate indicators to the cycle caps, the waxing and waning of the mega-monsoon may have influenced high frequency (10 to 20 k.y.) eustasy, which generated the carbonate cycles (Jacobs and Sahagian 1993).

In summary, the development and subsequent dolomitization of the Late Triassic Hungarian platform appears to have been strongly affected by climate. Milankovitch climate forcing likely generated the highly cyclic platform carbonates. High frequency eustasy interacting with a relatively arid, mega-monsoonal climate caused intense dolomitization of the lower platform (Main Dolomite). With cooling and increasingly humid conditions, dolomitization of the platform cycles decreased, to form the limestone-dominated upper platform in which dolomite is restricted to cycle caps overlain by clayey paleosols. Analogous climate-controlled regional dolomitization of carbonate platforms may be a widespread phenomenon in the Cenozoic, as exemplified by the widespread Miocene dolomitization events worldwide (Sibley 1980).

CONCLUSIONS

(1) The Late Triassic carbonate platform of Hungary is a 200 km wide, 3 km thick platform segment of the southern passive margin of the Tethys ocean. The platform succession is highly cyclic, and composed of meter-scale, probably precessional (≈20 k.y.) cycles. The lower platform (Main Dolomite) is dominated by pervasively dolomitized cycles, capped by caliche laminites and vadose pisolites, whereas the upper platform (Dachstein Limestone) contains limestone-dominated cycles, with dolomitization restricted to the intertidal laminites, which are capped by clayey paleosols.
(2) The abundant marine calcite was originally high Mg-calcite marine cement, contains microdolomite inclusions and has Mg/Sr ratios that suggest a Late Triassic sea-water composition similar to the present ocean. Delta ^{18}O and $\delta^{13}C$ values of these marine

cements are compatible with published Triassic values. Precursor sediments likely were mixtures of aragonite and high Mg-calcite.

(3) The Hungarian Triassic carbonates show little evidence of a late burial overprint. Most of the dolomite in the Hungarian platform was formed in and beneath tidal flats . During each high frequency cycle, algal laminites were dolomitized by marine water made reducing by organic algal mat in the sediments, to form dolomites slightly enriched in $\delta^{18}O$ relative to marine calcite, and relatively high amounts of Fe^{2+}. Subtidal dolomites of the lower platform were dolomitized by refluxing brine beneath the flats to form dolomites that have the heaviest $\delta^{18}O$ values, and low Fe^{2+} and Mn^{2+} reflecting low organic content of the subtidal sediment. Paleosols in the Dachstein Limestone appear to be depleted in ^{13}C, reflecting vegetated flats, and are enriched in Mn^{2+}, perhaps related to moderate reducing waters, and a windblown source of Mn^{2+}. Mn-rich dolomites in the Main Dolomite also may be supratidal facies. Na^{+} and Sr^{2+} contents of early dolomites indicate that they were reset by meteoric or mixed fluids, either during emergence following deposition of each carbonate cycle, and perhaps by long term emergence in the Late Mesozoic and Early Cenozoic.

(4) Coarse-grained platform margin dolomites with low Fe^{2+} and Mn^{2+} and light $\delta^{18}O$ values were formed from warm (74 to 130 °C), thermally driven, oxidizing marine water during early burial, possibly associated with Jurassic rifting.

(5) The distribution of early dolomitization on the platform was controlled by high frequency, low amplitude sea-level changes, but not by longer term eustasy. Instead, the intense early dolomitization of the lower platform reflects hot, semi-arid subtropical conditions associated with the Late Triassic "mega-monsoon". The more limited dolomitization of the upper platform reflects global cooling, shrinkage of the monsoon belt, and northward movement of the platform. These brought the platform into cooler, more humid climate that inhibited pervasive dolomitization, except in more arid interior platform areas. The strong climate control on dolomitization evidenced by the Hungarian Triassic platform may be a recurring theme on many Phanerozoic platforms.

REFERENCES CITED

Aharon, P., Socki, R.A., and Chan, L., 1987, Dolomitization of atolls by sea water convective flow: test of a hypothesis at Niue, South Pacific: Journal of Geology, v. 95, p. 187-203.

Aigner, T., and Bachmann, G.H., 1992, Sequence-stratigraphic framework of the German Triassic: Sedimentary Geology, v. 80, p. 115-135.

Anderson, H.M., and Anderson, J.M., 1970, A preliminary review of the Uppermost Permian, Triassic and lowermost Jurassic of Gondwanaland: Paleontol. Afr. Suppl., v. 13, p. 1-22.

Baker, P.A., and Kastner, M., 1981, Constraints on the formation of sedimentary dolomite: Science, v. 213, p. 214-216.

Balla, Z., 1988, Clockwise paleomagmatic rotations in the Alps in the light of the structural pattern of the Transdanubian Range (Hungary): Tectonophysics, v. 145, p. 277-292.

Balog, A., Haas, J., 1990, Sedimentological features and diagenesis of the Dachstein Limestone of the Nagyszal Mt. at Vac (A Vaci Nagyszalhegy Dachsteini meszkovenek szedimentologiai jellegei es diagenezise): Bull. Hung. Geol. Soc. (Foldtani Kozlony), v. 120, p. 11-18.

Balog, A., Haas, J., and Read, J.F., 1995, Shallow marine record of orbitally forced cyclicity in a Late Triassic carbonate platform, Hungary: Journal of Sedimentary Research (In press).

Banner, J.L., and Hanson, G.N., 1990, Calculation of simultaneous isotopic and trace element variations during water-rock interaction with applications to carbonate diagenesis: Geochimica et Cosmochimica Acta, v. 54, p. 3123-3137.

Barnard, P.D.W., 1973, Mesozoic floras, *in* Hughes, N.F., ed., Organisms and Continents through Time: p.

Behrens, E.W., and Land, L.S., 1972, Subtidal Holocene dolomite, Baffin Bay, Texas: Journal of Sedimentary Petrology, v. 42, p. 155-161.

Bodnar, R.J., 1992, Revised equation and table for freezing point depression of H_2O-salt fluid inclusions: PACROFI IV.

Bottinga, Y., 1968, Calculation of fractionation factors for carbon and oxygen exchange in the system calcite-carbon dioxide-water: Journal of Physical Chemistry, v. 72, p. 800-808.

Carballo, J.D., Land, L.S., and Miser, D.E., 1987, Holocene dolomitization of supratidal sediments by active tidal pumping, Sugarloaf Key, Florida: Journal of Sedimentary Petrology, v. 57, p. 153-165.

Carpenter, A.B., and Oglesby, T.W., 1976, A model for the formation of luminescently zoned calcite cements and its implications [abs.]: Geological Society of America, Abstracts with Programs, v. 8, p. 469-470.

Carpenter, S.J., Lohmann, K.C., Holden, P., Walter, L.M., Huston, T.J., and Halliday, A.N., 1991, $\delta^{18}O$ values, $^{87}Sr/^{86}Sr$ and Sr/Mg ratios of Late Devonian abiotic marine calcite: implications for the composition of ancient seawater: Geochimica et Cosmochimica Acta, v. 55, p. 1991-2010.

Crowley, T.J., Hyde, W.T., and Short, D.A., 1989, Seasonal cycle variations on the supercontinent of Pangaea: Geology, v. 17, p. 457-460.

Dawans, J.M., and Swart, P.K., 1988, Textural and geochemical alternations in Late Cenozoic Bahamian dolomites: Sedimentology, v. 35, p. 385-403.

De Groot, K., 1973, Geochemistry of tidal flat brines at Umm Said, SE Qatar, Persian Gulf, *in* Purser, B.H., ed., The Persian Gulf: New York, Springer-Verlag, p. 377-394.

Dickson, J.A.D., 1965, A modified staining technique for carbonates in thin section: Nature, v. 205, p. 587.

Dubiel, R.F., Parrish, J.T., Parrish, J.M., and Good, S.C., 1991, The Pangean megamonsoon — evidence from the Upper Triassic Chinle Formation, Colorado Plateau: Palaios, v. 6, p. 347-370.

Fischer, A.G., 1982, Long-term climatic oscillations recorded in stratigraphy, *in* Berger, W., ed., Climate in Earth History [National Academy of Sciences, Studies in Geophysics]: Washington, D.C., National Academy Press, p. 97-104.

Fischer, A.G., and Arthur, M.A., 1977, Secular variations in the pelagic realm, *in* Cook, H.E., and Enos, P., eds., Deep-water Carbonate Environments: Tulsa, OK, SEPM Special Publication No. 25, p. 19-49.

Frakes, L.A., Francis, J.E., and Syktus, J.I., 1992, Climate modes of the Phanerozoic. The history of the Earth's climate over the past 600 million years, Cambridge University Press, 274 p.

Friedman, I., and O'Niel, J.R., 1977, Compilation of stable isotope fractionation factors of geochemical interest [Data of Geochemistry, Sixth Edition]: U. S. Geological Survey Professional Paper 440-KK, 12 p.

Gregg, J.M., Howard, S.A., and Mazzullo, S.J., 1992, Early diagenetic recrystallization of Holocene (<300 years old) peritidal dolomites, Ambergris Cay, Belize: Sedimentology, v. 39, p. 143-160.

Haas, J., 1982, Facies analysis of the cyclic Dachstein Limestone Formation (Upper Triassic) in the Bakony Mountains, Hungary: Facies, v. 6, p. 75-84.

Haas, J., Csaszar, G., Kovacs, S., and Voros, A., 1990, Evolution of the western part of the Tethys as reflected by the geological formations Hungary: Acta Geod. Geoph. Mont. Hung., v. 25, p. 325-344.

Haas, J., and Dobosi, K., 1982, Felso-Triasz ciklusos karbonatos kozetek vizsgalata bakonyi alapszelvenyeken: Magyar Allami Foldtani Intezet Evi Jelentese 1980-rol, p. 135-168.

Haq, B.U., Hardenbol, J., and Vail, P.R., 1987, Chronology of fluctuating sea levels since the Triassic: Science, v. 235, p. 1156-1167.

Hay, W.W., Behensky, J.F., Barron, E.J., and Sloan, J.L., 1982,, Late Triassic Paleoclimatology of the proto-central North Atlantic rift system: Paleogeography, Paleoclimatology, Paleoecology, v. 40, p. 13-30.

Hein, J.R., Gray, S.C., Richmond, B.M., and White, L.D., 1992, Dolomitization of Quaternary reef limestone, Aitutaki, Cook Islands: Sedimentology, v. 39, p. 645-661.

Hoffman, A., Gruszczynski, M., and Malkowski, K., 1991, On the interrelationship between temporal trends in $\delta^{13}C$, $\delta^{18}O$, and $\delta^{34}S$ in the world ocean: Journal of Geology, v. 99, p. 355-370.

Humphrey, J.D., 1988, Late Pleistocene mixing zone dolomitization, southeastern Barbados, West Indies: Sedimentology, v. 35, p. 327-348.

Illing, L.V., Wells, A.J., and Taylor, J.C.M., 1965, Penecontemporary dolomite in the Persian Gulf, *in* Pray, L.C., and Murray, R.C., eds., Dolomitization and Limestone Diagenesis: Tulsa, OK, SEPM Special Publication No. 13, p. 89-111.

Jacobs, D.K., and Sahagian, D.L., 1993, Climate-induced fluctuations in sea level during non-glacial times: Nature, v. 361, p. 710-712.

Juhasz, E., Korpas, L., and Balog, A., 1995, 200 million years of karst history, Dachstein Limestone, Hungary: Sedimentology, v. 42 (in press).

Kaufman, J., 1994, Numerical models of fluid flow in carbonate platforms: implications for dolomitization: Journal of Sedimentary Research, Section A: Sedimentary Petrology and Processes, v. A64, p. 128-139.

Kazmer, M., and Kovacs, S., 1985, Triassic and Jurassic oceanic/paraoceanic belts in the Carpathian-Pannonian region and its surroundings, *in* Sengor, A.M.C., ed., Tectonic evolution of the Tethyan region: Dordrecht, London,, Kluwer Academic Publishers, p. 698.

Klimetz, M.P., 1983, Speculations on the Mesozoic plate tectonic evolution of eastern China: Tectonics, v. 2, p. 139-166.

Kohout, F.A., Henry, M.R., and Banks, J.E., 1977, Hydrogeology related to geothermal conditions of the Floridan plateau, *in* Smith, K.L., and Griffin, G.M., eds., The Geothermal Nature of the Floridan Plateau: Talahassee, FL, Florida Department of Natural Resources Special Publication 21, p. 1-34.

Kovacs, S., 1982, Problems of the "Pannonian Median Massif" and the distribution of Late-Paleozoic - Early Mesozoic isopic zones: Geologische Rundschau, v. 71, p. 617-648.

Kutzbach, J.E., 1994, Idealized Pangean climates: Sensitivity to orbital change, *in* Klein, G.D., ed., Pangea: Paleoclimate, Tectonics, and Sedimentation during Accretion, Zenith and breakup of a supercontinent, Vol. Special Paper, 288.: The Geological Society of America, p. 41-55.

Kutzbach, J.E., and Gallimore, R.G., 1989, Pangaean climates: megamonsoons of the megacontinent: Journal of Geophysical Research, v. 94, p. 3341-3357.

Land, L.S., 1973, Holocene meteoric dolomitization of Pleistocene limestone, north Jamaica: Sedimentology, v. 20, p. 411-424.

Land, L.S., 1983, The application of stable isotopes to studies of the origin of dolomite and to problems of diagenesis of clastic sediments, *in* Arthur, M.A., ed., Stable Isotopes in Sedimentary Geology: Tulsa, OK, SEPM Short Course No. 10, p. 4-1 to 4-22.

Land, L.S., 1985, The origin of massive dolomite: Journal of Geological Education, v. 33, p. 112-125.

Land, L.S., 1991, Dolomitization of Hope Gate Formation (N. Jamaica) by seawater: reassessment of mixing zone dolomite, *in* Taylor, H.P., O'Neil, J.R., and Kaplan, I.R., eds., Stable Isotope Geochemistry: a tribute to Samuel Epstein, Vol. Specia. Publication 3.: Geochemical Society, p. 121-133.

Land, L.S., and Hoops, G.K., 1973, Sodium in carbonate sediments and rocks: a possible index to the salinity of diagenetic solutions: Journal of Sedimentary Petrology, v. 43, p. 614-617.

Lohmann, K.C., and Walker, J.C.G., 1989, The $\delta^{18}O$ record of Phanerozoic abiotic marine calcite cements: Geophysical Research Letters, v. 16, p. 319-322.

Lorens, R.B., 1981, Sr, Cd, Mn, and Co distribution coefficients in calcite as a function of calcite precipitation rate: Geochimica et Cosmochimica Acta, v. 45, p. 553-561.

Manspeizer, W., 1994, The breakup of Pangea and its impact on climate: consequences of Variscian-Alleghanide orogenic collapse, *in* Klein, G.D., ed., Pangea: Paleoclimate, Tectonics, and Sedimentation during Accretion, Zenith and breakup of a supercontinent, Vol. Special Paper, 288.: The Geological Society of America, p. 169-185.

Marton, E., 1986, Paleomagnetism and tectonics in the Mediterranean region: Journal of Geodynamism, v. 7, p. 33-57.

Mazzullo, S.J., Reid, A.M., and Gregg, J.M., 1987, Dolomitization of Holocene Mg-calcite supratidal deposits, Ambergris Cay, Belize: Geological Society of America Bulletin, v. 98, p. 224-231.

McKenzie, J.A., 1981, Holocene dolomitization of calcium carbonate sediments from the coastal sabkhas of Abu Dhabi, U.A.E.: a stable isotope study: Journal of Geology, v. 89, p. 185-198.

McKenzie, J.A., 1991, The dolomite problem: an outstanding controversy, *in* Muller, D.W., McKenzie, J.A.a., and Weissert, H., eds., Controversies in modern geology: London, San Diego, Academic Press, p.

McKenzie, J.A., Hsu, K.J., and Schneider, J.F., 1980, Movement of subsurface waters under the sabkha, Abu Dhabi, UAE, and its relation to evaporative dolomite genesis, *in* Zenger, D.H., Dunham, J.B., and Ethington, R.L., eds., Concepts and Models of Dolomitization: Tulsa, OK, SEPM Special Publication No. 28, p. 11-30.

Miller, J.K., and Folk, R.L., 1994, Petrographic, geochemical and structural constraints on the timing and distribution of postlithification dolomite in the Rheatian Portoro (Calcare Nero) of the Portovenere Area, La Spezia, Italy, *in* Purser, B., Tucker, M., and Zenger, D., eds., Dolomites, Vol. Special Publication 21: International Association of Sedimentary Geologists, p. 187-202.

Montañez, I.P., and Read, J.F., 1992, Eustatic control on early dolomitization of cyclic peritidal carbonates: evidence from the Early Ordovician Upper Knox Group, Appalachians: Geological Society of America Bulletin, v. 104, p. 872-886.

Morse, J.W., and Bender, M.L., 1990, Partition coefficients in calcite: Examination of factors influencing the validity of experimental results and their application to natural systems: Chemical Geology, v. 82, p. 265-277.

Olsen, P., 1986, A 40-million-year lake record of Early Mesozoic orbital forcing: Science, v. 234, p. 842-848.

Parrish, J.M., Parrish, J.T., and Ziegler, A.M., 1986, Permian-Triassic paleogeography and paleoclimatology and implications for therapsid distributions, *in* Hotton, N.H., III, MacLean, P.D., Roth, J.J., and Roth, E.C., eds., The Ecology and Biology of Mammal-like Reptiles: Washington, D.C., Smithsonian Press, p. 109-132.

Parrish, J.M., and Peterson, F., 1988, Wind direction predicted from global circulation models, and wind directions determined from eolian sandstones of the Western United States - a comparison: Sedimentary Geology, v. 56, p. 261-282.

Parrish, J.T., 1993, Climate of the supercontinent Pangea: Journal of Geology, v. 101, p. 215-233.

Parrish, J.T., and Curtis, R.L., 1982, Atmospheric circulation, upwelling and organic rich rocks in the Mesozoic, Cenozoic eras: Palaeogeography, Palaeoclimatology, v. 40, p. 31-66.

Patterson, R.J., and Kinsman, D.J.J., 1982, Formation of diagenetic dolomite in coastal sabkha along Arabian (Persian) Gulf: American Association of Petroleum Geologists Bulletin, v. 66, p. 28-43.

Perlmutter, M.A., and Matthevws, M.D., 1989, Global cyclostratigraphy - a model, *in* Cross, T.A., ed., Quantitative dynamic stratigraphy: New Jersey, Prentice Hall, p. 233-260.

Railsback, L.B., 1990, Influence of changing deep ocean circulation on the Phanerozoic oxygen isotopic record: Geochimica et Cosmochimica Acta, v. 54, p. 1501-1509.

Railsback, L.B., and Anderson, T.F., 1987, Control of Triassic seawater chemistry and temperature on the evolution of post-Paleozoic aragonite-secreting faunas: Geology, v. 15, p. 1002-1005.

Randazzo, A.F., and Hickey, E.W., 1978, Dolomitization in the Floridan aquifer: American Journal of Science, v. 278, p. 1177-1184.

Read, J.F., 1974, Calcrete deposits and Quaternary sediments, Edel Province, Western Australia, *in* Logan, B.W., Read, J.F., Hagan, G.M., Hoffman, P., Brown, R.G., Woods, P.J., and Gebelein, C.D., eds., Evolution and Diagenesis of Quaternary Carbonate Sequences, Shark Bay, Western Australia: Tulsa, OK, American Association of Petroleum Geologists Memoir 22, p. 250-282.

Robinson, P.L., 1973, Paleoclimatology and continental drift, *in* Tarling, D.H., and Ronov, A.B., eds., A comparative estimate of volcanic intensity on continents and in oceans, Vol. 22: International Geology Review, p. 1383-1389.

Rossignol-Strick, M., 1983, African monsoons, an immediate response to orbital insolation: Nature, v. 303, p. 46-49.

Saller, A.H., 1984, Petrologic and geochemical constraints on the origin of subsurface dolomite, Enewetak Atoll: an example of dolomitization by normal sea water: Geology, v. 12, p. 217-220.

Sandberg, P.A., 1983, An oscillating trend in Phanerozoic non-skeletal carbonate mineralogy: Nature, v. 305, p. 19-22.

Schwarzacher, W., and Haas, J., 1986, Comparative statistical analysis of some Hungarian and Austrian Upper Triassic peritidal carbonate sequences: Acta Geologica Hungarica, v. 29, p. 175-196.

Scotese, C.R., and Golonka, J., 1992, PALEOMAP paleographic atlas, *in* , PALEOMAP Progress Report, Vol. 20: Department of Geology, University of Texas, at Arlington,

Sengor, A.M.C., 1985, The story of Tethys: How many wives did Okeanus have?: Episodes, v. 8, p. 3-12.

Sibley, D.F., 1980, Climatic control of dolomitization, Seroe Domi Formation (Pliocene), Bonaire, N.A., *in* Zenger, D.H., Dunham, J.B., and Ethington, R.L., eds., Concepts and Models of Dolomitization: Tulsa, OK, SEPM Special Publication No. 28, p. 247-258.

Sibley, D.F., Dedoes, R.E., and Bartlett, T.R., 1987, Kinetics of dolomitization: Geology, v. 15, p. 1112-1114.

Simms, M.A., 1984, Dolomitization by groundwater-flow systems in carbonate platforms: Transactions of the Gulf Coast Association of Geological Societies, v. 34, p. 411-420.

Tollman, A., 1987, Neue Wege in der Ostalpengeologie und die Beziehungen zum Ostmediterran: Mitteilungen der Österreichischen Geologischen Gesellschaft, v. 80, p. 47-113.

Tucker, M., and Benton, M.J., 1982, Triassic environments, climates and reptile evolution: Palaeogeography, Palaeoclimatology, Palaeoecology, v. 40, p. 361-379.

Vahrenkamp, V.C., and Swart, P.K., 1990, New distribution coefficient for the incorporation of strontium into dolomite and its implications for the formation of ancient dolomites: Geology, v. 18, p. 387-391.

Vahrenkamp, V.C., and Swart, P.K., 1991, Episodic dolomitization of late Cenozoic carbonates in the Bahamas: evidence from strontium isotopes: Journal of Sedimentary Petrology, v. 61, p. 1002-1014.

Veizer, J., 1983, Chemical diagenesis of carbonates: theory and application of trace element technique, *in* Arthur, M.A., ed., Stable Isotopes in Sedimentary Geology: Tulsa, OK, SEPM Short Course No. 10, p. 3-1 to 3-100.

Ward, W.C., and Halley, R.B., 1985, Dolomitization in a mixing zone of near-seawater composition, Late Pleistocene, northeastern Yucatan Peninsula: Journal of Sedimentary Petrology, v. 55, p. 407-420.

Weems, R.E., 1992, The "terminal Triassic catastrophic extinction event" in respective: a rewiev of Carboniferous through Early Jurassic terrestrial vertebrate extinction patterns: Paleogeography, Paleoclimatology, Paleoecology, v. 94, p. 1-29.

Whitaker, F.F., and Smart, P.L., 1990, Active circulation of saline ground waters in carbonate platforms: evidence from the Great Bahama Bank: Geology, v. 18, p. 200-203.

Wilkinson, B.H., 1982, Cyclic cratonic carbonates and Phanerozoic calcite seas: Journal of Geological Education, v. 30, p. 189-203.

Wilson, E.N., Hardie, L.A., and Phillips, O.M., 1990, Dolomitization front geometry, fluid flow patterns, and the origin of massive dolomite: the Triassic Latemar buildup, northern Italy: American Journal of Science, v. 290, p. 741-796.

Wilson, K.M., Rosol, M.J., and Hay, W.W., 1989, Global Mesozoic reconstruction using revised continental data and terrain histories: A progress report:, *in* W., H.J., ed., Deep structure and past kinematics of accreted terraine, Vol. 50: Geophysical monograph, p. 1-41.

Ziegler, A.M., Scotese, C.R., and Barrett, S.F., 1983, Mesozoic and Cenozoic paleographic maps, *in* Borsche, P., and Sundermann, J., eds., Tidal friction and the earth's rotation, II: New York, Springer-Verlag, p. 240-252.

Chapter 4: Spectral analysis of lithologic and wireline logs, and synthetic modelling of Late Triassic Hungarian platform carbonates

ABSTRACT

Spectral analysis and modelling were done on sections from the Late Triassic Hungarian platform, a two to 3 km thick highly cyclic carbonate succession that was originally part of the Alpine Triassic Tethyan passive margin. The meter scale cycles consist of subtidal carbonates, tidal flat laminites and supratidal/subaerial caliches or clayey paleosols. The cycles include transgressive, regressive and symmetrical transgressive-regressive cycles. Spectral analysis of lithologic logs and wireline logs, and of synthetic stratigraphic sections generated under known Milankovitch sea level curves, indicate that the Late Triassic platform carbonates of Hungary, formed as a result of Milankovitch climate forcing, actually preserve a relatively poor record of orbital forcing.

Spectra of time series based on lithologic logs and wireline logs show peaks centered around 2.5m (interpreted to be the basic precessional cycle), 3.4 m, 4.4 to 5.6 m (obliquity), 8.5 to 12 m (100 k.y.) and 28 to 40 m (possibly 400 k.y.). Lithologic logs gave the best spectra, whereas spectra from the gamma ray logs and self potential logs were more sensitive for the lower frequency signals. However spectra from neutron logs appeared to be relatively sensitive to all frequencies. The poor spectra of the wireline logs may reflect the fact that the logs used were done in the early 70's and better results might be obtained from logs done with more modern tools.

Spectra from computer-generated synthetic stratigraphies formed under known input sea level curves involving various Milankovitch signals, closely resemble the actual spectra from lithologic logs of the cores. Best fits of spectra were obtained with 19 to 23 k.y. sea level changes of 5 m, 100 k.y. of 5 m and a relatively small signal for obliquity and long term eccentricity. In view of the relatively poor radiometric time control, the similarity between synthetic and spectra from the cores provide the best evidence that Milankovitch eustasy involving a dominant precessional signal and a lesser eccentricity signal were important in the formation of the Hungarian cycles. Obliquity and long term eccentricity apparently had a lesser effect the cycle bundling.

INTRODUCTION

Since the pioneering work of (Gilbert 1895; Milankovitch 1941; Emiliani 1966; Imbrie and Imbrie 1979; Berger 1984; Berger and Vincent 1986) study has focused on how Milankovitch orbital forcing is expressed in the sedimentary record.

The main statistical method used is spectral analysis (Weedon 1990; Weedon 1993), whose major limitation is that sedimentary cycles are measured in thickness and not time scale (Weedon 1990). Conversion of stratigraphic thickness to time relies on radiometric dating of the stratigraphic record, which generally is poorly constrained. Another problem is the presence of hiatuses in shallow water platform carbonates.

The Late Triassic highly cyclic Hungarian platform carbonates provide a data set for a spectral analysis that can be compared to the excellent, near complete Milankovitch record of the Late Triassic rift lake deposits of the Newark Supergroup (Haas 1982; Olsen 1986; Balog et al. 1995). The duration of the meter-scale elementary cycles of the Hungarian carbonates appear to be precessional cycles (~20 k.y.) and there is a weak bundling into longer period cycles (Balog et al. 1995). The cyclic record is complicated by hiatuses represented by paleosol horizons. In this study we analyzed several time-series based on lithology, gamma-ray logs, self-potential and neutron density logs to assess which logs, if any appeared to preserve the best signal of orbital forcing. Spectra were then compared spectra based on synthetic cyclic platform successions generated using PHIL (Bowman 1994). Although preliminary, the study suggests that wireline logs through shallow platforms may provide informations on stratigraphic forcing mechanisms.

STRATIGRAPHIC SETTING

The large Late Triassic carbonate platform of the Transdanubian Range, Hungary were part of the southwestern passive margin of the Tethys seaway (Fig. 4.1) (Kazmer and Kovacs 1985). They were originally situated between the Northern and Southern Alps and moved eastward to their present location along strike slip faults during the Paleogene (Kazmer and Kovacs 1985; Balla 1988; Balog et al. 1995). They occur a in a single, fault-bounded megatectonic unit.

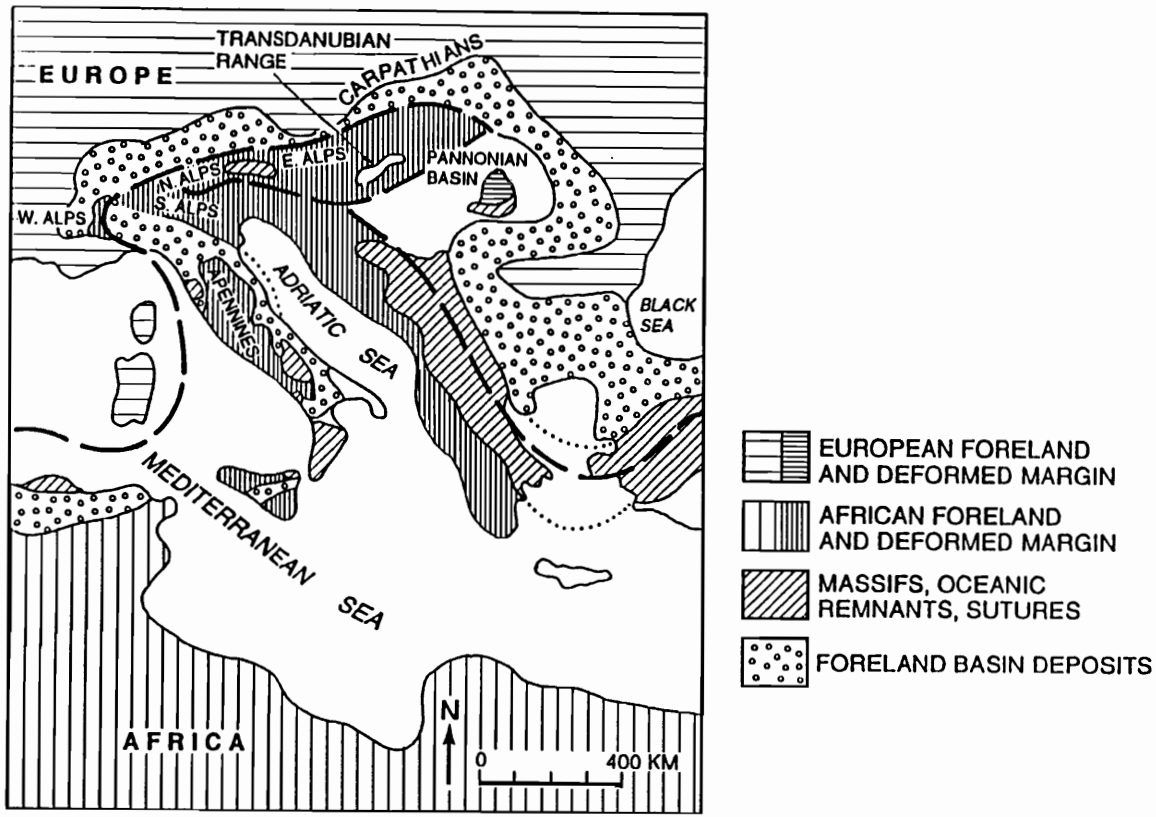

Fig. 4.1. Regional geological location map of the Triassic carbonates of the Transdanubian Range (arrowed), Hungary. Boundaries of major lithotectonic blocks bounded by heavy dashed lines. The Transdanubian carbonates are allochthonous, and were transported by strike-slip faulting from their original position between the Northern and Southern Alps.

The Late Triassic carbonate platform was an aggraded, flat-topped platform. The "lower platform unit" is the Main Dolomite Formation (600-1500 m thick) which contains completely dolomitized carbonate
cycles. The Main Dolomite is overlain by the "upper platform" Dachstein Limestone (up to 1200 m thick), composed of limestone cycles in which only cycle caps are dolomitized (Fig. 4.2).

These carbonates are highly cyclic and have complex early diagenetic history (Haas and Dobosi 1982; Balog et al. 1995). Meter-scale cycles are from less than 1 m to over 5 m thick, and consist of, from base to top (Fig. 4.3):

1. Supratidal Sediments: These are generally dolomitized caliche laminite and vadose pisolite in the dolomitized lower platform. In the upper platform, they consist of red, or green, partly dolomitized clayey lime mudstone.

2. Transgressive Tidal Flat Laminite: These dolomites have well developed microbial lamination, fenestrae, and mudcracks. The fenestrae are filled by internal sediment, crystal-silt, pellet-silt and/or pendant, radiaxial or blocky calcite or rarely dolomite cement overlain by marine calcite.

3. Subtidal Facies: These are completely dolomitized in the lower platform, and are mainly limestone in the upper platform. They include peloidal skeletal wackestone/packstone with rare oolitic grainstone.

4. Regressive Tidal Flat Laminites: These dolomites are similar to transgressive laminites, but commonly are more leached, especially in the Dachstein Limestone cycles, with abundant internal sediment and mudcracks filled by internal sediment.

These are overlained by a disconformity, paleosols, transgressive laminites or subtidal facies of the next cycle.

These cycles can be either upward deepening, upward shallowing or symmetrical transgressive-regressive cycles (Haas and Dobosi 1982; Balog et al. 1995).

CONSTRUCTION AND ANALYSIS OF THE TIME SERIES

"Time-series" used in the analysis are actually amplitude vs. depth plots, because stratigraphic distance is used as a proxy for "time" (Schwarzacher and Haas 1986).

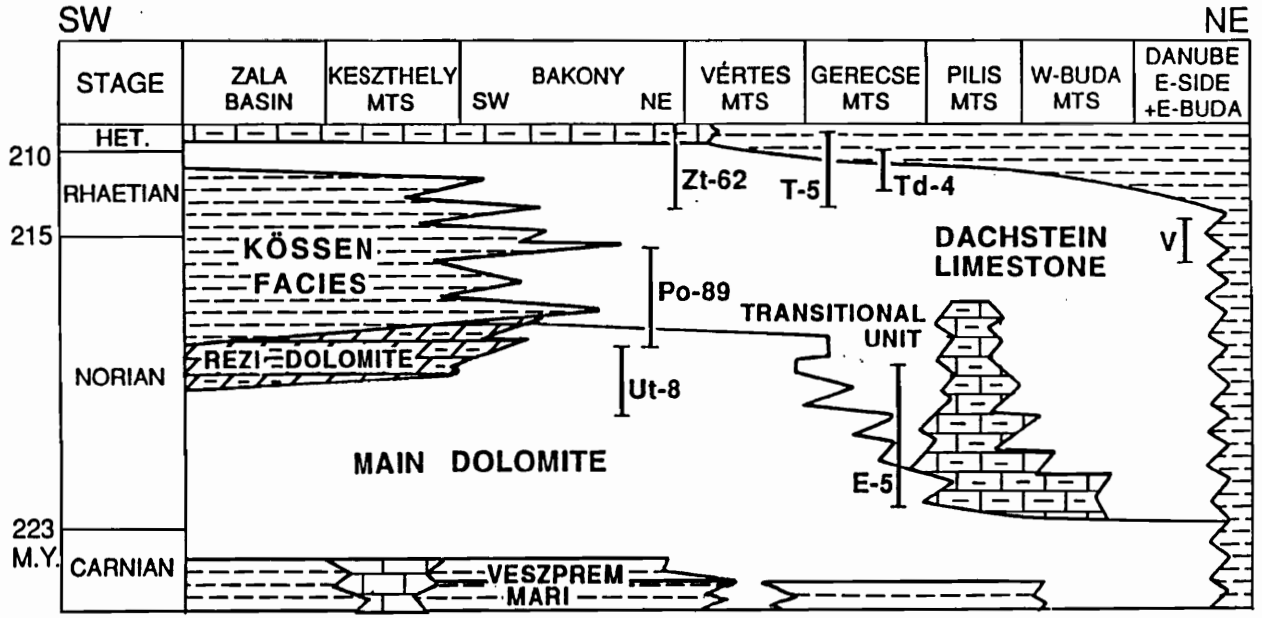

Fig. 4.2. Depth-distance stratigraphic chart showing stratigraphic units of the Triassic carbonate platform, Transdanubian Range. Stratigraphic positions of the cores are shown by heavy vertical bars. Modified from Haas (1988). Time (m.y.) shown alongside depth section for reference. Landward is to left (southwest), and seaward edge of platform is to right (northeast).

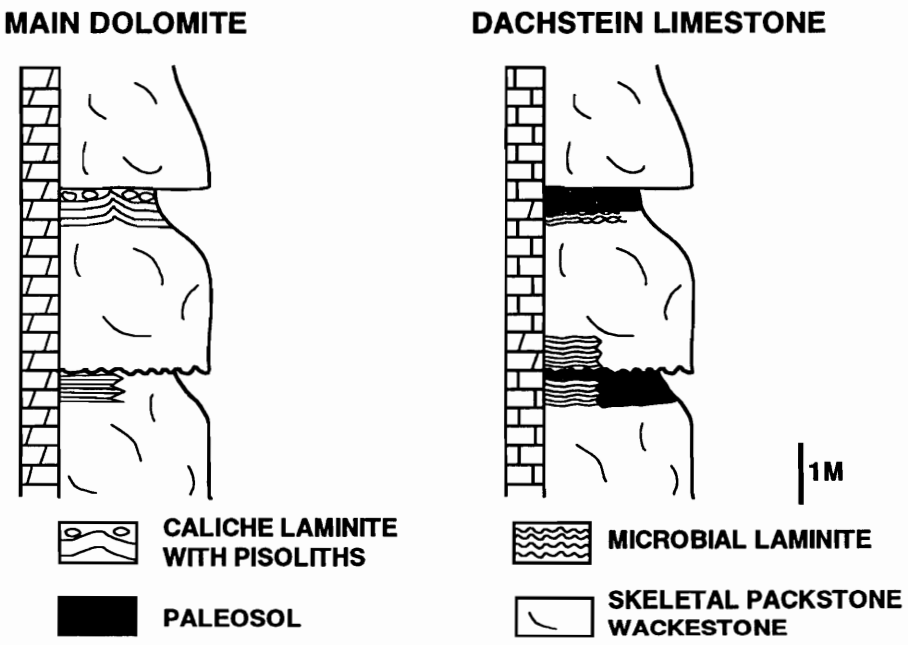

Fig. 4.3. Small portions of representative stratigraphic columns showing typical cyclic successions in Main Dolomite and Dachstein Limestone. Cycles in the Main Dolomite are completely dolomitized, whereas those in the Dachstein Limestone are limestone with dolomite.

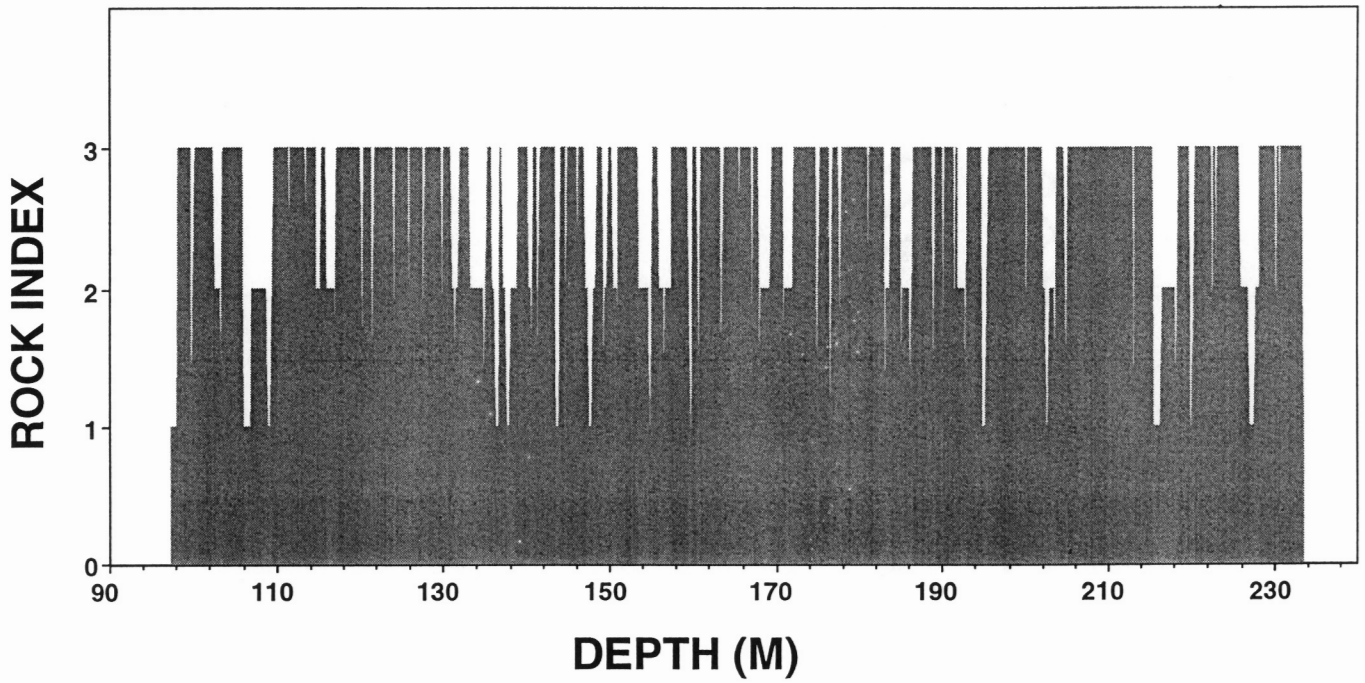

Fig. 4.4. Time-series of part of the core Po-89 showing rock index (1=paleosol, supratidal carbonates; 2=intertidal carbonates; 3=subtidal carbonates) vs. stratigraphic depth.

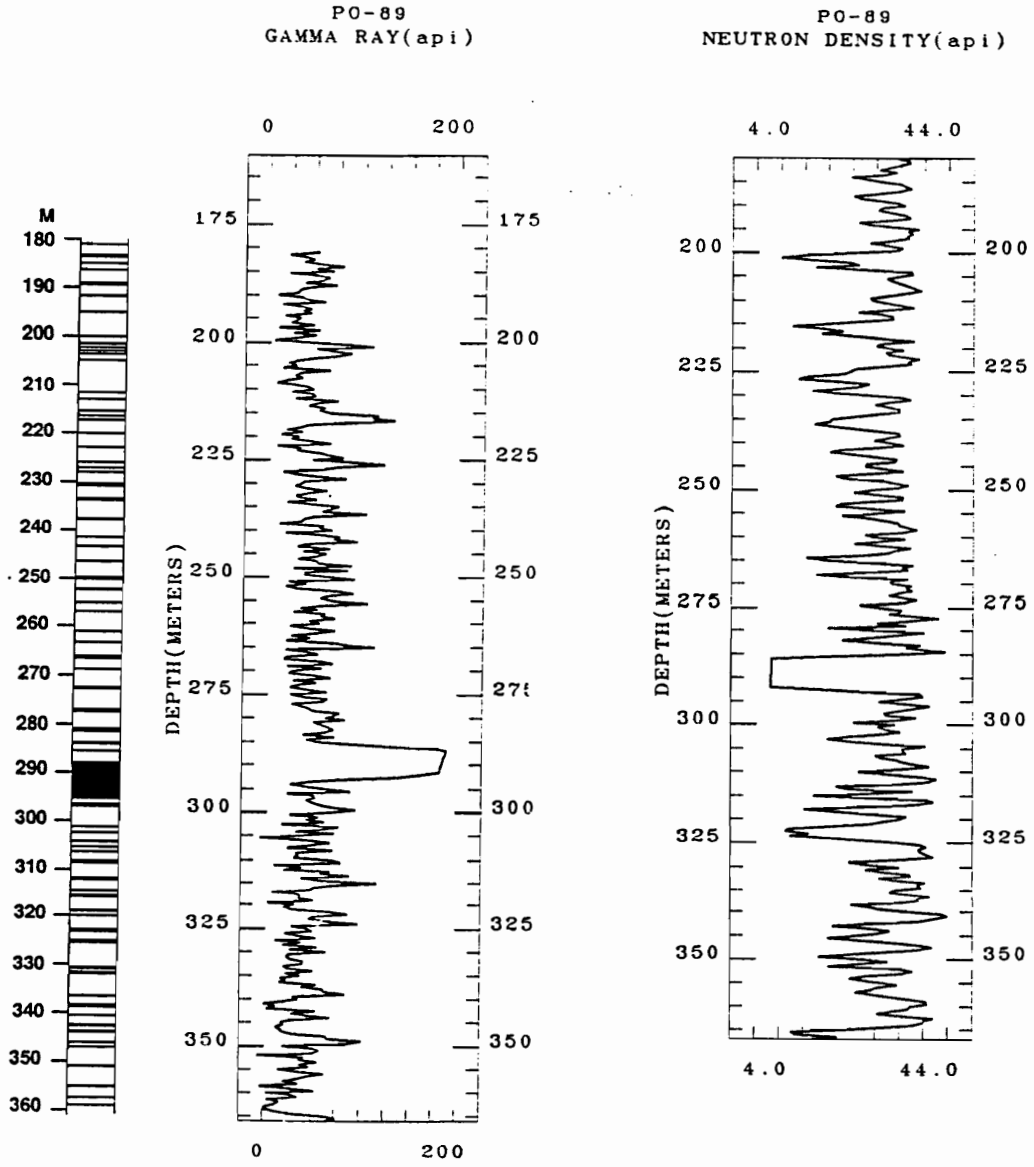

Fig. 4.5. Simplified stratigraphic column of Po-89 core (black represents cycle caps with clayey mud in them) along with gamma ray and neutron log. The thick clayey horizon around 290 m is a younger clay filled fracture.

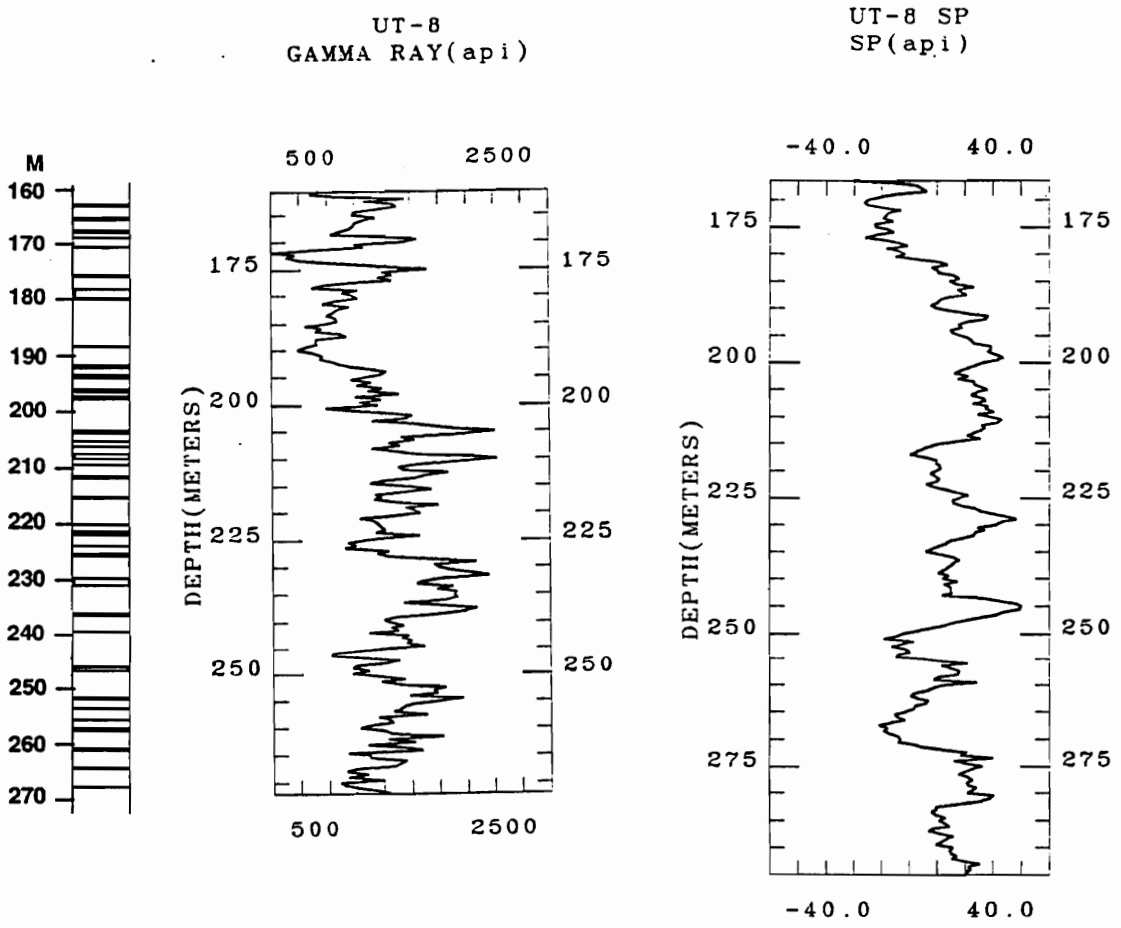

Fig. 4.6. Simplified stratigraphic column of Ut-8 core (black represents cycle caps with clayey mud in them) along with gamma ray and Self Potential logs.

Data in this paper are from cores from the Hungarian carbonate platform (Fig.4.2). Detailed bed-by bed logs were made of the continuous diamond drill cores of Po-89 (400 m) and Ut-8 (300 m) (Fig. 4.2). The lithologic "time series" were generated from these bed by bed logs using a rock type index of relative water depth (1 = paleosol, supratidal carbonates; 2 = intertidal carbonates; 3 = subtidal carbonates) with a sampling interval of 0.2 m (Fig. 4.4).

Gamma ray, neutron-, and self potential logs of the wells were constructed from the original logs by digitizing the stratigraphic position of peaks and trough, which were than automatically sampled at 0.5 m (Figs. 4.5, 4.6).

Synthetic cyclic sections were generated for the Late Triassic carbonate platform using PHIL modeling program (Bowman 1994). Synthetic platform stratigraphies constrained by field data were made using a digitized initial platform topography, subsidence rate increasing basinward, a tropical carbonate production curve, and 3rd order sea level curve with superimposed Milankovitch sea level curves which were altered between runs (Table 4.1, Fig 4.7.). We generated a stratigraphic column for each model at the 175 km position on the platform which appeared to generate the most complete cycle stratigraphies that resembled the actual stratigraphies. From the lithologic columns, we created time-series based on rock index sampled every 0.2 m (Fig 4.8).

A Fast Fourier Transform (FFT) algorithm was used to generate the amplitude spectrum of each the time series. Spectral mapping of the logs was performed using a Short-Time Fourier Transform (STFT) (Nawab and Quatieri 1988). In this method, the data are sampled within a sliding window and the Fourier amplitude spectrum is calculated separately for each window in turn. A cosine or Hamming window is used to sample the data instead of a rectangular window, as this reduces possible side-lobe "ringing" in the amplitude spectra. The resulting map provides information on the variability of amplitude spectrum with depth. Parameters for window length and depth-step were chosen to optimize both the frequency and depth resolution. Values for window length and depth-step were iterated until the reconstructed logs were nearly identical to the original logs. We used a 20 m window length and a 2.8 m depth step.

Amplitude Spectrum of "Time Series" Based on Lithology:

The amplitude spectrum of the lithologic time-series of cores Po-89 and Ut-8 show well developed peaks that correspond reasonably well on both plots (Table 4.2, Figs. 4.9, 4.10). At the high frequency end of the spectrum, peaks are centered around 2.2 to 2.4 m

Table 4.1

Model	19 k.y.	22 k.y.	40 k.y.	100 k.y.	400 k.y.	1 M.A.
A	5m	5m	2.5m	5m	2.5m	7m
B	5m	5m	2.5m	2.5m	2.5m	7m
C	5m	5m	0	2.5m	2.5m	7m
D	5m	5m	2.5m	0	2.5m	7m

Table 4.2

	λ/M	A	λ/M	A	λ/M	A	λ/M	A	λ/M	A	λ/M	A	λ/M	A	λ/M	A	λ/M	A
Lithology time series																		
Po-89	40	6.4	26	4.9	12	10	8.5	9.7	5.6	4	4.4	5.2	3.4	14	3	9.2	2.4	5.4
Ut-8			29	17	9.1	15	8.5	14	5.4	15	4.3	12	3.8	6	3	6.4	2.3	6
Synthetic/A	28	27	12	15	10	18	7.7	21	5.6	10	4.8	19			3.2	9.5	2.4	5
Synthetic/B	33	26	17	9.2	7.7	27			5.9	24.5	4.5	17	3.9	8.2	3.3	11.2	2.6	5.6
Synthetic/C (40 k.y. absent)	31	36	22	25	9	22	7.4	8.5	6.4	7	4.8	5.5	3.9	7.5	3.2	12	2.6	10
Synthetic/D (100 k.y. absent)			19	15	13	17	7.5	18	5.3	26.7	4.7	12	3.9	12	3.2	10	2.6	3
Gamma-ray time series																		
Po-89	40	6	28	13	12	12	8.7	3.5	5.7	2.8	4.4	3.4						
Ut-8			28	13	11	2.5	8.6	3.5	5.6	5	4.8	2.8	3.5	13				
Neutron-log time series																		
Po-89			29	16	12	13	8.7	8.2	5.2	8	4.4	3.9	3.9	6	3.5	3.2	2.9	6.2
SP-log time series																		
Ut-8	40	36	25	11	16	23	8.9	4	6.8	2								

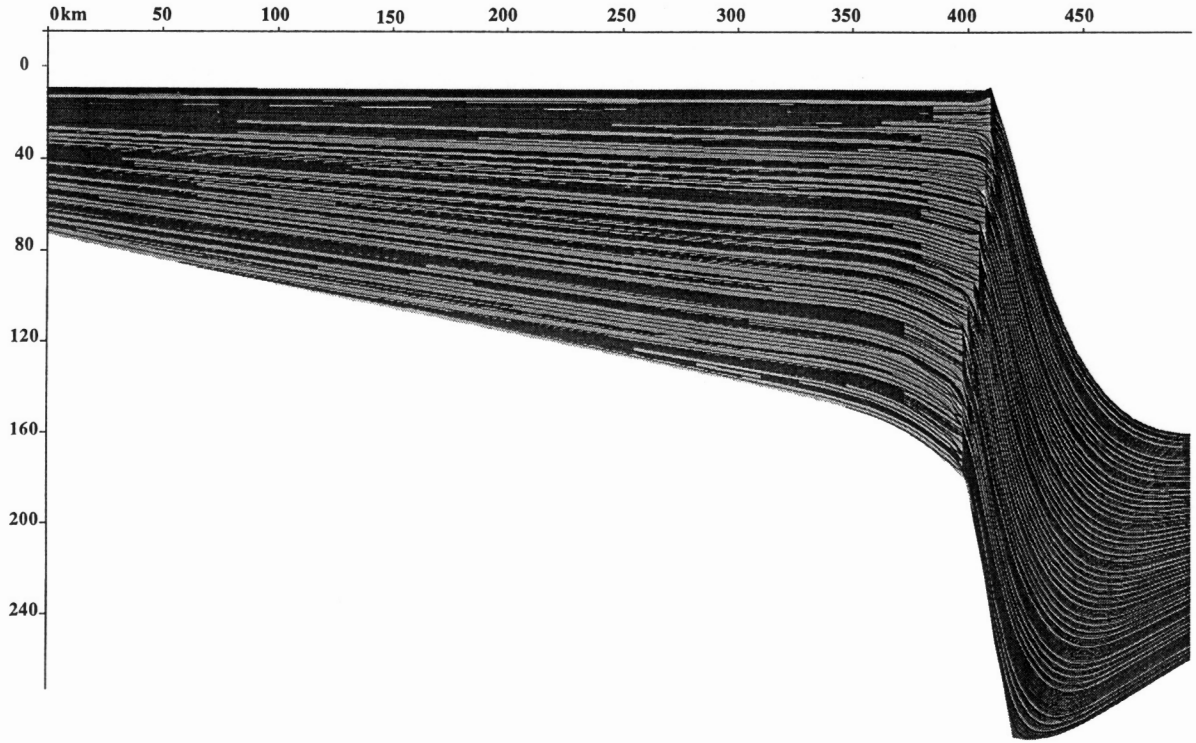

Fig. 4.7. Synthetic model of the Late Triassic carbonate platform generated by using PHIL modeling program (Bowman 1994). Platform stratigraphies were generated using a digitized initial platform topography, subsidence rate increasing basinward, a tropical carbonate production curve, and 3rd order with superimposed Milankovitch sea level curve of 19 to 23 k.y.=5 m, 40 k.y.=2.5 m, 100 k.y.=5 m, 400 k.y.=2.5 superimposed on a third order sea level change of 7 m. On the platform stratigraphy gray represents subtidal, and dark gray represents supratidal carbonates.

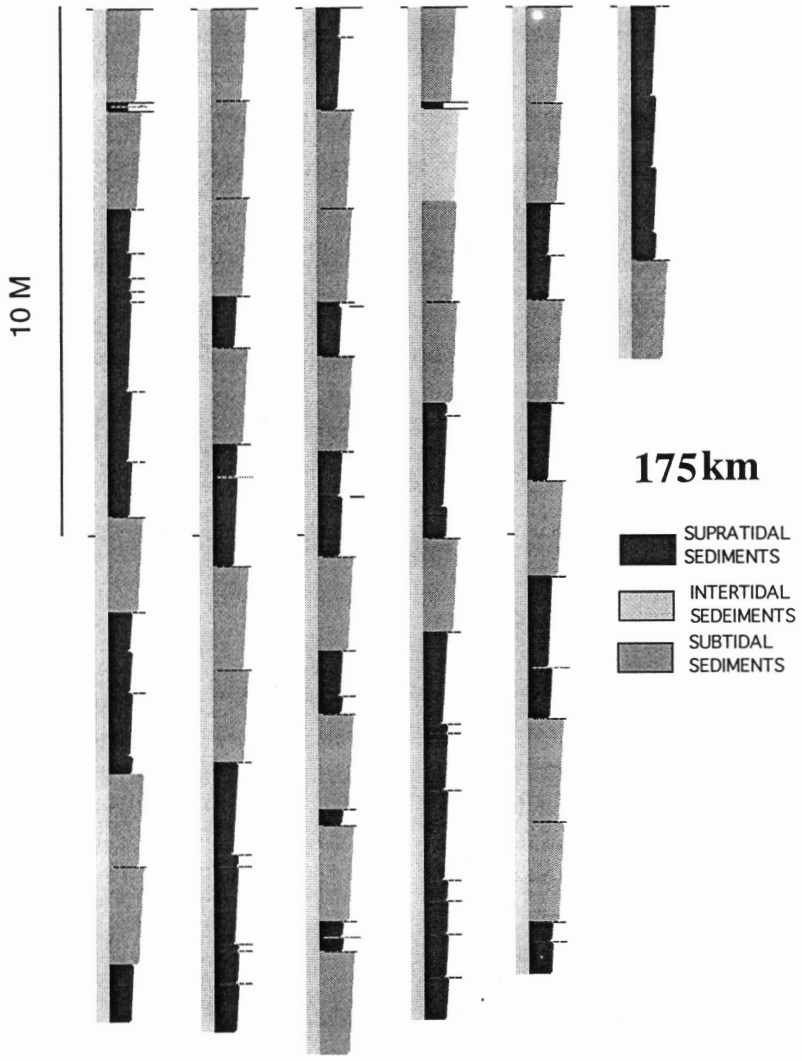

Fig. 4.8. Stratigraphic column generated from the synthetic Late Triassic carbonate platform shown on Fig. 4.7. using PHIL modeling program. The column is constructed at the 175 km position on the platform which appeared to generate the most complete cycle stratigraphies. From the lithologic columns, we created time series based on rock index sampled every 0.2 m .

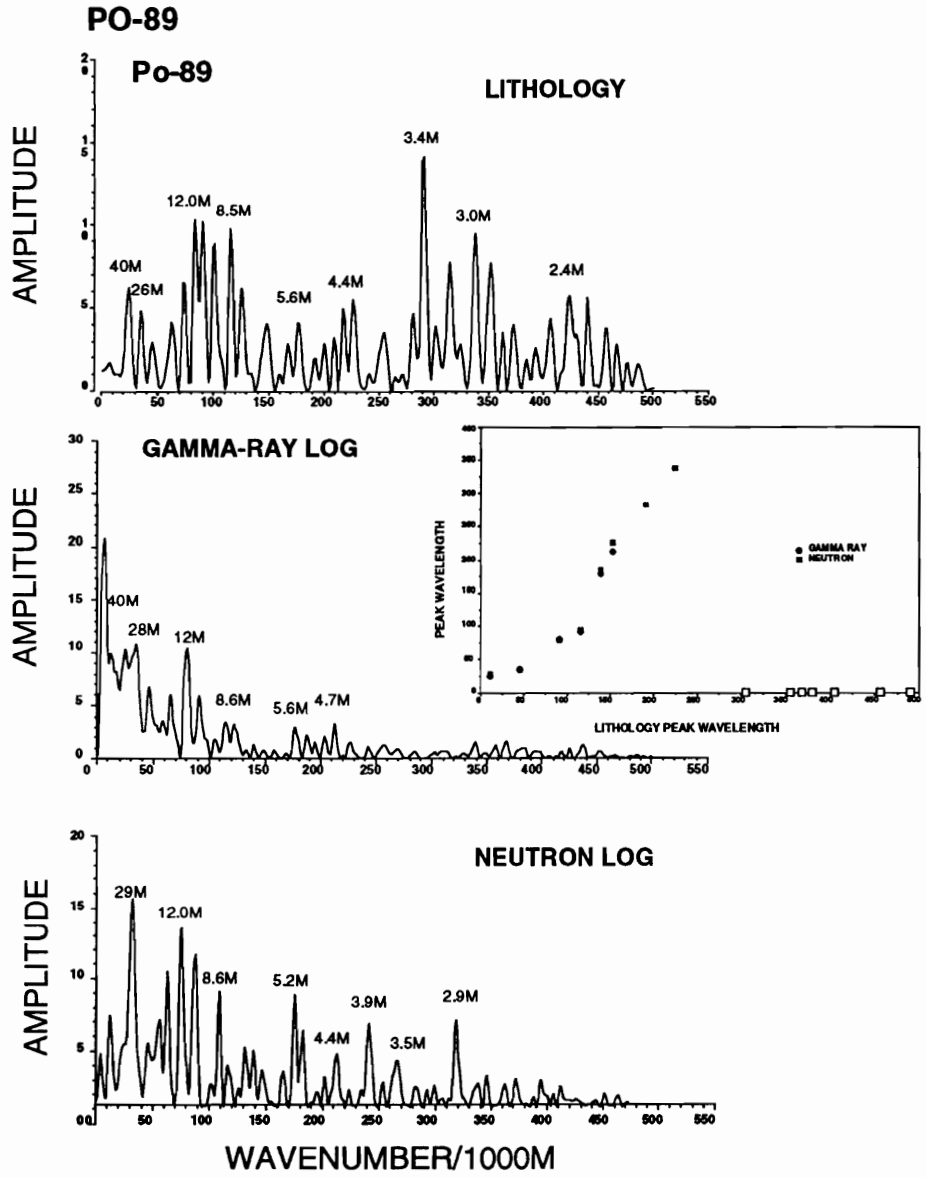

Fig. 4.9. Fast-Fourier amplitude spectral analysis of PO-89 using debiased time-series based on water depth rank (subtidal, intertidal, supratidal/paleosol) vs. stratigraphic position. Sampling interval is 0.2 m. The second and third figures show the debiased FFT spectra of the gamma-ray log and neutron log of Po-89 core with 0.5 m sampling distance. Wavelengths of cycles (in meters) shown by numbers above peaks. Inset shows a cross plot of the different time series.

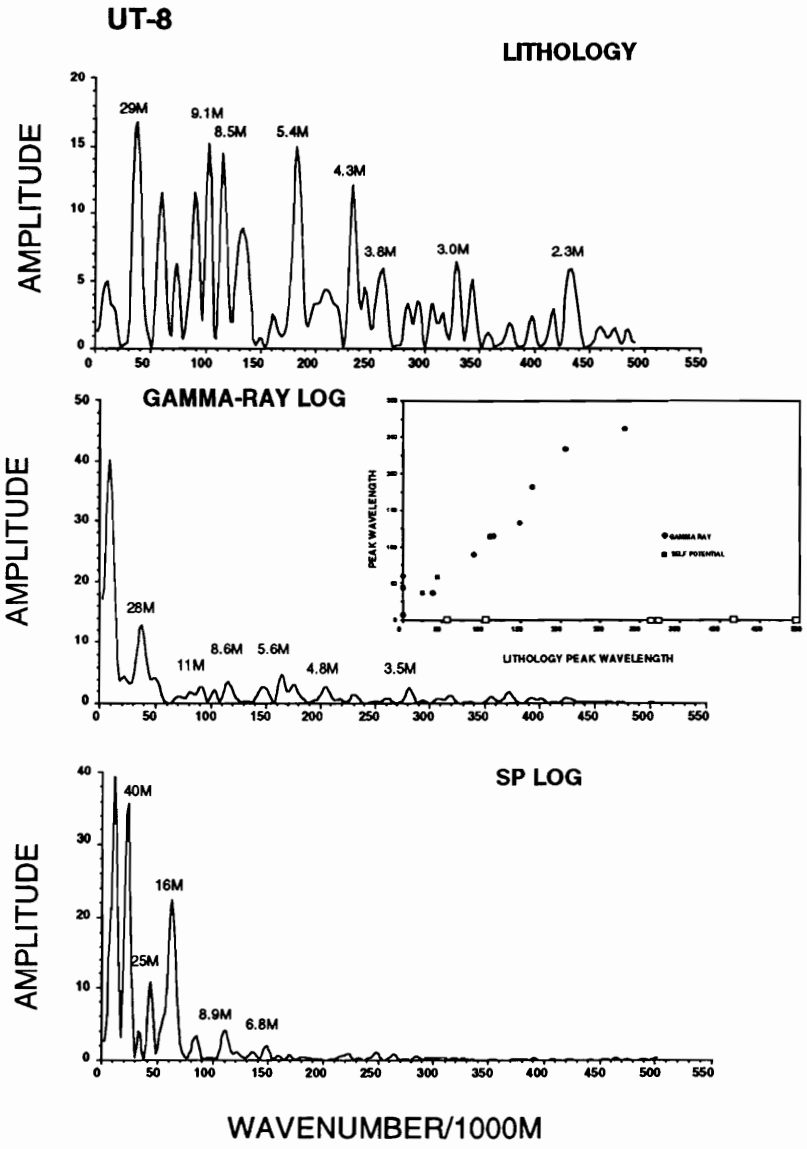

Fig. 4.10. Fast-Fourier amplitude spectra of Ut-8 core using debiased time-series based on water depth rank (subtidal, intertidal, supratidal/paleosol) vs. stratigraphic position. Sampling interval is 0.2 m. The second and third figures show the debiased FFT spectra of the gamma-ray log and neutron log of Po-89 core using 0.5 m sample distance. Wavelengths of cycles (in meters) shown by numbers above peaks. Inset shows a cross plot of the different time series.

wavelength have cognate amplitude (Table 4.2, Figs. 4.9, 4.10). The second group of peaks occur at 3.0 to 3.4 m on Po-89 and 3.0 on Ut-8 (Table 4.2, Figs. 4.10, 4.11). Another peak occurs at 4.4 m on Po-89 and 4.3 m (strong) on Ut-8. A peak also occurs at 5.4 m on Ut-8 and a much weaker one at 5.6 m on Po-89. A strong cluster of peaks occur between about 8.5 and 12 m on both Po-89 and Ut-8. Finally at the low frequency end, there are peaks at 26 to 40 m wavelength on Po-89 and 29 m on Ut-8.

Frequency maps were generated to determine whether the various frequencies were uniformly distributed throughout the stratigraphic section. The most dense areas on the frequency map have very similar frequencies to the frequencies of the significant peaks on the single amplitude spectrums of the different time series (Fig. 4.11). However, the frequency map shows that they have different relative importance as a function of depth. Longer wavelengths peaks (8 to 12.5 m or about 100 cycles/km) are dominant on the top and the bottom of the Po-89 time-series (Fig. 4.11). Three to 3.5 m wavelengths are dominant throughout the Po-89 core, but 2.4 m wavelength only are important in the lower part (Fig. 4.11).

Comparison of Wireline Log Spectra with Spectra Based on Lithology

The gamma ray signal in the cores is mainly generated by clayey units associated with tops of cycles, the more pure subtidal carbonate parts of the cycles generally being clay-poor.

Amplitude spectra from the gamma-ray logs in the two cores have very similar peaks (Table 2. Figs. 4.9, 4.10). At the low frequency end, peaks are similar to the spectra of the lithologic time-series except for a very low frequency peak at 100 wavelength. The relatively short time-series (140 m) suggests that this peak may be artifact. However at the high frequency end of the spectrum below about 4 m wavelength there is little signal evident (Table 2. Figs. 4.9, 4.10).

The neutron log is sensitive to all hydrogen nuclei, thus it is sensitive to both free and bound water. In a tight, relatively nonporous carbonate sequence such as the Hungarian Triassic it would tend to detect bound water in clay rich horizons (Rider 1986). The peaks in the spectra of the time-series of the neutron log of Po-89 are very similar to spectra generated from the lithologic time-series (Table 2. Fig. 4.9). However peaks below 2.9 m are very subdued while at the low frequency end, the 40 m peak evident in the lithologic spectra is present as a small shoulder on the much larger peak around 29 m (Table 4.2. Fig. 4.9).

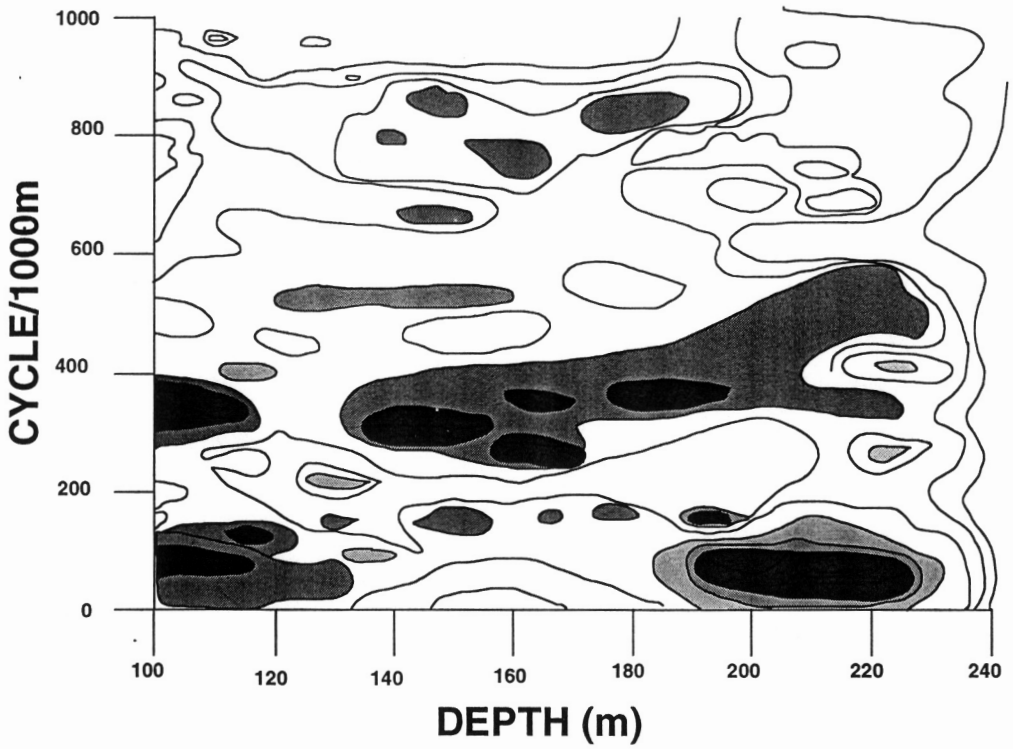

Fig. 4.11. Short-Time Fourier Transform (STFT) spectral map using lithologic time series of Po-89 core. The data are sampled within a sliding window and the Fourier amplitude spectrum is calculated separately for each window in turn. X coordinate represents frequency in wavelength/km, Y shows depth in the section. The contour lines represent the amplitude of the frequencies.

The self potential (SP) log is a measure of the natural potential differences or self-potential between an electrode in a borehole and the reference electrode at the surface, and it is most commonly used as a method to calculate the formation self potential. Since SP deflects slowly these logs generally have poor bed resolution (Rider 1986). The peak locations on the spectrum from the self potential log of Ut-8 have some similarity to those on the lithologic spectra, but only the low frequency wavelengths (above 6 m) are strongly developed; peaks are centered around 9 m, 16 m, and 25 to 40 m. Note the presence of a very low frequency wavelength (100m) in this spectra, which is also evident on the spectra from the gamma ray time-series (Table 2, Fig. 10).

Conversion of Thickness to Time

In the cyclic Hungarian Late Triassic carbonates, the average thickness of the elementary cycle is about 2.5 (Schwarzacher 1993) and this has been assumed by most workers to be the precessional cycle (Schwarzacher and Haas 1986; Schwarzacher 1993; Balog et al. 1995). The calculated duration of an elementary cycle is 20 to 23 k.y. (Haas and Dobosi 1982; Schwarzacher and Haas 1986; Balog et al. 1995). However, the lack of accurate radiometric time controls in the Late Triassic puts a large possible error into the calculation (Balog et al. 1995). Harland (1990) suggests that the Norian had a duration of 13.9 m.y. and the Rhaetian 1.5 m.y. and that 2000 m of carbonates accumulated accumulated in Hungary at this time. Based on this Schwarzacher (Schwarzacher 1993) assigns the 400 m of Po-89 approximately 3 m.y. This suggested that the 12 m megacycles and the 2.5 m basic cycles were roughly 100 k.y. cycles and 20 k.y. respectively. Balog et al (1995) showed that in the Hungarian Triassic there are numerous missing cycles, manifested in the Dachstein Limestone by thick paleosols, or by calichified zones in the Main Dolomite. Cycle bundling on Fischer plots indicated that they are rarely contain the five cycles (100 k.y. eccentricity bundle) or the 40 cycles (400 k.y. bundle) suggesting that about 25% of the total cycles are missing from the succession (Balog et al. 1995).

If the basic cycle is 2.5 m, than the 4 to 5 m peak (roughly twice the basic cycle) is likely to be the obliquity peak and the ~12 m peak the 100 k.y. eccentricity peak (approximately 5 times the basic cycle). The peak between 28 to 40 m may represent the long term eccentricity cycle (Schwarzacher and Haas 1986; Balog et al. 1995).

Comparison of Spectra Based on Actual and Synthetic Lithologic Time Series

Various spectra were derived from the succession of lithologies at location 175 km on the synthetic platform, generated from various input Milankovitch signals. Figure 11 and 12 show spectra of the lithologic time-series, and spectra from the synthetic time-series. Note that simple sea level curves were generated from asymmetric sine waves for the 100 k.y. signal and symmetrical sine waves for the 40 and 19-23 k.y. signal. However the resulting stratigraphic sections clearly show that the stratigraphic record of the platform preserves very poor Milankovitch signal. This partly results from some of the sea level oscillations not flooding the platform, and variation in sedimentation rates with water depth, and cycle capping hiatuses being of highly variable durations, and not being able to be included in the time-series based on thickness.

The spectra from the synthetic platform generated under Milankovitch sea level fluctuations (model A) in which the dominant signals were 100 k.y.=5 m and 19 and 23 k.y. = 5 m respectively, are the most like the actual spectra generated from the cores (Tables 4.1, 4.2, Fig. 4.12). They show peaks centered at 2.4 m (the basic cycle), 3 to 3.4 m (although peaks in the synthetic are more subdued) 4.4 to 4.8, 7 to 12 m, and around 26 to 28 m (close to the 29 m peak in Ut-8). The synthetic runs did not generate a 40 m peak, evident in Po-89 spectra.

In synthetic runs with a low 100 k.y. input signal (model B), the peaks between 7 to 12 m were much more subdued than the spectra from the cores (Tables 4.1, 4.2, Fig. 4.12, 4.13) peak centered around 13 m, which probably was due to the 19 to 23 k.y. input signal generating a precessional beat around 100 k.y (Tables 4.1, 4.2, Fig. 4.13).

For the synthetic run with the 40 k.y. input sea level signal absent, peaks centered around 4 to 4.5 m were suppressed, particularly when compared to core Ut-8 spectrum and to a lesser extent Po-89 (Tables 4.1, 4.2, Fig. 4.13).

Thus the poor record of Milankovitch sea level changes in the synthetic data which was generated by a "clear" synthetic Milankovitch input sea level signal, is very similar to the record preserved on the actual platform. It seems likely based on the modelling that the actual sea level signal was dominated by precessional forcing (19 to 23 k.y. periods) each of which were associated with at least 5 m of sea level change, and eccentricity (~100 k.y.) forcing with an et least 5 m of sea level change. There is a strong suggestion of an obliquity signal in the data/modelling runs, as well as a suggestion of 400 k.y. forcing. The comparison of the real and synthetic data sets suggest that the lack

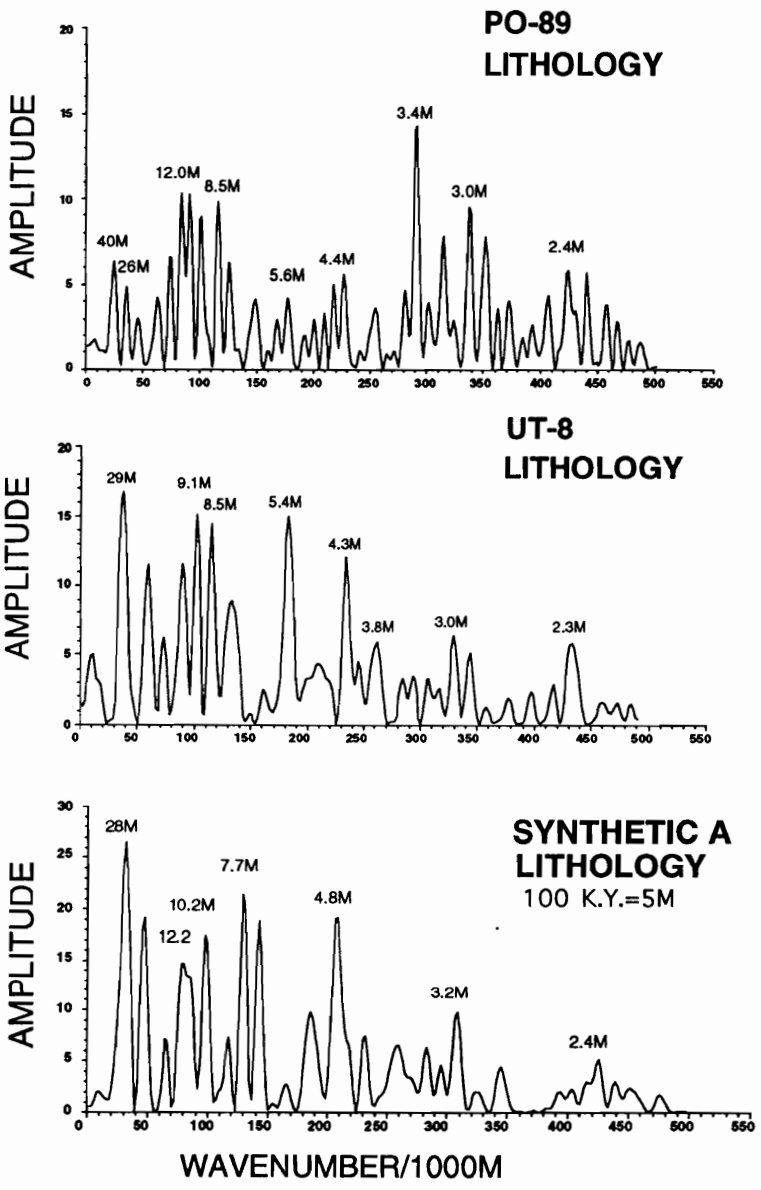

Fig. 4.12. Fast-Fourier amplitude spectra of the lithologic time-series from Po-89 and Ut-8 compared to synthetic amplitude spectra from model A, using debiased time-series based on water depth rank (subtidal, intertidal, supratidal/paleosol) vs. stratigraphic position. Sampling interval is 0.2 m. Wavelengths of cycles (in meters) shown by numbers above peaks.

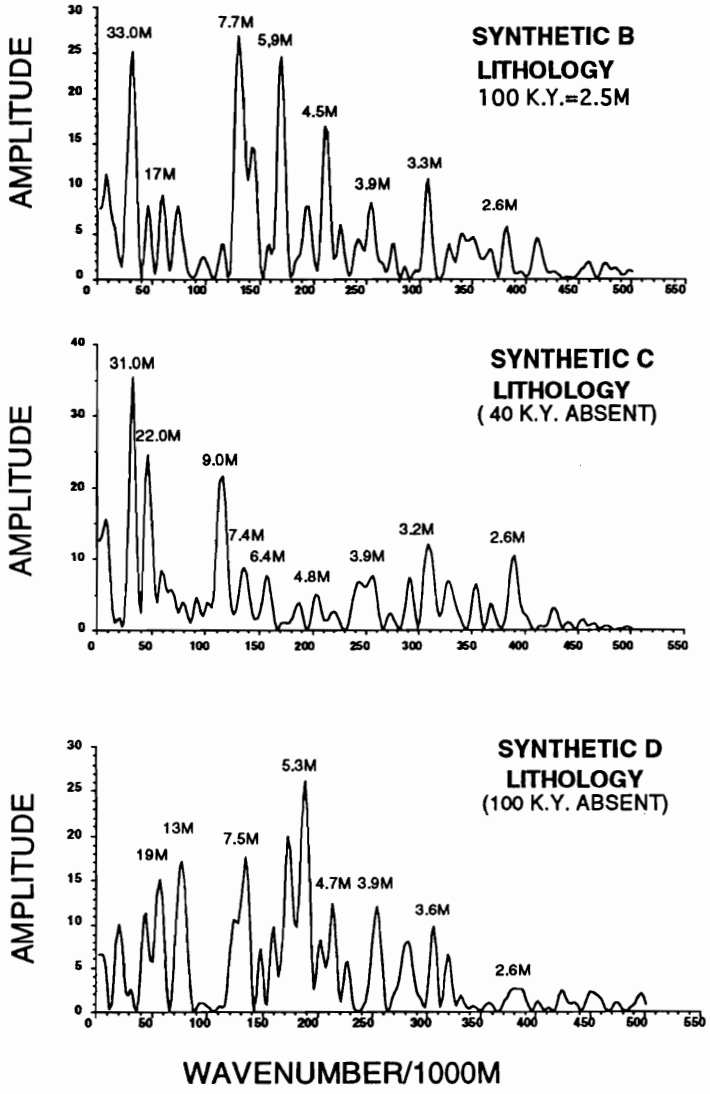

Fig. 4.13. Fast-Fourier amplitude spectra of the lithologic time-series from synthetic model B, C, and D. using debiased time-series based on water depth rank (subtidal, intertidal, supratidal/paleosol) vs. stratigraphic position. Sampling interval is 0.2 m. Wavelengths of cycles (in meters) shown by numbers above peaks.

of a clear Milankovitch sea level signal in shallow water carbonate platform stratigraphies thus should not be used to assess the relative role of autocyclic vs. allocyclic processes.

CONCLUSIONS

(1) Spectral analysis of lithologic logs and wireline logs, and of synthetic stratigraphic sections generated under known Milankovitch sea level curves, support but do not prove the idea that the Late Triassic platform carbonates of Hungary formed as a result, at least in part, of Milankovitch climate forcing.

(2) Spectra of lithologic logs in which time-series were generated by "relative water depth rank" have peaks centered around 2.5 to 3.4 m, 4.4 to 5.6 m, 8.5 to 12 m and 28 to 40m. Spectra from neutron log gave peaks similar to the lithologic log spectra. Spectra from the time-series of gamma ray logs and self potential logs were only sensitive for the lower frequency signals, the higher frequency cycles being very subdued. The poor spectra from the wireline logs may reflect the fact that the logs used were done in the early 70's and better results might be obtained with more modern logs.

The data suggest that precession and short-term eccentricity were important, along with obliquity, and perhaps long term eccentricity, during the deposition of the Late Triassic Hungarian carbonates.

(3) Spectra generated from computer-generated synthetic stratigraphies formed under known input sea level curves involving various Milankovitch signals show a relatively poor Milankovitch signal even though the synthetic columns were generated using a clear Milankovitch sea level curve. The synthetic spectra resemble the actual spectra from the lithologic logs of the Triassic platform. Overall the data support the ideas that Milankovitch eustasy involving a dominant precessional signal and a lesser eccentricity signal were important in the formation of the Hungarian cycles. Obliquity and long term eccentricity also appear to have influenced the cycle bundling. The model results suggests that spectra from carbonate platforms reflect imperfect recording of any Milankovitch orbital forcing.

REFERENCES CITED

Balla, Z., 1988, Clockwise paleomagmatic rotations in the Alps in the light of the structural pattern of the Transdanubian Range (Hungary): Tectonophysics, v. 145, p. 277-292.

Balog, A., Haas, J., and Read, J.F., 1995, Shallow marine record of orbitally forced cyclicity in a Late Triassic carbonate platform, Hungary: Journal of Sedimentary Research (In press).

Berger, A., 1984, Accuracy and frequency stability of the Earth's orbital elements during the Quaternary, *in* Berger, A., Imbrie, J., Hays, J., Kukla, G., and Saltzman, B., eds., Milankovitch and Climate [NATO ASI Series C, Vol. 126]: Boston, D. Reidel Publishing Co., p. 510.

Berger, W.H., and Vincent, E., 1986, Deep-sea carbonates: reading the carbon-isotope signal: Geologische Rundschau, v. 75, p. 249-269.

Bowman, S., 1994, PHIL Tm 1.5 Manual, Huston, Marco Polo Software, Inc.

Emiliani, C., 1966, Paleotemperature analysis of Caribbean cores P6304-8 and P6304-9 and a generalized temperature curve for the past 425,000 years: Journal of Geology, v. 74, p. 109-126.

Gilbert, G.K., 1895, Sedimentary measurement of Cretaceous time: Journal of Geology, v. 3, p. 121-127.

Haas, J., 1982, Facies analysis of the cyclic Dachstein Limestone Formation (Upper Triassic) in the Bakony Mountains, Hungary: Facies, v. 6, p. 75-84.

Haas, J., and Dobosi, K., 1982, Felso-Triasz ciklusos karbonatos kozetek vizsgalata Bakonyi alapszelvenyeken: Magyar Allami Foldtani Intezet Evi Jelentese 1980-rol, p. 135-168.

Harland, W.B., Armstrong, R.L., Cox, A.V., Craig, L.E., Smith, A.G., and Smith, D.G., 1990, A Geologic Timescale 1989: Cambridge, University Press, 263 p.

Imbrie, J., and Imbrie, K.P., 1979, Ice Ages: Solving the Mystery: Short Hills, NJ, Enslow Publ., 224 p.

Kazmer, M., and Kovacs, S., 1985, Triassic and Jurassic oceanic/paraoceanic belts in the Carpathian-Pannonian region and its surroundings, *in* Sengor, A.M.C., ed., Tectonic

evolution of the Tethyan region: Dordrecht, London,, Kluwer Academic Publishers, p. 698.

Milankovitch, M., 1941, Cannon of insolation and ice age problems [in German]: Belgrade, Academy Royale Serbe (Belgrade), Special Publication 133, 633 p.

Olsen, P., 1986, A 40-million-year lake record of Early Mesozoic orbital forcing: Science, v. 234, p. 842-848.

Rider, M.H., 1986, The geological interpretation of well logs: New York, John wiley and Sons, 175 p. 135.

Schwarzacher, W., 1993, Cyclostratigraphy and the Milankovitch Theory, v. 52: Amsterdam, Elsevier, 225 p.

Schwarzacher, W., and Haas, J., 1986, Comparative statistical analysis of some Hungarian and Austrian Upper Triassic peritidal carbonate sequences: Acta Geologica Hungarica, v. 29, p. 175-196.

Weedon, G.P., 1990, The spektral analysis of stratigraphic time series, *in* Einsele, G., Ricken, W., and Seilacher, A., eds., Cycles and Events in Stratigraphy: Berlin, Springer-Verlag, p. 840-863.

weedon, G.P., 1993, The recognition and stratigraphic implications of orbital-forcing of climate and sedimentary cycles, *in* Wright, V.P., ed., Sedimentology review/1: Oxford, Blackwell Scientific Publications, p. 31-50.

VITA

Anna Balog was born in Kaposvar, Hungary on May 6 1954. She attended Szabo Jozsef High School which was specialized in geology and she graduated in 1972. She graduated in geology at Eötvös University, Budapest, Hungary, in 1978. She immediately started to work for the Department of Mineralogy, and two years later for the Department of Petrology and Geochemistry at the Eötvös University, Budapest as an assistant professor. She received her doctorate in mineralogy and geochemistry in 1984 at the same department. In 1983 she became an assistant professor at the Technical University of Budapest, where she was promoted to associate professor in 1986. Five years later, in 1990 she received a scholarship from Szécheny István Foundation (Hungary), and moved to Blacksburg and worked at Virginia Tech. In the following year she entered the Ph.D. program in Geological Sciences Virginia Tech. She is employed as an adjunct Associate Professor at the Geology Department of Virginia Western Community College.